TUG

Doctoral Thesis

Low Complexity Ultra-Wideband (UWB) Communication Systems in Presence of Multiple-Access Interference

Jimmy Baringbing

Faculty of Electrical Engineering and Information Technology
Graz University of Technology, Austria

Examiners:
Univ.-Prof. Dr. techn. Gernot Kubin, Graz University of Technology,
Austria
Dr. ir. Gerard J. M. Janssen, Delft University of Technology,
The Netherlands

Co-Advisor:
Dipl.-Ing. Dr. Klaus Witrisal, Graz University of Technology, Austria

Graz, December 19, 2008

Education is hanging around until you've caught on

Abstract

Ultra-wideband (UWB) communication systems use radio signals with a bandwidth in the range of some hundred MHz to several GHz. Radio channels with dense multipath propagation achieve high multipath diversity, which can be used to improve the robustness and capacity of the communication channel. Furthermore the large bandwidth allows to transmit signals with a small power spectral density such that the interference to other radio signals will be negligible, even if they lie within the same frequency band. In this work the focus is on low-complexity receiver architectures for communication systems in presence of multiple-access interference (MAI). The main objective of this thesis is to develop and to study a framework for communications for transmitted reference (TR) UWB systems and energy detection UWB systems.

First, we study the hybrid matched-filter (HMF) receiver for TR UWB systems, which employs matched filters in front of the autocorrelation receiver (AcR). We investigate optimization of the combining weights in the matched filters with the purpose of suppressing MAI. For that goal, we included MAI contributions in an equivalent system model for the HMF-TR UWB receiver and derived a modified pre-combining minimum mean-square error solution for multiuser detection. The obtained solution is novel, due to the non-linear behavior of the autocorrelation operation. The proposed detectors are shown to yield improved performance over the multi-channel autocorrelation receiver. Second, the performance of a dual-pulse TR UWB system is presented in presence of MAI. We derive an analytical expression of the channel-averaged signal-to-interference ratio for a TR UWB receiver in two asynchronous scenarios, based on random time-hopping codes. Analytical results and numerical results are presented for illustration. We further show the impact of the chosen system parameters (e.g., symbol duration and delay hopping code) to better understand their influence on the multi-user performance. Third, we introduce optimization of the energy detection UWB receiver system. We have considered a weighted energy detection receiver that alleviates the noise effect in a single user scenario and the multiple-access influence in a multiple-access environment. We have demonstrated that the weighted receiver outperforms the conventional energy detection receiver.

Kurzfassung

Ultra-Breitband (engl.: ultra-wideband, UWB) Kommunikationssysteme verwenden Funksignale mit einer Bandbreite von wenigen hundert MHz bis zu mehreren GHz. Funkkanäle mit einer dichten Mehrwegeausbreitung erreichen eine starke Frequenzdiversität, was zu einer Steigerung der Robustheit und der Kapazität des Kommunikationskanals genutzt werden kann. Außerdem erlaubt die große Bandbreite ein Übertragen des Signals mit geringem Leistungsdichtespektrum, so dass die gegenseitige Beeinflussung anderer Funksignale vernachlässigbar ist, sogar wenn diese im selben Frequenzband liegen. In dieser Arbeit liegt der Schwerpunkt auf Empfängerarchitekturen mit geringer Komplexität für Kommunikationssysteme bei Vorliegen von Mehrfachzu- griffstörungen (engl.: multiple-access interference, MAI). Das Hauptanliegen dieser Doktorarbeit ist die Entwicklung und Analyse einer Kommunikationsstruktur für Transmitted-Reference (TR) UWB Systeme und UWB Systeme mit Energiedetektorempfängern.

Zuerst untersuchen wir eine Hybride Matched-Filter (HMF) Empfängerarchitektur für TR UWB Systeme. Wir führen eine Optimierung der Kombinationsgewichte des analogen Matched-Filters zur Unterdrückung von MAI durch. Wir haben dafür MAI durch ein äquivalentes Systemmodell für den HMF TR UWB Empfänger ausgedrückt und damit eine modifizierte Minimum Mean-Square Error Lösung für Mehrbenutzerdetektion (engl.: multiuser detection, MUD) abgeleitet. Die erzielte Lösung ist wegen des nichtlinearen Verhaltens des hybriden Autokorrelationsempfängers neuartig. Es wird gezeigt, dass die vorgeschlagenen Detektoren eine verbesserte Leistung gegenüber herkömmlichen Mehrkanal-Autokorrelations UWB Empfängern liefern. Zweitens präsentieren wir die Leistung von Zweipuls TR UWB Systemen in Gegenwart von MAI. Wir leiten einen analytischen Ausdruck für das über Kanalrealisierungen gemittelte Signal-zu-Störverhältnis für den TR UWB Empfänger her, für zwei asynchrone Szenarien basierend auf Mehrfachzugriff mittels zufälligen Time-Hopping Codes. Wir zeigen den Einfluss der gewählten Systemparameter (z.B.: Symboldauer und Time-Hopping Code) auf die Leistung des Mehrfachbenutzer-Systems, um deren Einfluss besser verstehen zu können. Drittens optimieren wir UWB Empfängersysteme mit Energiedetektion. Wir untersuchen einen gewichteten Energiedetektionsempfänger, der die Rauscheffekte in einem Einbenutzer Szenario und die Mehrfachzugriffstörungen (MAI) in einer Mehrbenutzerumgebung reduziert. Wir zeigen, dass der gewichtete Empfänger den gewöhnlichen Energiedetektionsempfänger leistungsmäßig übertrifft.

Acknowledgment

I would very much like to express my sincere gratitude to Prof. Gernot Kubin for encouraging me prior to and during my PhD study and for his excellent guidance throughout this work. From the initial stage until completion of this work he gave me valuable inspiration. I thank for his insightful comments and remarks about this work.

I am in great debt to my doctoral thesis advisor, Dr. Klaus Witrisal. His idea and visions for Ultra Wideband (UWB) have been a great motivation. He encouraged me to try out new ideas and helped me to question them critically. Also, I am thankful for his technical suggestions improving my work considerably and for his effort in helping me make this thesis more graspable and the presentation of the content. He has guided me and encouraged me all the way during my PhD study and also for supporting me in the difficult time.

I would also like to thank to Dr. ir. Gerard J. M. Janssen from Delft University of Technology (TU Delft) for serving in my dissertation examiner, for reviewing my dissertation and bringing questions.

I would like to thank a lot to my colleagues at the Signal Processing and Speech Communication Laboratory that over these years have provided an excellent working environment and were really helpful to me.

I would like to thank OAD (Austrian Exchange Service) to support this research. I thank our parents for their support during our study and who have been a source of encouragement throughout my life.

A big thank you goes to the woman in my life, my dearest wife Evi for her understanding during many hours I was occupied with my work. You are the very best, for all your love and care.

Graz,   Jimmy Baringbing
December 19, 2008

xi

to our family,
 and to my beloved wife Evi.

Contents

List of Figures

List of Tables

List of Symbols

$\mathbf{a}^{(k)}[i]$	$\cdots$	Polarities of all pulses having impact on received symbol i
$\tilde{\mathbf{b}}^{(k)}$	$\cdots$	Amplitude code vectors of user k
$b_{l_{\mathbf{d}}}$	$\cdots$	Despreading vectors for the data pulses
$b_{l_{\mathbf{r}}}$	$\cdots$	Despreading vectors for the reference pulses
$c_{l_{\mathbf{d}}}$	$\cdots$	Time-hopping sequences of data pulses
$c_{l_{\mathbf{r}}}$	$\cdots$	Time-hopping sequences of reference pulses
$\mathsf{E}(.)$	$\cdots$	Expectation operation
$f_{rx}(t)$	$\cdots$	Impulse response of the front-end filter receiver
$g^{(k)}(t)$	$\cdots$	Response of the channel to one transmitted monocycle of user (k)
$h^{(k)}$	$\cdots$	Time-hopping burst position
h_0	$\cdots$	Bias term
$\mathbf{h_1}$	$\cdots$	Linear coefficients
$\mathbf{h_2}$	$\cdots$	Quadratic terms
i	$\cdots$	Symbol index
$j_{\mathbf{r}}(j)$	$\cdots$	Mapping of index j onto $j_{\mathbf{r}}$
$j_{\mathbf{d}}(j)$	$\cdots$	Mapping of index j onto $j_{\mathbf{d}}$
N_{cr}	$\cdots$	Number of correlators
N_d	$\cdots$	Number of data pulses
N_0	$\cdots$	Single-sided power spectral density
N_r	$\cdots$	Number of reference pulses
$\widetilde{\otimes}$	$\cdots$	Reduced version of the Kronecker product for binary vectors
$R_\nu(\kappa)$	$\cdots$	Autocorrelation function of noise process
$s^{(k)}(t)$	$\cdots$	Transmitted signal of user (k)
$t_{i,l}^{(k)}$	$\cdots$	Pulse timing for single channel of user (k)
τ_{rms}	$\cdots$	RMS delay spread
T_B	$\cdots$	Burst duration
T_{BPM}	$\cdots$	BPPM time shift
T_c	$\cdots$	Chip duration
T_I	$\cdots$	Integration interval
$\mathbf{Y}^{(j_{\mathbf{r}},j_{\mathbf{d}})}_{(k,k')}$	$\cdots$	Interference among the pulses due to multiple existing users
$\mathbf{w}_{ref}$	$\cdots$	Linear combiners for reference pulses
$\mathbf{w}_{dat}$	$\cdots$	Linear combiners for data pulses
$w(t)$	$\cdots$	Transmitted pulse shape
$\mathbf{y}_\nu[i]$	$\cdots$	Vector of zero-mean noise samples

List of Abbreviations

AWGN	$\cdots$	Additive White Gaussian Noise
AcR	$\cdots$	Auto Correlation Receiver
ACF	$\cdots$	Auto Correlation Function
APDP	$\cdots$	Average Power Delay Profile
BER	$\cdots$	Bit Error Rate
BPSK	$\cdots$	Binary Phase Shift Keying
CCF	$\cdots$	Cross Correlation Function
CIR	$\cdots$	Channel Impulse Response
CDMA	$\cdots$	Code Division Multiple Access
ED	$\cdots$	Energy Detector
FCC	$\cdots$	Federal Communications Commission
FD	$\cdots$	Frame Differential
HMF	$\cdots$	Hybrid Matched Filter
IFI	$\cdots$	Inter Frame Interference
ISI	$\cdots$	Inter Symbol Interference
IPDP	$\cdots$	Instantaneous Power Delay Profile
IPI	$\cdots$	Inter Pulse Interference
LDR	$\cdots$	Low Data Rate
MAI	$\cdots$	Multi Access Interference
MIMO	$\cdots$	Multiple-Input-Multiple-Output
MMSE	$\cdots$	Minimum Mean Squared Error
MUD	$\cdots$	Multiuser Detection
PHY	$\cdots$	Physical Layer
PPM	$\cdots$	Pulse Position Modulation
SNR	$\cdots$	Signal-to-Noise Ratio
SIR	$\cdots$	Signal-to-Interference Ratio
TH	$\cdots$	Time Hopping
TR	$\cdots$	Transmitted Reference
UWB	$\cdots$	Ultra Wideband
WPAN	$\cdots$	Wireless Personal Area Networks

1 Introduction

Ultra wideband (UWB) impulse radio systems transmit data by modulation of sub-nanosecond pulses. UWB technology has been around since 1960, when it was mainly used for radar and military applications. UWB does not use a sinusoidal carrier to raise the signal to the radio frequency (RF) band, which means a UWB radio may be manufactured inexpensively [2].

1.1 Motivation for Ultra Wide-Band Communications

According to the Federal Communication Commission (FCC), UWB impulse radio is a communications system whose 10 dB bandwidth is greater than 20 percent of its center frequency or exceeds 500 MHz [3]. The first criterion is the fractional bandwidth B_f, defined as

$$B_f = 2\frac{f_H - f_L}{f_H + f_L} \tag{1.1}$$

with f_H being the upper frequency of the -10 dB emission point and f_L the lower frequency of the -10 dB emission point. The center frequency of the transmission was simply defined as $f_c = \frac{f_H + f_L}{2}$. The UWB systems with $f_c > 2.5$ GHz need to have a -10 dB bandwidth of at least 500 MHz, while UWB systems with $f_c < 2.5$ GHz need to have fractional bandwidth of at least 0.20. Traditionally, UWB impulse radio communication systems transmit data and operate at baseband that can be free of sine-wave carriers and do not require IF processing. These narrow pulses are distorted by the channel, but often can resolve many distinct propagation paths (multipath) because of their very fine time resolution. The UWB concept was used to develop impulse radio, where baseband pulses are transmitted over the channel [4]. This technique greatly simplifies the transmitter and receiver designs; however, the transmitted bandwidth extends to the GHz range. The unique features of UWB systems also suggest very accurate ranging applications. Ultra-wide bandwidth radio communication systems have the potential for great capacity and robustness. However, the potential benefits promised by UWB technology pose great challenges to the design of low-cost and low-complexity UWB communication systems.

Any application of UWB technology must conform to the regulations imposed on radio-frequency transmission. Since the power spectrum of UWB devices overlaps

with various other technologies, transmission power is restricted by a spectral mask. For the United States, the Federal Communication Commission (FCC) permits transmission of signals in the 3.1 to 10.6 GHz band as shown in Fig. 1.1. It requires that the transmitted signals have an effective isotropic radiated power (EIRP) below -41.3 dBm in this band and a minimum bandwidth of 500 MHz. This very conservative limit equals the threshold for the electromagnetic compatibility (EMC) and ensures the non-interference of a UWB signal source.
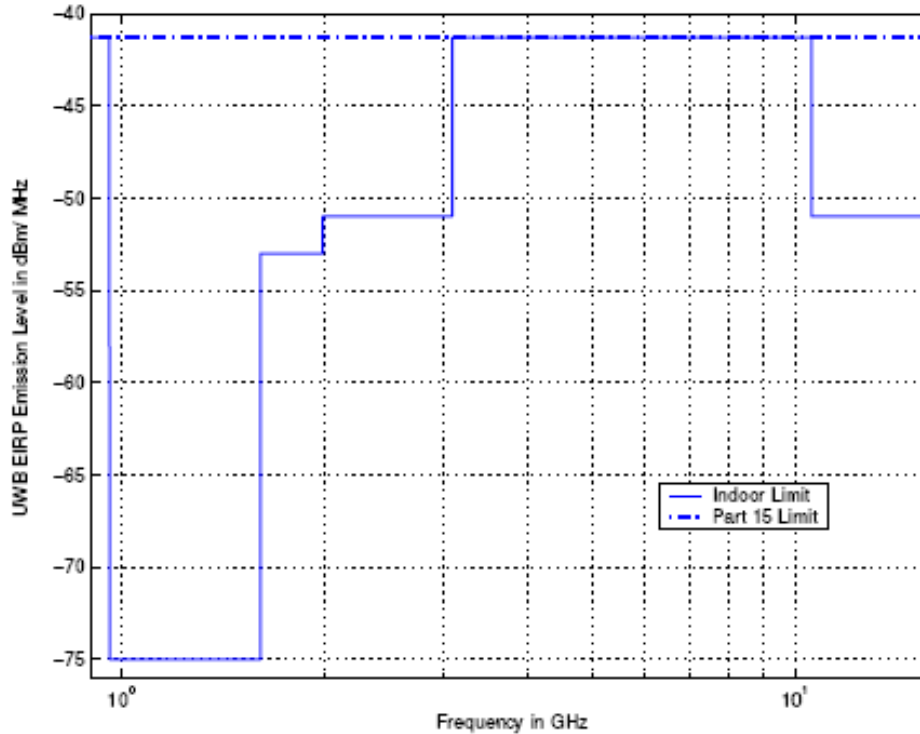
Figure 1.1: FCC Spectral Mask for Indoor Application

The extremely large bandwidth of UWB systems promises the following outstanding air interface features: (i) The power spectral density (PSD) of UWB signals could be kept very low such that existing inband narrowband services would not be as strongly affected by UWB signals than by any other radio signals. (ii) The extremely large bandwidth would provide very high channel capacity and thus enable multiuser communication at high data rates. (iii) The large bandwidth causes a large diversity which enables robust communication links resulting in simple transmitter and receiver circuits.

Consequently, when designing a UWB system, the fading margin in link budgets

can be significantly reduced, which allows for low transmit power operations. Since UWB devices operate at a power level as low as the background noise, they will less likely interfere with the existing narrowband systems.

Due to the extremely large bandwidths of UWB signals, the transmitted UWB signal duration is very small. Experimental results have shown that in typical indoor environments, maximum channel delay spreads of 60-70 ns are observed. This implies that, by transmitting subnanosecond pulses, the signal energy will be spread over a large number of multipath components (MPCs) [5, 6, 7]. The unique channel structure of UWB systems has many implications. To fully collect the signal energy, commonly-used rake receivers are essential for coherent signal detection; the receiver has to lock on these multipath components to collect the energy [8, 9]. Rake receivers typically require the estimation of the timings, amplitudes/phase and the pulse shapes at individual arrivals. To have satisfactory energy capture, the number of Rake fingers required may be large in a dispersive UWB channel, which may considerably increase the receiver complexity.

Transmitted-reference and energy detector receivers are two other practical and lower-complexity transceiver types, which we consider in this dissertation. The original idea of the transmitted reference (TR) scheme dates back to the 1960s and was firstly applied to UWB systems in [10]. The TR UWB system has several advantages over the rake receiving system in terms of implementation complexity [11, 12, 13]. First, it simply needs an autocorrelation receiver (AcR) with delays instead of many rake fingers to capture the multipath energy. Second, it does not require channel estimation, thus it is not sensitive to the channel estimation errors that may deteriorate the performance of rake receivers. In addition, instead of requiring timing synchronization for each rake finger, the TR scheme only needs synchronization for one correlation operation. The drawback of such a design is the implementation challenge of delay lines. However, the simplicity of the TR UWB system is achieved at the expense of certain amount of performance degradation. Simply put, it wastes power and time to transmit the reference pulses, which effectively degrades the detection performance and sacrifices the information rate. Moreover, because a noisy reference is used as the template signal for correlation, the noise effect is enhanced by introducing an additional noise-times-noise term, which further degrades the detection performance [14, 15].

Energy detection receivers are appealing for IEEE 802.15.4a low data-rate networks because of their low complexity. With a reasonable energy consumption, these receivers can exploit the ranging capabilities and multipath resistance of impulse-radio UWB (IR-UWB) [16, 17]. They make no attempts to gather information on the channel response. For example, assume binary pulse position modulation (2-PPM) with rate $1/T$. Symbol zero corresponds to transmitting a pulse in the first half of the interval $(0, T)$ while symbol one corresponds to transmitting a pulse in

the second half. Its data decisions are based only on signal energy measurements. The receiver measures the signal energies on both halves and selects the symbol with the largest energy. However, the performance of energy-detection receivers can be severely degraded by multiple-access interference (MAI). The simplicity of this approach comes at the cost of a lower immunity to interference from other users or other systems. This energy-capture scheme appears as a valid solution in terms of complexity, cost and power consumption and, for these reasons, has been employed in this work.

1.2 Concept of This Work

In this dissertation, based on the preliminary discussion in the previous section, we try to address certain challenges related to practical low-cost and low-complexity UWB transceiver design in the presence of multiple-access interference (MAI). Multiple access is an essential part of UWB systems to accommodate many users within the same channel. Possible multiple access options for UWB networks are time-division multiple access (TDMA), frequency-division multiple access (FDMA), code-division multiple access (CDMA). Time-hopping (TH) and direct-sequence (DS) UWB are popular CDMA based approaches that are applicable to UWB systems, where TH UWB systems are studied in this dissertation.

The transmission of the signals close to the noise level and the extreme dispersion of the received signal impose many challenges on practical implementations of multiuser UWB systems. The main focus of this work is put on simple, low-power and robust receivers for low data-rate communication in the presence of MAI [3, 18, 19, 20, 21]. Simple receiver architectures can be found by realizing the receiver tasks that require fast signal processing. Receiver types that work without channel estimation are noncoherent or energy collecting receivers such as transmitted-reference and energy detection receivers.

It is also observed that the effect of noise and multiuser interference are worse for the TR and ED approaches. In particular, noise-square terms and MAI-square terms degrade the detection performance. Therefore, even though TR and ED perform better at high SNR due to better energy capture, they have poor performance when the noise and MAI variances are large. While exact analysis of TR and ED require Chi-square statistics to be used; through all chapters, we consider Gaussian approximations to the Chi-square statistics, which becomes valid under certain conditions, and allows a unified analysis of the transceiver schemes.

1.3 Outline

This thesis is organized as follows. Chapter 2 describes an overview of the properties of the UWB TR with their equivalent system model and is a basis to understand the subsequent chapters.

In Chapter 3 we study and optimize the hybrid matched filter (HMF) receiver, which employs a linear matched filter in front of an autocorrelation receiver (AcR), in a multiuser (MU) scenario. We derive the equivalent system model for the HMF receiver in a similar form as presented in [22]. This equivalent system model is then used for the optimization of the combining weights in the (pre-AcR) matched filters, with the purpose of suppressing multiple access interference (MAI). MAI refers to the interference between different users due to multiple users transmitting over the same radio channel. The solution to this problem cannot use standard minimum mean-square error (MMSE) techniques, due to the non-linear behavior of the (post-combining) autocorrelation operation. We present a modified MMSE solution for this problem. To verify this solution, structural modifications are applied to the HMF front-end, which allow the employment of standard MMSE and maximum-likelihood (ML) detectors for MAI suppression. However, these structurally expanded receivers are less feasible for a hardware implementation, but they provide reliable benchmark results for the studied optimized HMF AcR. We also compare the performance to conventional, optimized multi-channel AcRs (MC-AcR) receivers [1, 23], which are most feasible from a practical point of view.

In Chapter 4, we study the conventional TR UWB scheme for dual-pulse systems in multi-user scenarios. We derive the equivalent system model for the TR UWB receiver in a similar form as presented in [22, 1]. The objective of this chapter is to study the statistical characterization of the MAI in terms of channel-averaged signal-to-interference ratio (SIR) and the influence of system parameters on the receiver. The authors in [24, 25, 26] have developed the theoretical framework of the statistical signal properties of the auto-and cross-correlations functions of the received pulse in UWB autocorrelation receiver (AcR) systems. We directly apply their theoretical framework, which will enable us to analyze the channel-averaged output SIR of the TR UWB system [27]. This chapter studies the performance of dual-pulse TR UWB systems in presence of MAI. We derive an analytical expression of the channel-averaged signal-to-interference ratio (SIR) for a TR UWB receiver in two asynchronous scenarios, based on random time-hopping (TH) codes. Both analytical results and numerical results are presented for illustration. We further show the impact of the chosen system parameters (e.g. symbol duration and delay hopping code) to better understand their influence on the multi-user performance.

In Chapter 5, we consider a simple yet flexible receiver based on weighted processing. In spite of the low duty cycle usually exhibited by UWB signals, some of

the envisioned application scenarios imply that multiple competing transmissions produce harmful collisions. In the presence of multiple users, single-user detection is typically suboptimal and special effort is needed to cope with MAI effects. This chapter is devoted to such issues with the aim to cope with MAI at the physical layer (PHY), using weighted energy detection receivers in single and multiuser scenarios [28].

Chapter 6 contains the conclusions and an outlook to future research.

1.4 Contributions

The major contributions of this work are :

- We present a derivation of a modified pre-combining minimum mean-square error (MMSE) solution for the HMF TR UWB receiver that is novel, due to the non-linear behavior of the autocorrelation operation. The equivalent system model for the HMF receiver in a similar form as presented in [22, 1] is then used for the optimization of the combining weights in the (pre-AcR) matched filters, with the purpose of suppressing MAI.

- We present the statistical characterization of the MAI in terms of channel-averaged signal-to-interference ratio (SIR) of the dual-pulse TR UWB systems and the influence of system parameters on the receiver.

- We present derivation of the weighting coefficients for weighted energy detection receiver based on maximization of a signal-to-interference metric in single and multiuser scenarios.

The results in this dissertation have been presented and published in the following papers:

- J. Baringbing, "Multiple Access Performance of TH UWB BPM Energy Detection Receiver", *Oral Presentation in Privatissimum at Signal Processing and Speech Communication Laboratory SPSC TUGraz*, Graz, Austria, October 2, 2008.

- J. Baringbing and K. Witrisal, "Performance Evaluation of Multiple-Access Dual-Pulse Transmitted Reference UWB Systems", *in Proceeding of IEEE International Wireless Communications and Mobile Computing Conference*, IWCMC, Crete, Greece, pp. 1-5, August 6-8, 2008.

- J. Baringbing and K. Witrisal, "MMSE Optimisation of the Hybrid Matched-Filter Receiver for Transmitted-Reference UWB", *in Proceeding of IEEE International Symposium on Personal, Indoor and Mobile Radio Communications*, PIMRC, Athens, Greece, pp. 214-219, September 3-7, 2007.

- J. Baringbing and K. Witrisal, "MMSE Optimisation of the Hybrid Matched-Filter Receiver for Transmitted-Reference UWB", *Oral Presentation in IEEE UWB Forum on Sensing and Communication*, Linz, Austria, March 12, 2007.

2 Channels, Transmitted-Reference Signaling and Multiple-Access Interference Modeling

Autocorrelation receiver (AcR) front-ends promise to provide a low-complexity, sub-optimal alternative to coherent reception for differentially modulated impulse radio (IR) ultra-wideband (UWB) signals and for transmitted-reference (TR) modulation. Due to the high processing gain, UWB-IR signals can be used for random multiple access by a large number of users, when detected coherently. Unfortunately, much of this capability is lost when a non-coherent AcR front-end is used. Delay hopping has been proposed as a basic priciple for multiple access in TR systems. Based on a data model for multiple access TR schemes, a favorable signaling scheme is proposed, which employs short bursts of UWB pulses, leading to a (non-linear) memoryless multi-user data model, even in the absence of synchronization among users. The performance of linear detectors is presented.

Multiple access communication allow users to communicate with each other with tolerable interference. Today, the demand for accessing the Internet from virtually anywhere motivates a reliable wireless multiple access scheme. Code division multiple access (CDMA) systems have been extensively investigated in the last two decades. In realistic propagation conditions, multipath phenomena cause degradation in the performance and, even with large fading margin design, an ongoing communication may be disconnected. Multipath phenomenons happen due to the electromagnetic wave reflections from objects, persons, building, trees, mountains or anything in the surrounding environment at which the wireless communication takes place.

To allow for multiple access, two approaches have been proposed, time-hopping (TH) and direct sequence (DS). In TH-UWB systems, each user is assigned a unique pseudo-random sequence, which determines time shift to the pulse position within each frame, in order to avoid the catastrophic collisions among different users. In DS-UWB systems, rather than sending one pulse per frame in TH-UWB systems, each symbol is represented by a series of consecutive pulses which are pulse-amplitude modulated by a user-specific spreading sequence. In this thesis, we only consider the more classical TH-UWB systems.

2.1 Introduction to Transmitted Reference UWB

In transmitted reference UWB receivers, the received signal consisting of a train of distorted pulses is correlated with a delayed version of itself. This is done by a 'pulse-pair' correlator with a fixed correlation lag. If there exist pulses spaced by this lag in the received signal, a high correlation output is obtained, which can be used to detect the data symbols. Generally, the first pulse is called the reference pulse and the second pulse the data pulse and data can be transmitted by changing the polarity of the second pulse.

Autocorrelation receivers (AcRs), in combination with transmitted-reference (TR) signaling [10, 29, 13], have the big advantage of capturing energy from all multipath components at low receiver complexity. The drawback of an AcR is the performance loss due to its nonlinear nature, which leads to cross-products between any signals at the receiver input (including the desired pulse sequence, noise, multiple access interference, narrowband interference, etc.). Recently, it has been shown that ISI leads to non-linear equivalent system models having a second-order Volterra structure [15, 22]. This result has been generalized to a multiuser system in [1].

We consider multiuser systems whose equivalent system model is a multiple-input multiple-output (MIMO) model. The multiple input signals are the transmitted signals of multiple users. The outputs are samples of various AcR channels with different correlation lags and also fractionally-spaced samples of these AcRs. Parallel second order Volterra systems accurately model such discrete-time MU MIMO channels [1]. This model is nonlinear, i.e., an output signal in a multiuser case is not equal to the sum of the output signals due to each individual user.

Knowledge of the exact system structure allows the derivation of detectors for the back-end of the receiver, processing the parallel output sample streams. We will formulate a minimum-mean-square-error (MMSE) detector, a maximum-likelihood (ML) detector and a maximum likelihood sequence detector (MLSD) [30], assuming AWGN and introducing decision feedback (DF) for complexity reduction. In memoryless multiple access channels, a conventional, memoryless ML detector can be used [31, 32].

The model is used to compare various multiple access schemes. A novel scheme is proposed for MU communications up to medium data rates (symbol period greater or equal to the channel excess delay), which transmits data encoded in short bursts of UWB pulses. Since a memoryless equivalent system model holds for this scheme, a memoryless MU detector is sufficient. But even a conventional threshold detector yields improved performance, since fatal collisions between pulse bursts are reduced due to the low duty-cycle of the signals. Furthermore, the implementation of the AcR frontend is simplified due to the shortened correlation lags. In [33], this scheme has been shown to yield efficient suppression of narrowband interference as well.

The chapter is organized as follows. In Section 2.2, the mathematical models of the TR signals and AcRs are introduced, including the description of the multiple access schemes. The detection algorithms are described in Section 2.3. In Section 2.4, performance results are discussed and conclusions are summarized in Section 2.5.

2.2 System Model

First of all, mathematical descriptions of the investigated delay-hopped transmitted-reference UWB systems are introduced for the case of multiple transmitting users. These models can represent various signaling schemes, including the original delay-hopped TR scheme of [10]. We also introduce three different multiple-access schemes.

2.2.1 Multiple Access Schemes

Impulse radio is a fast hopping system, which means that there are N_p impulses transmitted per symbol. Each data symbol $d_i^{(k)} \in \mathbb{B} = \{\pm 1\}$ is transmitted via N_p consecutive pulses/frame by modulating the pulse amplitudes $\{a_{i,l}^{(k)}\} \in \mathbb{B}$, where i is the symbol index, k indicates the user or transmit antenna, and l is the pulse index within a symbol, $l = 0, 1, ..., N_\mathrm{p} - 1$.

In Fig. 2.1, three different transmitted-reference schemes are illustrated for multiple access. User indices have been omitted in this figure. The method described by Hoctor and Tomlinson in [10], here called HT-scheme, encodes symbols in chips, each consisting of N_fpc pulse pairs or frames (see Fig 2.1(a)). Pulse pairs within a chip are spaced by the same delays $\{\check{D}_{l'}\}$ and modulated by the chip code $\{\check{b}_{l'}\}$ and data, for $l' = 0, 1, ..., N_\mathrm{chips} - 1$, which can be expressed in the above introduced notation by the code sequences $\{b_l^{(k)}\}_{l=0}^{N_\mathrm{p}-1}$ and $\{c_l^{(k)}\}_{l=0}^{N_\mathrm{p}-1}$, with $N_\mathrm{p} = 2N_\mathrm{fpc}N_\mathrm{chips}$. At the receiver, $N_\mathrm{cr} = N_\mathrm{chips}$ correlators are employed, matched to the delays $\{\check{D}_{l'}\}$.

Inherently more robust and preferable for high-rate transmission is the technique depicted in Fig 2.1(b), because each pulse is re-used as a data pulse as well as a reference pulse [22]. This scheme is referred to as the frame-differential scheme (FD-scheme). It requires a bank of $N_\mathrm{cr} = N_\mathrm{p}$ correlators at the receiver, assuming that each pair of pulses in a symbol is spaced differently.

A small modification to the previous scheme is much better suited for random multiple access, — however, at reduced data rates (see Fig 2.1(c)). One pulse is added per data symbol, i.e., $N_\mathrm{p} = N_\mathrm{cr} + 1$, comprising a so-called pulse-burst. Several pulse-bursts are separated by an idle period that is typically much longer than the burst duration. This makes a low-duty-cycle signal, which has the advantage that fatal collisions among bursts of several users are often avoided. This scheme is called low-duty-cycle (LDC) frame-differential scheme, in short LDC-scheme.
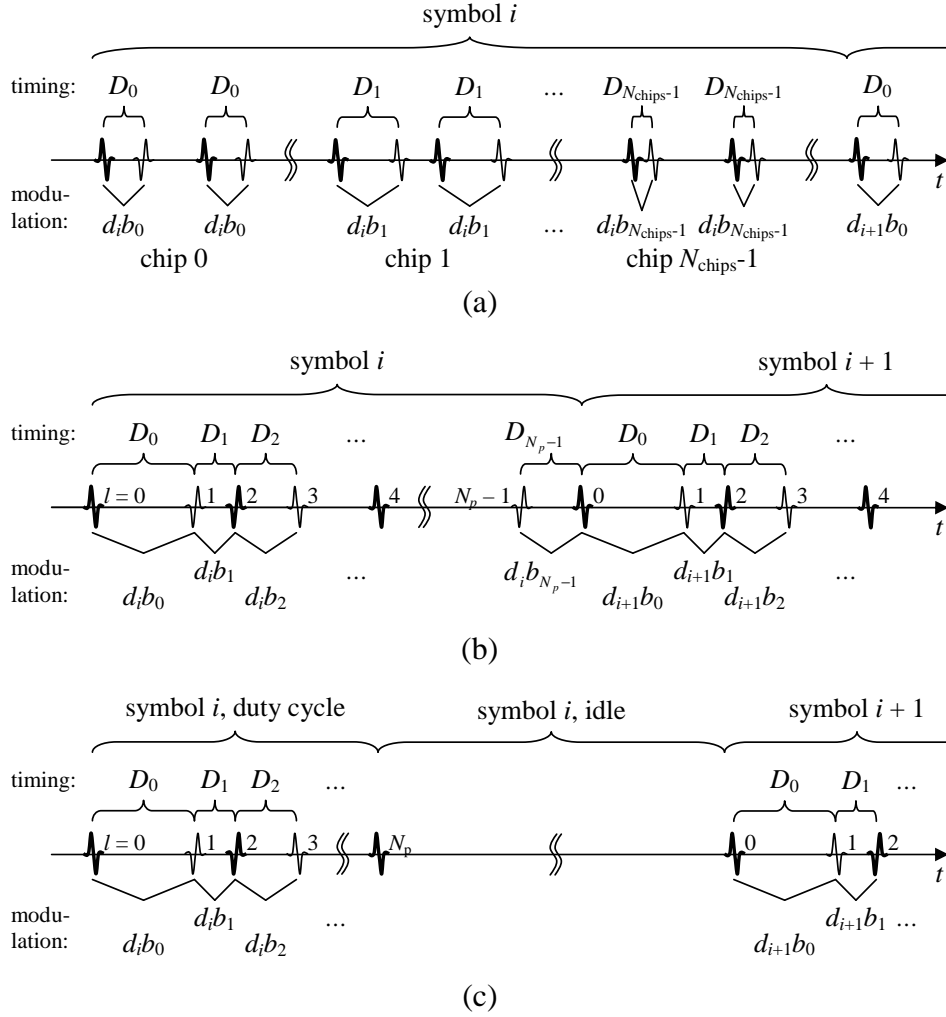
Figure 2.1: Transmitted pulse streams for various differential UWB schemes. Bold-face pulses are unmodulated reference pulses. (a): Hoctor and Tomlinson (HT) transmitted-reference scheme; (b): Frame-differential (FD) scheme; (c): Burst oriented low-duty-cycle (LDC) frame-differential scheme.

2.2.2 Frame-differential (FD) scheme

We defined the pulse stream of "user" k as

$$s^{(k)}(t) = \sum_{i=-\infty}^{\infty} \sum_{l=0}^{N_\mathrm{p}-1} a_{i,l}^{(k)} w(t - t_{i,l}^{(k)}), \qquad (2.1)$$

with $w(t)$ being the transmitted pulse shape and $\{t_{i,l}^{(k)}\}$ are the pulse timings.

Data are modulated differentially, superimposing an amplitude code $\{b_l^{(k)}\} \in \mathbb{B}$. Data and reference pulses are distinguished by the sequence $\{s_l\} \in \{0, 1\}$, see (2.2). Relative to the first pulse of each symbol, we define the pulse polarities as

$$a_{i,l}^{(k)} = a_{i,0}^{(k)} \overline{b}_l^{(k)} \begin{cases} d_i^{(k)} & s_l = 1 \\ 1 & s_l = 0 \end{cases} \qquad (2.2)$$

$$a_{i+1,0}^{(k)} \equiv a_{i,N_\mathrm{p}}^{(k)} = a_{i,0}^{(k)} \overline{b}_{N_\mathrm{p}}^{(k)}, \qquad (2.3)$$

where $\overline{b}_{i,l}^{(k)} = \prod_{\mu=0}^{l-1} b_{i,l}^{(k)}$ and $\{b_{i,l}^{(k)}\}$ refers to the differential amplitude code between pulses l and $l + 1$. This notation demands that pulse $l = 0$ is *not* data modulated, i.e., $s_0 = 0$.

The time instants of the pulses are defined as $t_{i,l}^{(k)} = iT_\mathrm{sym} + c_l^{(k)}$, where T_sym is the symbol-duration (assumed equal for all users k) and $\{c_l^{(k)}\}$ is the relative pulse timing within a symbol in seconds, representing time-hopping codes, average spacing between two pulses, and time offsets between users. Note that fixed codes $\{b_l^{(k)}\}$, $\{c_l^{(k)}\}$, and $\{s_l\}$ are used throughout. Since the receiver front-end is matched to the delays between pulse pairs, it is worthwhile defining the delay-hopping code $D_l^{(k)} = c_{l+1}^{(k)} - c_l^{(k)}$.

Time-hopping (TH) impulse radio (IR) is among the most developed UWB prototype systems. The time-hopping pattern is a way of spreading the signal spectrum. It also adds security with low probability of detection or interception. This is due to the fact that each user has its own time-hopping pattern that looks random to all other users, except for the receiver of interest. With ideal propagation conditions, ultra wideband radio promises a great multiple access capacity.

2.2.3 Channel Model

The channel model considered in this dissertation is a dispersive multipath radio channel. A detailed derivation of the underlying channel model is given in [34].

Due to multipath propagation, multiple copies of the originally transmitted pulse arrive at the receiver antenna. If the delay D between two pulses is smaller than

(a)

(b)
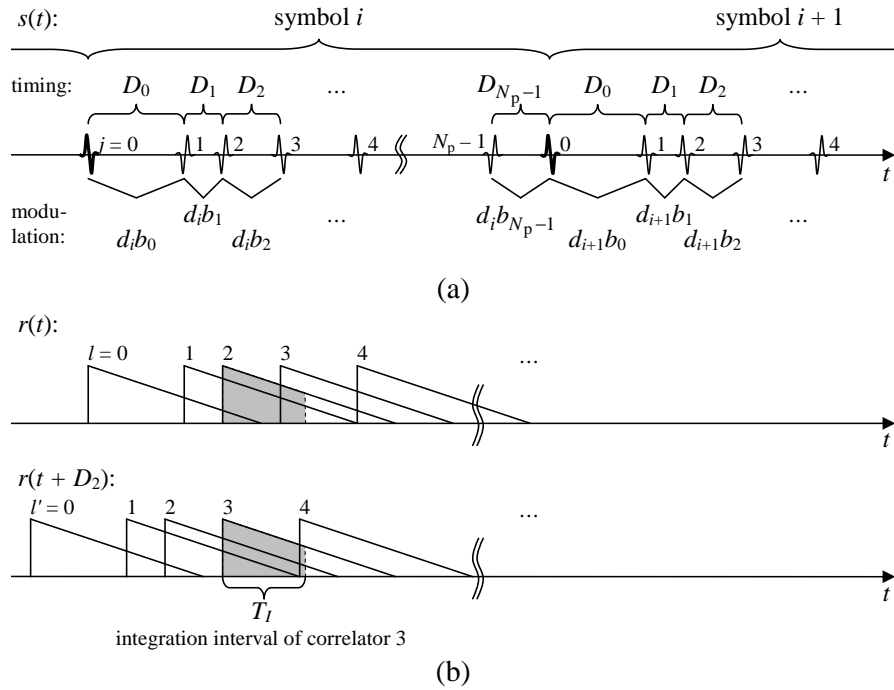
Figure 2.2: Transmitted and received signal in the frame-differential IR-UWB system.

the time until the last multipath component arrives, then these components lead to a distorted correlator output. See, Fig. 2.2(a) for a sketch of the received signal illustrating the multipath propagation leading to inter-frame interference (IFI). By increasing the data rate, which is equivalent to reducing the average frame duration T_f, ISI is created, which means that whole symbols interfere with others.

Throughout this dissertation, the time variance of the channel is assumed to be relatively slow compared to the symbol duration , implying a quasi-stationary system model.

The impulse response of the stochastic channel is modeled as a sum of delta pulses,

$$h(t) = \sum_{l=0}^{\infty} \alpha_l \delta(t - \tau_l) \tag{2.4}$$

where α_l are independent zero mean random variables. Only α_0 has no zero mean accounting for a dominant line-of-sight (LOS) path. τ_l are ray-arrival times, where τ_0 is the arrival time of the first multipath component.

For the characterization of the channel, which is assumed to be time invariant, its delay power spectrum (or average poser delay profile) is used and given by

$$P_h(t) = E\{h^2(t)\} = E\{\sum_{l=0}^{\infty} \alpha_l^2 \delta(t - \tau_l)\} \tag{2.5}$$

Two other characterization parameters are called multipath power gain

$$P_\alpha = \sum_l \alpha_l^2 \tag{2.6}$$

and RMS delay spread

$$\tau_{\mathrm{rms}} = \sqrt{\overline{\tau^2} - (\overline{\tau})^2} \tag{2.7}$$

where

$$\overline{\tau^n} = \frac{\int_{-\infty}^{\infty} \tau^n P_h(t)\ d\tau}{\int_{-\infty}^{\infty} P_h(t)\ d\tau} \tag{2.8}$$

2.2.4 Receiver Front-End

In Fig. 2.3, a bank of N_{cr} correlators is present at the input of the receiver, whose lags D_j are matched to the time shifts between pulse pairs $\{D_l^{(k)}\}$. The integrate-and-dump blocks are triggered at the arrival-times of the respective pulses $\{t_{i,l}^{(k)}\}$. We denote parameters of the receiver using the tilde ˜, and assume that the front-end is matched to user $k = 1$. The correlator outputs are sampled N_{fs} times per

symbol, at a rate defined by the integration interval T_{I}. Indexing the correlators by $j = 0, 1, ..., N_{\mathrm{cr}} - 1$ and the samples within a symbol by $n = 0, 1, ..., N_{\mathrm{fs}} - 1$, we can write the output samples as

$$y_{j,n}[i] = \int_{\tilde{t}_{i,j,n}}^{\tilde{t}_{i,j,n+1}} r(t)r(t + \widetilde{D}_j) \, dt. \tag{2.9}$$

The integration start times are written as $\tilde{t}_{i,j,n} = \tilde{c}_j + iT_{\mathrm{sym}} + nT_{\mathrm{I}}$. Normally the time offsets $\tilde{c}_j$ are matched to the arrival times of the transmitted pulse-pairs spaced by the desired lags $\widetilde{D}_j$. For instance, $\tilde{c}_j = c_l^{(1)}$ and $\widetilde{D}_j = c_{l+1}^{(1)} - c_l^{(1)}$, if correlator j is used to demodulate the pulse pair l and $l + 1$.

The received signal in (2.9) is defined by

$$r(t) = \sum_{k=1}^{K} \sum_{i=-\infty}^{\infty} \sum_{l=0}^{N_{\mathrm{p}}-1} a_{i,l}^{(k)} g^{(k)}(t - t_{i,l}^{(k)}) + \nu(t), \tag{2.10}$$

where $g^{(k)}(t) = h^{(k)}(t) * w(t)$ is the response of the channel to a transmitted monocycle from user k and $\nu(t)$ is an additive noise process. The amplitude gain of channel k is incorporated in $g^{(k)}(t)$. We will use the constant $\eta = \lceil \tau_{\mathrm{max}}/T_{\mathrm{sym}} \rceil$ to specify the number of past symbols interfering on the current one, where we assume that the support of any $g^{(k)}(t) \in [0, \tau_{\mathrm{max}}]$. The excess delay of the channel impulse response is denoted as τ_{max}.

2.2.5 Discrete-Time Equivalent System Model

The equivalent system model relates the data streams of all users $\{d_i^{(k)}\}$, $\forall k \in \mathbb{K} = \{1, 2, ..., K\}$, to the sampled receiver output $y_{j,n}[i]$. For the single-channel, single-user, symbol-spaced case, such a model has been derived in [22]. In [1] it has been extended to the multiuser case.

It has been shown that the correlator output can be written as a second-order Volterra model of the input data,

$$\begin{aligned}
y_{j,n}[i] = h_{0,j,n} &+ \mathbf{h}_{1,j,n}^T \mathbf{d}[i] \\
&+ \mathbf{d}^T[i] \mathbf{H}_{2,j,n} \mathbf{d}[i] + \nu_{j,n}[i].
\end{aligned} \tag{2.11}$$

The vector $\mathbf{d}[i]$ is a stacked version of each user's data up to a finite memory depth η plus the current and one consecutive symbol. I.e., $\mathbf{d}[i] = [\mathbf{d}^{(1)}[i], \mathbf{d}^{(2)}[i], \cdots, \mathbf{d}^{(K)}[i]]^T$ with $\mathbf{d}^{(k)}[i] = [d^{(k)}[i - \eta], d^{(k)}[i - \eta + 1], \cdots, d^{(k)}[i + 1]]$. Three components comprise the Volterra model describing the data dependence of each of the samples $y_{j,n}[i]$ — a bias $h_{0,j,n}$, a linear transversal FIR component expressed by the vector product
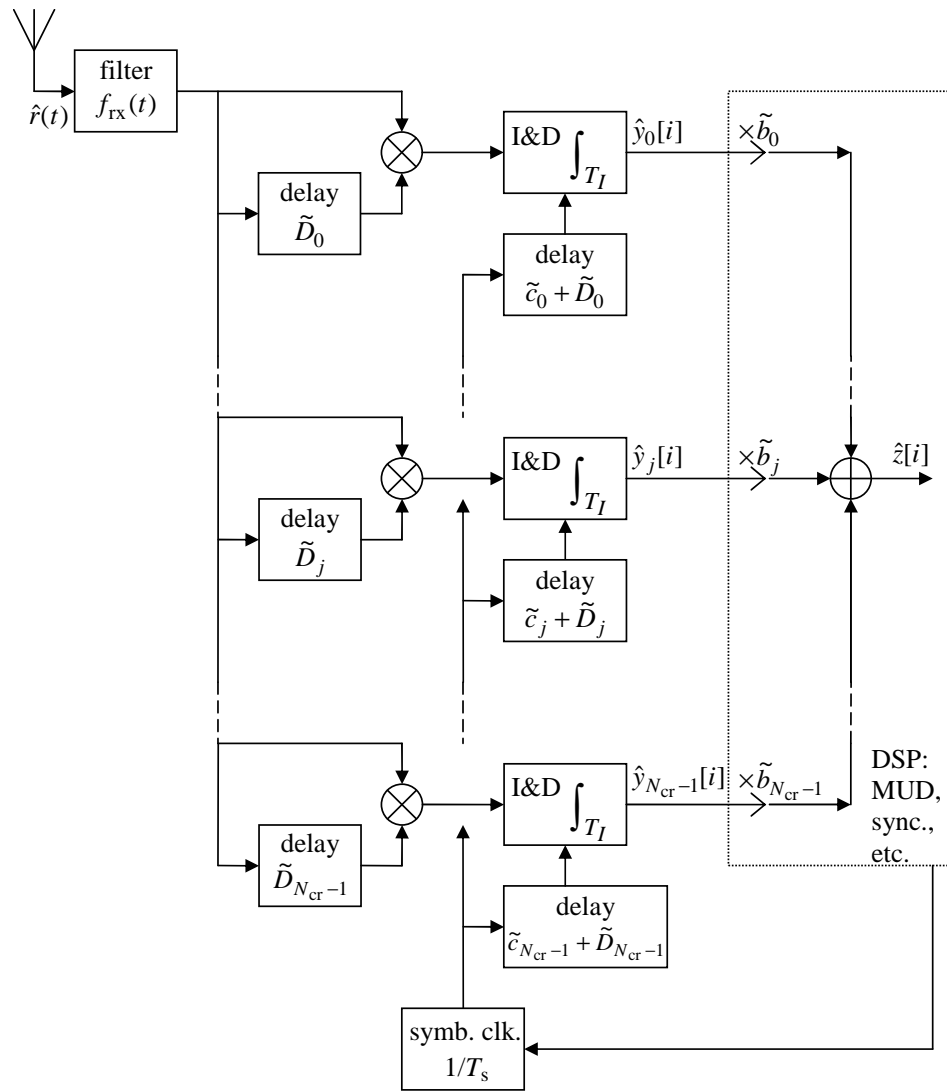
Figure 2.3: Receiver Front-End.

$\mathbf{h}_{1,j,n}^T \mathbf{d}[i]$, and quadratic terms involving products of data symbols, $\mathbf{d}^T[i]\mathbf{H}_{2,j,n}\mathbf{d}[i]$. The bias term is due to interference among reference pulses or among *equally* data modulated pulses. Product coefficients are caused by interference of data pulses of different symbols, i.e., interference between symbols of multiple users and multiple symbols in time.

We re-write the MU-MIMO data model for a length $N_{\mathrm{rx}} = N_{\mathrm{fs}}N_{\mathrm{cr}}$ vector $\mathbf{y}[i]$ stacking the output samples $y_{j,n}[i]$ as

$$\begin{aligned}
\mathbf{y}[i] &= \mathbf{h}_0 + \mathbf{H}_1^T \mathbf{d}[i] + \mathbf{H}_2^T(\mathbf{d}[i] \,\widetilde{\otimes}\, \mathbf{d}[i]) + \mathbf{y}_\nu[i] \\
&= [\mathbf{h}_0\ \mathbf{H}_1^T\ \mathbf{H}_2^T] \begin{bmatrix} 1 \\ \mathbf{d}[i] \\ \mathbf{d}[i] \,\widetilde{\otimes}\, \mathbf{d}[i] \end{bmatrix} + \mathbf{y}_\nu[i] \qquad (2.12) \\
&= \mathbf{H}^T \widetilde{\mathbf{d}}[i] + \mathbf{y}_\nu[i],
\end{aligned}$$

where $\widetilde{\otimes}$ is a reduced version of the Kronecker product for binary vectors, omitting all redundant duplicate products and trivial squares. The vector $\mathbf{h}_0$ contains the bias terms $h_{0,j,n}$ of all channels, the column vectors of $\mathbf{H}_1$ contain the linear coefficients $\mathbf{h}_{1,j,n}$, and the product kernels $\mathbf{H}_{2,j,n}$ are re-arranged into $\mathbf{H_2}$. Matrix $\mathbf{H}$ collects all model coefficients. The vector $\mathbf{y}_\nu$ is a vector of zero-mean noise samples, which are generally correlated and non-stationary. It is well approximated by a white Gaussian process, which will be used in this chapter.

2.3 Data Detection

After devising the equivalent system model of the UWB schemes under investigation, we will next apply this knowledge about the system structure in order to develop data detection algorithms.

2.3.1 Conventional Threshold Detector

A conventional threshold detector combines the samples in $\mathbf{y}[i]$ by de-spreading the amplitude code. I.e., it computes a combined decision variable

$$z[i] = \widetilde{\mathbf{b}}^T \mathbf{y}[i]$$

and performs detection against some threshold γ by

$$d[i] = \mathrm{sign}\{z[i] - \gamma\}. \qquad (2.13)$$

For the de-spreading combiner, the elements of $\widetilde{\mathbf{b}}$ are $\tilde{b}_{j,n} = b_l^{(1)}$, for correlator j being matched to the pulses l and $l+1$ of user $k = 1$. So we also have $\widetilde{D}_j = c_{i,l+1}^{(1)} - c_{i,l}^{(1)}$.

The bias term of the Volterra data model is a logical choice for the decision threshold, $\gamma = \widetilde{\mathbf{b}}^T \mathbf{h}_0$. But it is not exactly optimal due to the non-stationarity of the additive noise process. Nevertheless, we will choose the bias term as a decision threshold, since we neglect the exact noise model throughout this section.

2.3.2 MMSE Detector

The minimum-mean-square-error (MMSE) algorithm tries to minimize the variance of the error σ_e^2 which is the difference between the desired bit and the linearly combined data vector $\mathbf{w}^T \mathbf{y}[i]$, where $\mathbf{w}$ is the linear combiner to be optimized. The linear operator can be viewed as a multiuser detector that operates on the output of the AcR.

We consider data are uncorrelated with variance $\sigma_d^2 = 1$. It is easily shown that also the products of data symbols are then uncorrelated, and $\sigma_d^2 = \sigma_d^4 = 1$. Furthermore, $d^{(1)}[i] = \mathbf{e}_1^T \widetilde{\mathbf{d}}[i]$ where $\mathbf{e}_1$, that can be expressed as $[0, \cdots, 0, 1, 0, \cdots, 0]$ is tuned to the desired bit of user one. Without loss of generality, we can drop the index i in this calculation. The variance of the error σ_e^2 for user one is thus written as

$$\sigma_e^2 = \mathsf{E}\{(d^{(1)} - \mathbf{w}^T(\mathbf{H}^T \widetilde{\mathbf{d}} + \mathbf{y}_\nu))^2\}, \tag{2.14}$$

Expanding this equation we obtain

$$\sigma_e^2 = \mathbf{e}_1^T \mathbf{e}_1 + \mathbf{w}^T \mathbf{H}^T \mathbf{H} \mathbf{w} - 2\mathbf{e}_1^T \mathbf{w} \mathbf{H}^T + \mathbf{w}^T \mathbf{w} \sigma_\nu^2. \tag{2.15}$$

Then we equate the derivative with respect to $\mathbf{w}$ to zero

$$\frac{\partial \sigma_e^2}{\partial \mathbf{w}} = 2(\mathbf{H}^T \mathbf{H} + \sigma_\nu^2 \mathbf{I})\mathbf{w} - 2\mathbf{e}_1^T \mathbf{H}^T = 0. \tag{2.16}$$

Therefore the solution is

$$\mathbf{w} = (\mathbf{H}^T \mathbf{H} + \sigma_\nu^2 \mathbf{I})^{-1} \mathbf{e}_1^T \mathbf{H}^T. \tag{2.17}$$

We note that $\mathbf{H}^T \mathsf{E}\{\widetilde{\mathbf{d}} d^{(1)}\} = \mathbf{H}^T \mathbf{e}_1 = \mathbf{h}_1^{(1)}$ is a column vector containing the linear model coefficients of the desired bit of user one. Appropriate synchronization has been assumed. So we can re-write the combiner

$$\mathbf{w} = (\mathbf{H}^T \mathbf{H} + \sigma_\nu^2 \mathbf{I})^{-1} (\mathbf{h}^{(1)})^T. \tag{2.18}$$

2.3.3 Maximum Likelihood Sequence Detector

Using the principle of maximum likelihood sequence detection (MLSD), optimum detectors can be derived for signals affected by ISI. Knowledge about the Volterra system structure can be incorporated, see [35] and the references therein, which presents such a detector in the context of differential UWB systems. The MLSD is also applicable for MIMO channels [30, 32].

The Viterbi algorithm is used to jointly detect the symbol sequences $\{d_i^{(k)}\}$ of all users. At a memory depth of $\eta + 1$, this results in a trellis of $2^{(\eta+1)K}$ states, with 2^K possible transitions per state, since K bits are taken into consideration at each time-step. Using the i.i.d. AWGN assumption for the noise vector $\mathbf{y}_\nu[i]$, the branch metrics from state $\mathbf{q}_1[i] = [d_{i-\eta}^{(1)}, d_{i-\eta+1}^{(1)}, \ldots, d_i^{(K)}]^T$ to state $\mathbf{q}_2[i] = [d_{i-\eta+1}^{(1)}, d_{i-\eta+2}^{(1)}, \ldots, d_{i+1}^{(K)}]^T$ are given by

$$m_{\mathrm{mlsd}}(\mathbf{q}_1[i], \mathbf{q}_2[i]) = \|\mathbf{y}[i] - \mathbf{h}_0 - \mathbf{H}_1^T \mathbf{d}[i] - \mathbf{H}_2^T (\mathbf{d}[i] \widetilde{\otimes} \mathbf{d}[i])\|^2,$$

where $\mathbf{d}[i] = [d_{i-\eta}^{(1)}, d_{i-\eta+1}^{(1)}, \ldots, d_{i+1}^{(K)}]^T$.

To reduce the complexity of the above MLSD, an MLSD with DF has been presented in [36]. This detector applies the Viterbi algorithm to a reduced-state trellis with only $2^{(\eta-L+1)K}$ states $(1 \leq L \leq \eta)$. For this reduced-state trellis, the branch metric from state $\mathbf{q}_1[i] = [d_{i-\eta+L}^{(1)}, d_{i-\eta+L+1}^{(1)}, \ldots, d_i^{(K)}]^T$ to state $\mathbf{q}_2[i] = [d_{i-\eta+L+1}^{(1)}, d_{i-\eta+L+2}^{(1)}, \ldots, d_{i+1}^{(K)}]^T$ is given by

$$m_{\mathrm{df}}(\mathbf{q}_1[i], \mathbf{q}_2[i]) = \|\mathbf{y}[i] - \mathbf{h}_0 - \mathbf{H}_1^T \hat{\mathbf{d}}[i] - \mathbf{H}_2^T (\hat{\mathbf{d}}[i] \widetilde{\otimes} \hat{\mathbf{d}}[i])\|^2,$$

where $\hat{\mathbf{d}}[i] = [\hat{\mathbf{d}}^{(1)^T}(\mathbf{q}_1[i]), d_{i-\eta+L}^{(1)}, d_{i-\eta+L+1}^{(1)}, \ldots, d_{i+1}^{(K)}]^T$, with $\hat{\mathbf{d}}^{(k)}(\mathbf{q}_1[i])$ denoting the $L \times 1$ vector of feedback decisions for user k, which depends on the state $\mathbf{q}_1[i]$ and is determined by the path histories.

2.3.4 ML Detection for Memoryless MIMO Channels

The complexity of a multiuser detector can be further reduced if only a single symbol of each user interferes at a time, as in the synchronous case in CDMA systems. This requires lower data rates, as ISI will prohibit such assumptions. Note that the validity of this approach can be taken for granted in the burst-oriented LDC-scheme proposed in Section 2.2.1, under the condition that the sum of burst duration, integration interval, and channel impulse response duration does not exceed the symbol duration, $c_{N_{\mathrm{p}}-1}^{(k)} - c_0^{(k)} + T_{\mathrm{I}} + \tau_{\max} \leq T_{\mathrm{sym}}, \forall k$.

A joint ML detector selects the data vector $\mathbf{d} = [d^{(1)}, d^{(2)}, ..., d^{(K)}]^T$, now consisting of a single bit per user, to maximize the likelihood function $f(\mathbf{y}[i]|\mathbf{d})$ [32, 31]. For a multiple-output system, this is a joint Gaussian PDF in the elements of $\mathbf{y}[i]$, as

demonstrated by the MIMO signal model (4.15). If we again make the simplifying assumption that the components of the additive noise vector are i.i.d. Gaussian, then maximizing $f(\mathbf{y}[i]|\mathbf{d})$ is equivalent to minimizing the Euclidean distance

$$\hat{\mathbf{d}}[i] = \arg\min_{\mathbf{d}} \|\mathbf{y}[i] - \mathbf{h}_0 - \mathbf{H}_1^T\mathbf{d} - \mathbf{H}_2^T(\mathbf{d}\widetilde{\otimes}\mathbf{d})\|^2.$$

2.4 Multiuser Results

The multiple access performance of the various transmission schemes introduced in Section 2.2.1 is studied in this section, applying the detectors derived in Section 2.3.

The following common system parameters are selected in all cases in order to obtain comparable results. The data rate has been set to 10 Mbit/s ($T_{\mathrm{sym}} = 100$ ns), accomodating $N_{\mathrm{p}} = 8$ pulses per symbol, with exception of the LDC-scheme, where $N_{\mathrm{p}} = 9$ pps. An integration interval of $T_{\mathrm{I}} = 20$ ns has been used. All schemes employ fixed sets of eight different pulse pair delays $\{D_l^{(k)}\}$ for all users, quantized in steps of 0.2 ns. However, the mean delays are different, 12.5 ns for the FD-scheme, and 2 ns for the LDC-scheme.

Furthermore, the amplitude gains of all users were set equal to one. A non line-of-sight channel has been simulated, with an exponentially decaying power delay profile (PDP) at an RMS delay spread of $\tau_{\mathrm{rms}} = 10$ ns [24]. The channel simulator produces random ray arrival times corresponding to a Poisson process, with a mean arrival rate of $\lambda = 5$ rays per ns. The ray-amplitudes are Rayleigh distributed with random signs. A second-derivative Gaussian monocycle with $\tau_m = 0.29$ ns, $w(t) = [1 - 4\pi(t/\tau_m)^2]\exp[-2\pi(t/\tau_m)^2]$, has been convolved with the such generated channel impulse responses, yielding $g^{(k)}(t)$.

2.4.1 Memoryless Multiuser Detection

Let us verify if the memoryless MIMO system model holds for the LDC-scheme, for asynchronous transmit signals. Subtracting the integration period from the idle period of the signal, we obtain the maximum allowable excess delay of the multipath channel, $\tau_{\mathrm{max}} \leq T_{\mathrm{sym}} - (c_{N_{\mathrm{p}}-1}^{(k)} - c_0^{(k)}) - N_{\mathrm{fs}}T_{\mathrm{I}} = 64$ ns, using the inequality discussed in Section 2.3.4. This is a delay, where the average power delay profile of an NLOS channel with $\tau_{\mathrm{rms}} = 10$ ns has already decayed to negligible values. The memoryless system model does not apply for the FD-scheme in the asynchronous case, since generally two symbols of each interfering user will disturb the desired symbol (*cf.* [37, 32]). To apply the memoryless ML detector, the interfering symbol with the maximum linear model coefficient has been selected for each user, obviously yielding a sub-optimal detector.
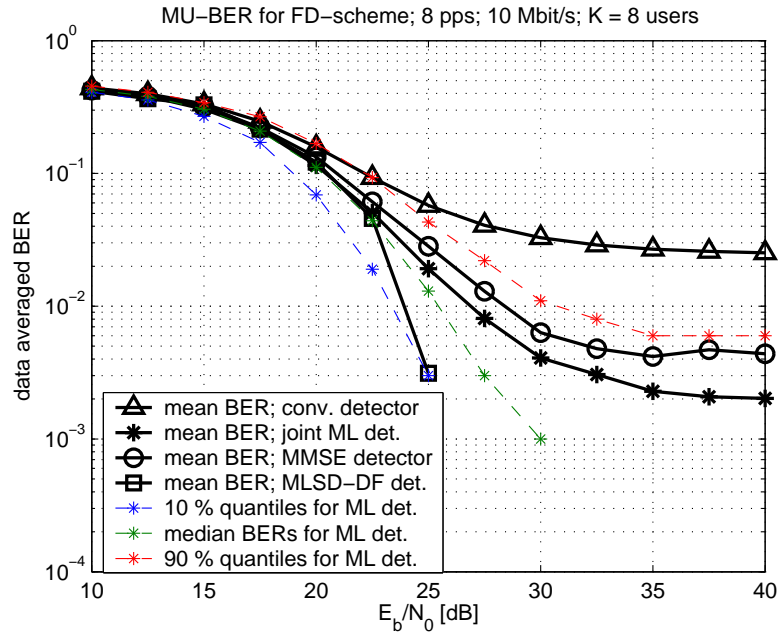
(a)
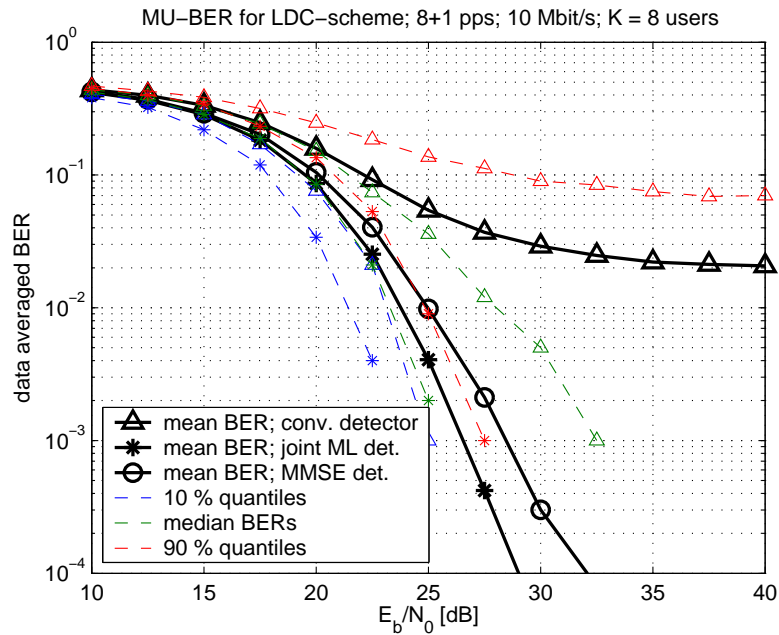
(b)

Figure 2.4: BER performance for eight users at 10 Mbit/s, comparing the conventional detector to the joint ML detector processing two samples of eight AcR channels. (a): Frame-differential scheme (FD-scheme); (b): Low-duty-cycle frame-differential scheme transmitting pulse bursts (LDC-scheme).

In the performance results given in Fig. 2.4, the MMSE detector, MLSD-DF detector and joint ML detector have been applied to a $K = 8$ input and $N_{\mathrm{rx}} = 16$ output MIMO system, namely the $K = 8$ users, $N_{\mathrm{cr}} = 8$ AcR channels, and $N_{\mathrm{fs}} = 2$ samples per symbol spaced by $T_{\mathrm{I}} = 10$ ns. For comparison, we also depict the mean performance results and quantiles for the conventional detector. Large gains are achieved for both schemes. In particular for the LDC-scheme, see Fig. 2.4(b), the error floor of the mean BER has been removed and the range between 10 and 90 % quantiles was reduced to acceptable 3.5 dB at a BER of one percent. For the FD-scheme, the sub-optimality of the detector is evident in irreducible error floors. Only a small penalty is evident for the MMSE detector w.r.t. the ML detector. For the FD scheme it was also attempted to simulate performance results for the MLSD-DF that should be capable of removing the error floor. However only a small number of channels have been simulated for this detector, thus the results are not very accurate. Nevertheless, they do indicate the expected trend.

2.5 Summary

Delay-hopped transmitted-reference systems are studied, which transmit data differentially encoded among pairs of UWB pulses. At the receiver, so-called autocorrelation receiver (AcR) front-ends are employed with correlation lags matched to the spacing of the pulse pairs. We consider data transmission at medium bit-rates (10 Mbit/s) over multipath channels typical for non-line-of-sight indoor scenarios ($\tau_{\mathrm{rms}} = 10$ ns), giving rise to severe MAI. Based on the discrete-time MIMO second-order Volterra equivalent system model of such multiuser systems, several detection schemes have been dervied.

A comparison of various multiple access schemes has been presented. Simulation results show that a frame-differential scheme achieves better performance than the classical transmitted-reference technique, by re-using each pulse as a data and as a reference pulse. We also introduce a novel multiple access scheme, which transmits each data symbol as a short burst of pulses. This method, having some penalty in the single user case due to increased inter-frame-interference, outperforms the others in multiuser scenarios, as collisions between bursts of multiple users are often avoided in asynchronous transmissions. Moreover, its optimum detector can be a memoryless (joint) ML detector. Blind and semi-blind detection techniques will be simplified due to the memoryless data model [38]. The reduced spacing of pulse pairs simplifies the implementation of the delay lines in the AcR frontend.

3 Hybrid Matched Filter TR UWB Systems

The hybrid matched-filter (HMF) receiver for transmitted reference (TR) ultra wideband (UWB) systems suffers substantial performance degradation in presence of noise and multiple-access interference (MAI) [3, 39, 40]. In this chapter, we present multiuser detection (MUD) techniques for the HMF-TR UWB receiver, derived by introducing a multiuser equivalent system model. We modified pre-combining minimum mean-square error (MMSE) solution for the HMF-TR UWB receiver that is novel, due to the non-linear behavior of the autocorrelation operation, and it is shown to yield improved performance over multi-channel autocorrelation receiver (MC-AcR) TR UWB receivers.

Ultra-wideband (UWB) impulse radio (IR) systems use extremely short duration pulses at low power with bandwidths of up to several GHz [41, 42]. One of the advantage of UWB communication is its ability to resolve individual multipath components. Autocorrelation receivers (AcRs), in combination with transmitted-reference (TR) signaling [10, 29, 43, 13, 44, 45], have the big advantage of capturing energy from all multipath components at low receiver complexity. The other advantage is to simplify signal synchronization and to avoid channel estimation, which is a key challenge in UWB systems. The drawback of an AcR is the performance loss due to its nonlinear nature, which leads to cross-products between any signals at the receiver input (including the desired pulse sequence, noise, multiple access interference, narrowband interference [33, 46], etc.). Recently, it has been shown that inter-symbol-interference (ISI) leads to non-linear equivalent system models having a second order Volterra structure [22]. This result has been generalized to a multiuser system in [1].

Recently, the idea of a hybrid matched-filter (HMF) receiver for TR UWB has been proposed by Tufvesson *et al.* [47, 14] and has been shown to reduce the performance loss due to the noise-by-noise product terms. The HMF performs a despreading of the data and reference pulse trains before the autocorrelation operation using a linear matched filter.

The objective of this chapter is to study and optimize the HMF receiver in a multiuser (MU) scenario. We derive the equivalent system model for the HMF receiver in a similar form as presented in [22, 1]. This equivalent system model is

then used for the optimization of the combining weights in the (pre-AcR) matched filters, with the purpose of suppressing multiple access interference (MAI). MAI refers to the interference between different users due to multiple users transmitting over the same radio channel. The solution to this problem cannot use standard minimum mean-square error (MMSE) techniques, due to the non-linear behavior of the (post-combining) autocorrelation operation. We present a modified MMSE solution for this problem. To verify this solution, structural modifications are applied to the HMF front-end, which allow the employment of standard MMSE and maximum-likelihood (ML) detectors for MAI suppression. However, these structurally expanded receivers are less feasible for a hardware implementation, but they provide reliable benchmark results for the studied optimized HMF AcR. We also compare the performance to conventional, optimized multi-channel AcR (MC-AcR) receivers [1, 23], which are most feasible from a practical point of view. In fact, our derivations start with the single-user case for clarity and the extension to multiuser case can be easily computed; simulation results will also include this case [48, 49].

3.1 System Model for Single User

First of all, mathematical descriptions of the investigated HMF transmitted-reference UWB systems are introduced for the single-user case.

3.1.1 Transmitted Signal

Each data symbol $d_i \in \mathbb{B} = \{-1, +1\}$ is transmitted via N_p consecutive pulses/frames by modulating the pulse amplitudes $\{a_{i,l}\} \in \mathbb{B}$, where i is the symbol index, and l is the pulse-index within a symbol, $l = 0, 1, ..., N_\mathrm{p} - 1$. We define the transmitted pulse stream as

$$s(t) = \sum_{i=-\infty}^{\infty} \sum_{l=0}^{N_\mathrm{p}-1} a_{i,l} w(t - t_{i,l}), \tag{3.1}$$

with $w(t)$ being the transmitted pulse shape including the influence of the transmitter and receiver antennae and $\{t_{i,l}\}$ are the pulse timings.

Data are modulated differentially, superimposing a frame-level BPSK code with an amplitude code $\{b_l\} \in \mathbb{B}$. The reference and data pulses are distinguished by the sequence $\{s_l\} \in \{0, 1\}$, see (3.2). Relative to the first pulse of each symbol, we define the pulse polarities as

$$a_{i,l} \;\; = \;\; a_{i,0} \bar{b}_l \begin{cases} d_i & s_l = 1 \\ 1 & s_l = 0 \end{cases} \tag{3.2}$$

$$a_{i+1,0} \;\; \equiv \;\; a_{i,N_\mathrm{p}} = a_{i,0} \bar{b}_{N_\mathrm{p}}, \tag{3.3}$$

where $\overline{b}_l = \prod_{\mu=0}^{l-1} b_{i,\mu}$ and $b_{i,l}$ refers to the differential amplitude code between pulses l and $l+1$. This notation demands that pulse $l=0$ is *not* data modulated, i.e., $s_0 = 0$. The BPSK code $b_{i,l}$ may change from symbol to symbol, denoted by the index i. This index may be dropped if the code length $N_{\mathrm{cd}} = N_{\mathrm{p}}$. In vector notation, $\mathbf{b} = [b_0, b_1, ..., b_{N_{\mathrm{p}}-1}]^T$ and $\mathbf{s} = [0, s_1, ..., s_{N_{\mathrm{p}}-1}]^T$.

The time-instants of the pulses are defined as $t_{i,l} = iT_s + c_l$, where T_s is the constant (average) symbol-duration and $\{c_l\}$ is the relative pulse timing within a symbol in seconds, representing time-hopping codes, average spacing between two pulses, and time offsets between users. Normally, the relative pulse timings are in the interval $c_l \in [0, T_{\mathrm{sym}})$. The time-hopping codes are defined as the pseudo-random sequences that determine the locations of the pulses, which reduce the probability of catastrophic collisions between two simultaneously transmitting users. We distinguish time-hopping sequences of reference pulses $\{c_{l_{\mathbf{r}}}\}$ and data pulses $\{c_{l_{\mathbf{d}}}\}$, which are subsets of $\{c_l\}$, with indices $l_r \subset \{l|s_l = 0\}$ and $l_d \subset \{l|s_l = 1\}$. The amplitude code of reference pulses $\{b_{l_{\mathbf{r}}}\}$ and of data pulses $\{b_{l_{\mathbf{d}}}\}$ are similarly defined as subsets of $\{\overline{b}_l\}$.

3.1.2 Multiple Access Scheme

The multiple access scheme is shown in Fig 3.1 where boldface pulses are unmodulated reference pulses. This scheme refers to a small modification to the previous scheme in [22]. It is much better suited for random multiple access, — however, at reduced data rates: One pulse and a guard interval are added per data symbol comprising so-called pulse bursts. Several pulse-bursts are separated by an idle period (guard interval) that is typically much longer than the burst duration, making up a low-duty-cycle signal, which has the advantage that fatal collisions among bursts of several users are often avoided. This scheme is called low-duty-cycle (LDC) frame-differential scheme, in short LDC-scheme (see Chapter 2).

3.1.3 HMF Receiver Front-End

Fig. 3.2 illustrates the typical block diagram of the proposed receiver front-end for a HMF receiver. The proposed receiver requires an analog correlator for the TH sequences of reference and data pulses, but is otherwise easier to implement. One correlator is present at the input of the receiver, whereas banks of delays $\{\tilde{c}_{j_{\mathbf{r}}}\}$ of the reference signal and $\{\tilde{c}_{j_{\mathbf{d}}}\}$ of the data signal are matched to the time hopping (TH) [1, 25] for the reference code $\{c_{l_{\mathbf{r}}}\}$ and data code $\{c_{l_{\mathbf{d}}}\}$ respectively. We denote parameters of the receiver using the tilde $\tilde{\ }$. The proposed receiver relies on the
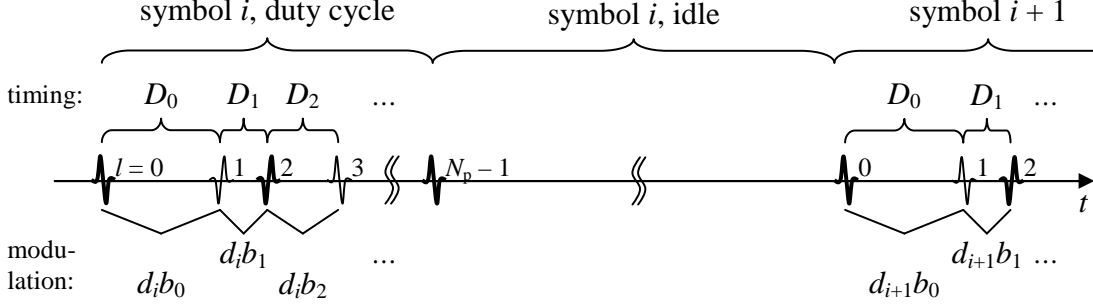
Figure 3.1: Burst oriented low-duty-cycle (LDC) frame-differential scheme.

availability of analog filters matched to the banks of delays. The key idea of this receiver is that prior to the autocorrelation operation between the reference and data signals, the proposed scheme performs a despreading. The despreading vectors are defined for the reference pulses $\{\tilde{b}_{j_{\mathbf{r}}}\} = \{b_{l_{\mathbf{r}}}\}$ and for the data pulses $\{\tilde{b}_{j_{\mathbf{d}}}\} = \{b_{l_{\mathbf{d}}}\}$. N_{ref} and N_{dat} denote the number of reference and data pulses, respectively. Thus, the SNR of the inputs to the multiplier is higher and the relative impact of the noise-noise cross terms is lower. The correlator output is sampled at the symbol rate; T_{I} is the integration interval.

$$\hat{z}[i] \;\; = \;\; \int_{\tilde{t}_i}^{\tilde{t}_i+T_I} \sum_{j_{\mathbf{r}}} \tilde{b}_{j_{\mathbf{r}}} \hat{r}(t + \tilde{c}_{j_{\mathbf{r}}}) \sum_{j_{\mathbf{d}}} \tilde{b}_{j_{\mathbf{d}}} \hat{r}(t + \tilde{c}_{j_{\mathbf{d}}}) dt \qquad (3.4)$$

where

$$\hat{r}(t) = r(t) + \nu(t) = s(t) * h(t) * f_{rx}(t) + \tilde{\nu}(t) * f_{rx}(t) \qquad (3.5)$$

is the received signal (of the desired user) with noise $\nu(t)$ and $r(t) = s(t) * h(t) * f_{rx}(t)$ is the received signal without noise. $h(t)$ denotes the impulse response of the UWB radio channel which is modeled as a sum of Dirac delta pulses $h(t) = \sum_{i=0}^{\infty} \alpha_i \delta(t - t_i)$ [22]. $f_{rx}(t)$ is the impulse response of the front-end filter of our receiver, which has to be the template pulse $w(t)$ to obtain the HMF described in [14]. $\tilde{\nu}(t)$ denotes an additive white Gaussian noise. $\nu(t)$ is a filtered noise process which is characterized by its autocorrelation function

$$R_\nu(\kappa) = E\{\nu(t)\nu(t + \kappa)\} = \frac{N_0}{2} f_{rx}(\kappa) * f_{rx}(-\kappa) \qquad (3.6)$$

where N_0 is the doubled-sided power spectral density of the white Gaussian noise process $\tilde{\nu}(t)$. The filter should be wide enough not to introduce and signal distortions and just limit the available noise. In case of an ideal, rectangular low-pass filter with cut-off frequency W, $R_\nu(\kappa)$ is given by $R_\nu(\kappa) = N_0 W \mathrm{sinc}(2W\kappa)$.

The filter is matched to the whole pulse train per one symbol. In this chapter, we assume a perfect match of integration start times and pulse timings $\tilde{t}_i = iT_s$, $\tilde{c}_{j_\mathbf{r}} = c_{j_\mathbf{r}}$, $\tilde{c}_{j_\mathbf{d}} = c_{j_\mathbf{d}}$, $\tilde{b}_{j_\mathbf{r}} = b_{j_\mathbf{r}}$ and $\tilde{b}_{j_\mathbf{d}} = b_{j_\mathbf{d}}$. For notational simplicity, we will drop the tilde ($\tilde{\ }$) in the rest of this chapter.
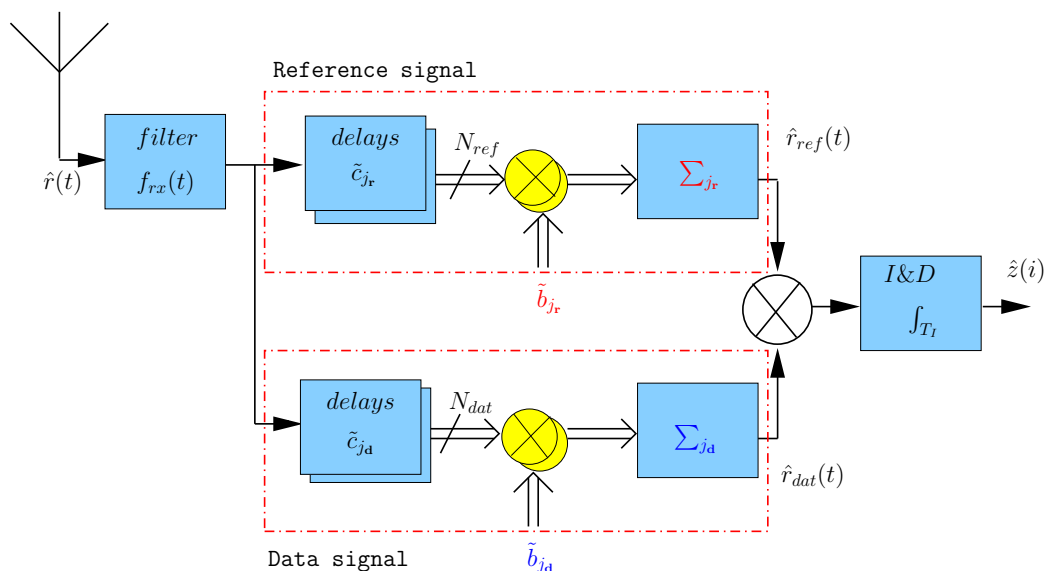
Figure 3.2: Proposed receiver front-end for the HMF differential UWB system.

3.2 Equivalent System Model for MU-HMF

In [22, 23], the detailed derivation of a non-linear equivalent system model is given, having a second-order Volterra structure. By using a similar method, the output of

the MU-HMF receiver in Fig 3.2 is analyzed. Without noise,

$$
\begin{aligned}
z[i] \;=\;& \int_{t_i^{(1)}}^{t_i^{(1)}+T_{\mathrm{I}}} \sum_{j_{\mathbf{r}}} b_{j_{\mathbf{r}}}^{(1)} \sum_{k=1}^{N_k} \sum_{l=0}^{N_{\mathrm{p}}-1} a_{i,l}^{(k)} g^{(k)}(t - t_{i,l}^{(k)} + c_{j_{\mathbf{r}}}^{(1)}) \\
& \times \sum_{j_{\mathbf{d}}} b_{j_{\mathbf{d}}}^{(1)} \sum_{k'=1}^{N_k} \sum_{l'=0}^{N_{\mathrm{p}}-1} \sum_{l'=0}^{N_{\mathrm{p}}-1} a_{i,l'}^{(k')} g^{(k')}(t - t_{i,l'}^{(k')} + c_{j_{\mathbf{d}}}^{(1)}) \, dt \\
=\;& \sum_{k=1}^{N_k} \sum_{k'=1}^{N_k} \sum_{l=0}^{N_{\mathrm{p}}-1} \sum_{l'=0}^{N_{\mathrm{p}}-1} a_{i,l}^{(k)} a_{i,l'}^{(k')} \sum_{j_{\mathbf{r}}} \sum_{j_{\mathbf{d}}} b_{j_{\mathbf{r}}}^{(1)} b_{j_{\mathbf{d}}}^{(1)} \qquad\qquad (3.7) \\
& \times \int_{t_i^{(1)}}^{t_i^{(1)}+T_{\mathrm{I}}} g^{(k)}(t - t_{i,l}^{(k)} + c_{j_{\mathbf{r}}}^{(1)}) g^{(k')}(t - t_{i,l'}^{(k')} + c_{j_{\mathbf{d}}}^{(1)}) dt
\end{aligned}
$$

where $g^{(k)}(t) = h^{(k)}(t) * w(t)$ is the response of the k-th channel to one transmitted monocycle at $t = 0$. The system of interest consists of N_k active users transmitting UWB signals simultaneously through a multipath channel, introducing the user index k. Superscript indices $^{(k)}$ denote the kth user's signal parameters. Without loss of generality, we assume that the first user ($k = 1$) is the desired one. Thus, the decision variable can be compactly defined in matrix notation as

$$
z[i] = \sum_{k=1}^{N_k} \sum_{k'=1}^{N_k} \mathbf{a}^{(k)}[i]^T \sum_{j_{\mathbf{r}}} \sum_{j_{\mathbf{d}}} b_{j_{\mathbf{r}}}^{(1)} b_{j_{\mathbf{d}}}^{(1)} \mathbf{Y}_{(k,k')}^{(j_{\mathbf{r}}, j_{\mathbf{d}})} \mathbf{a}^{(k')}[i]. \qquad (3.8)
$$

The polarities of all pulses having impact on received symbol i are represented by vectors $\mathbf{a}^{(k)}[i] = [a_{i,0}^{(k)}, a_{i,1}^{(k)}, \cdots, a_{i,N_p-1}^{(k)}]^T$. The autocorrelation integrals in (3.7) are defined by the matrix $\mathbf{Y}_{(k,k')}^{(j_{\mathbf{r}}, j_{\mathbf{d}})} = \int_{t_i^{(1)}}^{t_i^{(1)}+T_{\mathrm{I}}} g^{(k)}(t - t_{i,l}^{(k)} + c_{j_{\mathbf{r}}}^{(1)}) g^{(k')}(t - t_{i,l'}^{(k')} + c_{j_{\mathbf{d}}}^{(1)}) dt$, expressing the interference among the pulses due to multiple existing users.

The complexity of a multiuser signal model reduces if only a single symbol of each user interferes at a time, as in the synchronous case in CDMA systems. This requires lower data rates, as ISI will prohibit such assumptions. We consider the case where inter-symbol-interference (ISI) can be completely avoided by making the idle-period (plus integration interval) longer than the channel excess delay (see Chapter 2). In the multiuser case, a memoryless multiuser equivalent system model will result under this condition, as only up to one data symbol of each user will interfere within the capturing period of the desired signal—a desired property for the design of simple multiple-access-interference (MAI) suppression schemes. Therefore, a memoryless multiuser equivalent system model of single output variable $z[i]$ can be written as

[22, 1, 38]

$$z[i] = h_0 + \mathbf{h}_1^T \mathbf{d}[i] + \mathbf{h}_2^T (\mathbf{d}[i] \; \widetilde{\otimes} \; \mathbf{d}[i]) + z_\nu[i]$$

$$= [h_0 \; \mathbf{h}_1^T \; \mathbf{h}_2^T] \begin{bmatrix} 1 \\ \mathbf{d}[i] \\ \mathbf{d}[i] \; \widetilde{\otimes} \; \mathbf{d}[i] \end{bmatrix} + z_\nu[i]$$

$$= \mathbf{h}^T \begin{bmatrix} 1 \\ \mathbf{d}[i] \\ \mathbf{d}[i] \; \widetilde{\otimes} \; \mathbf{d}[i] \end{bmatrix} + z_\nu[i] \tag{3.9}$$

$$= \mathbf{h}^T \tilde{\mathbf{d}}[i] + z_\nu[i],$$

where $\mathbf{d}[i] = [d^1[i], \cdots, d^{N_k}[i]]^T$ and $\widetilde{\otimes}$ is a reduced version of the Kronecker product for binary vectors [38], omitting all redundant duplicate products and trivial squares, defined as

$$\mathbf{d} \; \widetilde{\otimes} \; \mathbf{d} = [d^{(1)}d^{(2)}, \cdots, d^{(1)}d^{(K)}, d^{(2)}d^{(3)}, \cdots, d^{(2)}d^{(K)}, d^{(3)}d^{(4)}, \cdots, d^{(K-1)}d^{(K)}] \tag{3.10}$$

The h_0 contains the bias term, the $\mathbf{h}_1$ contains the linear coefficients, and the quadratic terms are denoted as $\mathbf{h}_2$, their computation is addressed in [1]. Vector $\mathbf{h}$ collects all model coefficients. Vector $\tilde{\mathbf{d}}[i]$ collects the data vector and its cross-products [38]. The variable z_ν represents zero-mean noise samples [1].

3.3 Expanded System Model for the HMF Receiver

This section describes the construction of the expanded system model for the multi-user (MU) HMF UWB receiver. The scheme is equivalent to the proposed scheme in Section 3.2 but it will allow the application of well-known linear detection schemes. The main idea is to compute each of the corresponding correlations of the reference and data signals separately, as shown in Fig 3.3. After the delays operations follows despreading, the analog products are then integrated and coherently summed up yielding the decision variable. The number of correlators N_{cr} are equal to $N_{ref}N_{dat}$. The obtained multichannel output variable $z[i]$ in this scheme is equal to the output variable $z[i]$ in (3.9) which will be validated by simulation in Fig 3.5.

3.3.1 Expanded Receiver Front-End for HMF with Post-Combining

The receiver front-end for post-combining detection is depicted in Fig 3.4. This scheme is motivated by replacing the despreading coefficients in Fig 3.3 prior to
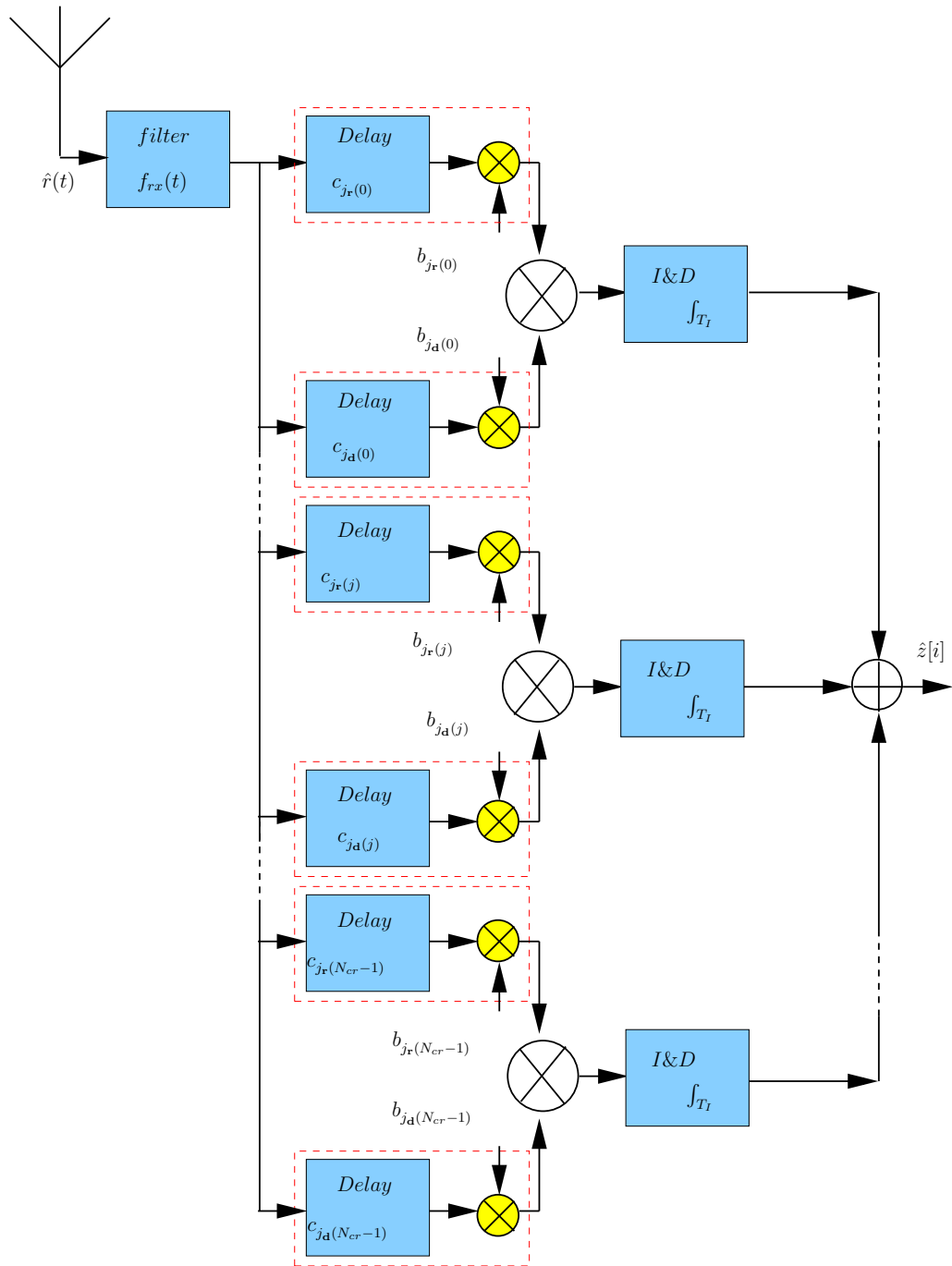
Figure 3.3: Expanded receiver front-end for the HMF receiver.

the correlators after integration as post-combining weight coefficients. The index of correlator branches is denoted as $j = \{0, 1, \ldots, N_{cr} - 1\}$ with $N_{cr} = N_{ref}N_{dat}$. The output decision variable for the MU-HMF is given as

$$
\begin{aligned}
z[i] &= \sum_{j=0}^{N_{cr}-1} \tilde{b}_j^{(1)} \int_{t_i^{(1)}}^{t_i^{(1)}+T_{\bar{I}}} \sum_{k=1}^{N_k} \sum_{l=0}^{N_{\mathrm{p}}-1} a_{i,l}^{(k)} g(t - t_{i,l}^{(k)} + c_{j_{\mathbf{r}}(j)}^{(1)}) \\
&\quad \times \sum_{k'=1}^{N_k} \sum_{l'=0}^{N_{\mathrm{p}}-1} a_{i,l'}^{(k')} g(t - t_{i,l'}^{(k')} + c_{j_{\mathbf{d}}(j)}^{(1)}) \, dt \\
&= \sum_{j=0}^{N_{cr}-1} \tilde{b}_j^{(1)} \sum_{k=1}^{N_k} \sum_{k'=1}^{N_k} \mathbf{a}^{(k)}[i]^T \mathbf{Y}_{(k,k')}^{(j_{\mathbf{r}}(j),j_{\mathbf{d}}(j))} \, \mathbf{a}^{(k)}[i] \\
&= \tilde{\mathbf{b}}^{(1)^T} \mathbf{y}[i]
\end{aligned}
\tag{3.11}
$$

where the amplitude code vector $\tilde{\mathbf{b}}^{(k)} = [(b_{j_{\mathbf{r}}(0)}^{(k)} \cdot b_{j_{\mathbf{d}}(0)}^{(k)})\ (b_{j_{\mathbf{r}}(1)}^{(k)} \cdot b_{j_{\mathbf{d}}(1)}^{(k)})\ \cdots\ (b_{j_{\mathbf{r}}(N_{cr}-1)}^{(k)} \cdot b_{j_{\mathbf{d}}(N_{cr}-1)}^{(k)})]^T$. This despreading vector is obtained from the Kronecker product of the reference and data codes. The notations $j_{\mathbf{r}}(j)$ and $j_{\mathbf{d}}(j)$ represent the mapping of index j onto $j_{\mathbf{r}}$ and $j_{\mathbf{d}}$. The vector $\mathbf{y}[i]$, stacking the output samples $y_j[i]$ for a multichannel data model with length N_{cr}, can be written as (see (3.9))

$$
\begin{aligned}
\mathbf{y}[i] &= \mathbf{h}_0 + \mathbf{H}_1^T \mathbf{d}[i] + \mathbf{H}_2^T (\mathbf{d}[i] \, \widetilde{\otimes} \, \mathbf{d}[i]) + \mathbf{y}_\nu[i] \\
&= [\mathbf{h}_0 \ \mathbf{H}_1^T \ \mathbf{H}_2^T] \begin{bmatrix} 1 \\ \mathbf{d}[i] \\ \mathbf{d}[i] \, \widetilde{\otimes} \, \mathbf{d}[i] \end{bmatrix} + \mathbf{y}_\nu[i] \\
&= \mathbf{H}^T \begin{bmatrix} 1 \\ \mathbf{d}[i] \\ \mathbf{d}[i] \, \widetilde{\otimes} \, \mathbf{d}[i] \end{bmatrix} + \mathbf{y}_\nu[i] \\
&= \mathbf{H}^T \tilde{\mathbf{d}}[i] + \mathbf{y}_\nu[i],
\end{aligned}
\tag{3.12}
$$

where the vector $\mathbf{y}_\nu[i]$ is a vector of zero-mean noise samples, which are weakly correlated and non-stationary [22, 1]. A stationary white noise model will be assumed throughout this chapter, for simplicity. The vector $\mathbf{h}_0$ contains the bias terms, the column vectors of $\mathbf{H}_1$ contain the linear coefficients, and the quadratic terms are arranged into $\mathbf{H_2}$. Matrix $\mathbf{H}$ collects all model coefficients.
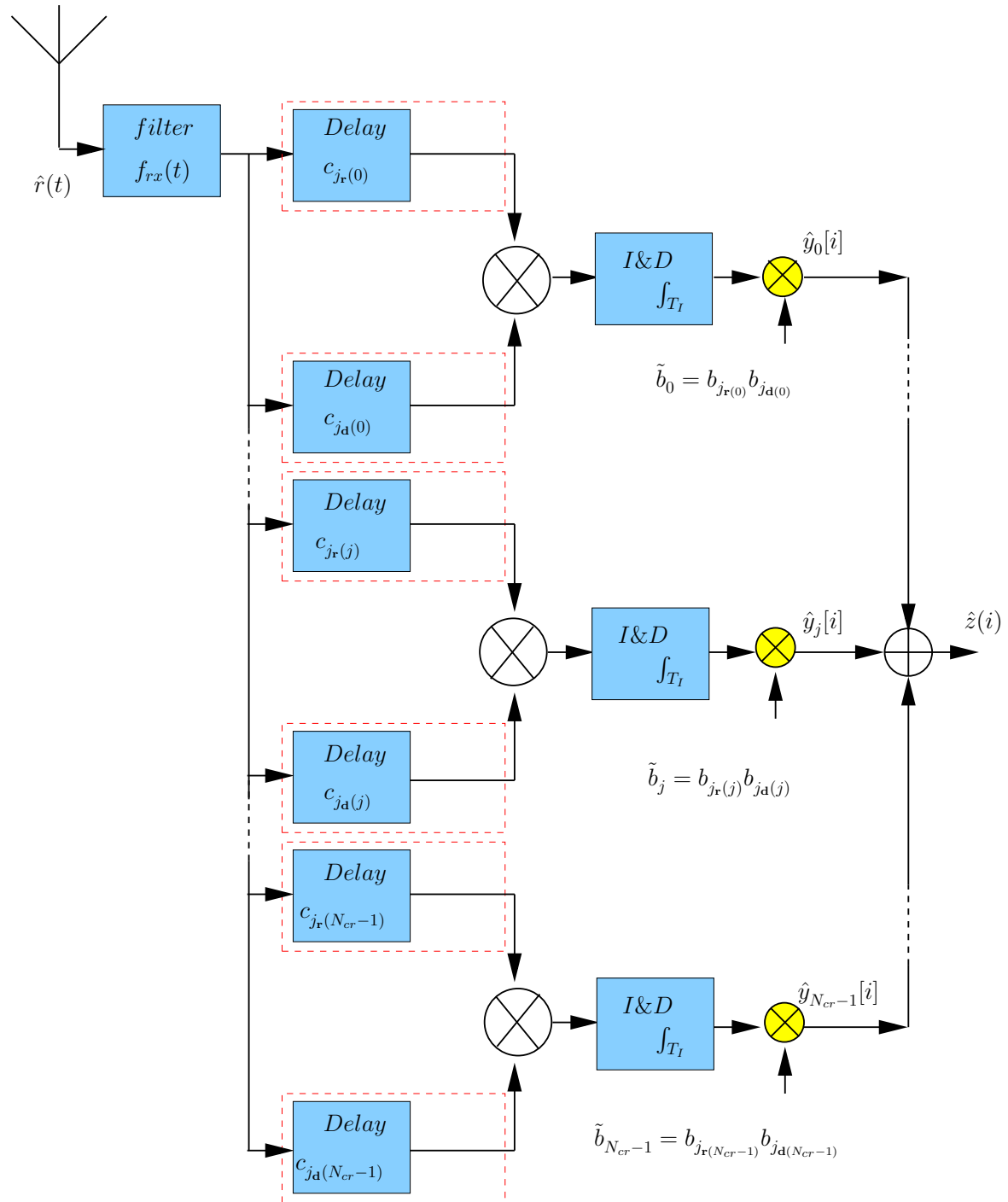
Figure 3.4: Expanded receiver front-end for the HMF receiver with post-combining.

3.4 Multiuser Detection

After devising the equivalent system model of the UWB schemes under investigation, we will next apply this knowledge about the system structure in order to develop data detection algorithms. Note that the detectors in Section 3.4.2 and Section 3.4.3 are our benchmark solutions for the receiver front-end in Fig 3.4. This is compared with our MMSE optimization in Section 3.4.4 for the HMF receiver in Fig 3.2.

3.4.1 Conventional Threshold Detector

A conventional threshold detector combines the samples $\mathbf{y}[i]$ by de-spreading the amplitude code (3.11). It performs detection against some threshold γ by

$$\hat{d}[i] = \text{sign}\{z[i] - \gamma\}. \tag{3.13}$$

For the de-spreading combiner, the elements of $\widetilde{\mathbf{b}}$ are $\tilde{b}_j = b_l^{(1)}$, for correlator j being matched to the pulses l and $l+1$ of user $k = 1$.

The bias term of the Volterra data model is a logical choice for the decision threshold, *i.e.*, $\gamma = \widetilde{\mathbf{b}}^T \mathbf{h}_0$ for the HMF receiver with post-combining of Section 3.3.1 and $\gamma = h_0$ for the HMF receiver of Section 3.2. But it is not exactly optimal due to the non-stationarity of the additive noise process. Nevertheless, we will choose the bias term as a decision threshold, since we neglect the exact noise model throughout this chapter.

3.4.2 Post-Combining MMSE

The linear minimum mean-square error (MMSE) algorithm tries to minimize the variance of the error σ_e^2. The linear operator can be viewed as a multiuser detector that operates on the output of the correlators. We consider the data are uncorrelated with variance $\sigma_d^2 = 1$. It is easily shown that also the products of data symbols are then uncorrelated. Furthermore, $d^{(1)}[i] = \mathbf{e}_1^T \tilde{\mathbf{d}}[i]$ where $\mathbf{e}_1$ that can be expressed as $[0, \cdots, 0, 1, 0, \cdots, 0]$, is tuned to the desired bit of user one. Without loss of generality, we can drop the index i in this calculation. The variance of the error σ_e^2 for user one is thus

$$\sigma_e^2 = \mathsf{E}\{(d^{(1)} - \mathbf{w}^T(\mathbf{H}^T\tilde{\mathbf{d}} + \mathbf{y}_\nu))^2\}, \tag{3.14}$$

where $\mathbf{w}$ is the linear combiner to be optimized. Expanding this equation, we obtain with $\sigma_d^2 = \sigma_d^4 = 1$

$$\sigma_e^2 = \mathbf{e}_1^T\mathbf{e}_1 + \mathbf{w}^T\mathbf{H}^T\mathbf{H}\mathbf{w} - 2\mathbf{e}_1^T\mathbf{w}\mathbf{H}^T + \mathbf{w}^T\mathbf{w}\sigma_\nu^2. \tag{3.15}$$

The noise variance of output samples $\mathbf{y}_\nu$ is obtained, where the data dependency is modeled by a second order Volterra system as

$$\mathsf{E}\{\mathbf{y}_\nu\mathbf{y}_\nu^T\} = (\mathbf{h}_{\nu,0} + \mathbf{H}_{\nu,1}^T\mathbf{d}[i] + \mathbf{H}_{\nu,2}^T(\mathbf{d}[i] \widetilde{\otimes} \mathbf{d}[i]))N_1 + T_I N_2 \qquad (3.16)$$

where $N_1 = \int_{-\infty}^{\infty} R_\nu(\kappa)d\kappa \propto N_0$ and $N_2 = \int_{-\infty}^{\infty} R_\nu^2(\kappa)\ d\kappa \propto N_0^2$. The vector $\mathbf{h}_{\nu,0}$ contains the bias terms of the noise terms, the column vectors of $\mathbf{H}_{\nu,1}$ contain the linear coefficients of the noise terms, and the non-linear terms of the noise terms are arranged into $\mathbf{H}_{\nu,2}$. The computation of this second-order Volterra system follows similar computational steps as derived in [23]. Then we equate the derivative with respect to $\mathbf{w}$ to zero,

$$\frac{\partial \sigma_e^2}{\partial \mathbf{w}} = 2(\mathbf{H}^T\mathbf{H} + \sigma_\nu^2\mathbf{I})\mathbf{w} - 2\mathbf{e}_1^T\mathbf{H}^T = 0. \qquad (3.17)$$

obtaining the solution

$$\mathbf{w} = (\mathbf{H}^T\mathbf{H} + \sigma_\nu^2\mathbf{I})^{-1}(\mathbf{h}^{(1)})^T. \qquad (3.18)$$

We note that $\mathbf{h}_1^{(1)} = \mathbf{e}_1^T\mathbf{H}^T$ is a column vector containing the linear model coefficients of the desired bit of user one.

3.4.3 Maximum Likelihood

A joint Maximum Likelihood (ML) detector [31, 32] selects the data vector for all users $\mathbf{d} = [d^{(1)}, d^{(2)}, \cdots, d^{(N_k)}]^T$, consisting of a single bit per user, to maximize the likelihood function $f(\mathbf{y}[i]|\mathbf{d})$. For a multiple-output system, this is a joint Gaussian PDF in the elements of $\mathbf{y}[i]$, as demonstrated by the multichannel data model (4.15). This detection is applied to the scheme in Fig 3.4. If we make the simplifying assumption that the components of the additive noise vector are i.i.d. Gaussian, then maximizing $f(\mathbf{y}[i]|\mathbf{d})$ is equivalent to minimizing the Euclidean distance

$$\hat{\mathbf{d}}[i] = \arg \min_{\mathbf{d}\in\{-1,+1\}^{N_k}} \|\mathbf{y}[i] - \mathbf{h}_0 - \mathbf{H}_1^T\mathbf{d} - \mathbf{H}_2^T(\mathbf{d}\widetilde{\otimes}\mathbf{d})\|^2.$$

3.4.4 Pre-Combining MMSE

Finally, we directly try to optimize the combining weights for the reference $\{b_{j_\mathbf{r}}\}$ and data $\{b_{j_\mathbf{d}}\}$ branches of the HMF in Fig 3.2 and Fig 3.3, written as $\mathbf{w}_{ref}$ and $\mathbf{w}_{dat}$ respectively. The optimization criterion of the minimum mean-square error (MMSE) solution minimizes the variance of the error σ_e^2 for user one, given as

$$\begin{aligned}
\sigma_e^2 &= \mathsf{E}\{(d^{(1)} - (\mathbf{w}_{dat} \otimes \mathbf{w}_{ref})^T(\mathbf{H}^T\mathbf{d} + \mathbf{z}_\nu))^2\} \\
&= \mathsf{E}\{(d^{(1)} - (\mathbf{w}_{dat} \otimes \mathbf{w}_{ref})^T\mathbf{H}^T\mathbf{d} \\
&\quad - (\mathbf{w}_{dat} \otimes \mathbf{w}_{ref})^T\mathbf{z}_\nu))^2\}
\end{aligned} \qquad (3.19)$$

where $\mathbf{w}_{ref}$ and $\mathbf{w}_{dat}$ are the linear combiners to be optimized. Expanding this equation we obtain

$$
\begin{aligned}
\sigma_e^2 &= \mathbf{e}_1^T\mathbf{e}_1 + (\mathbf{w}_{dat} \otimes \mathbf{w}_{ref})^T\mathbf{H}^T\mathbf{H}(\mathbf{w}_{dat} \otimes \mathbf{w}_{ref}) \\
&\quad + (\mathbf{w}_{dat} \otimes \mathbf{w}_{ref})^T(\mathbf{w}_{dat} \otimes \mathbf{w}_{ref})\sigma_\nu^2 \\
&\quad - 2(\mathbf{w}_{dat} \otimes \mathbf{w}_{ref})^T\mathbf{e}_1\mathbf{H}^T.
\end{aligned} \tag{3.20}
$$

We use some the following definitions for the vectors $\mathbf{w}_{ref}$ and $\mathbf{w}_{dat}$ of length N_{ref} and N_{dat}, respectively.

$$
\begin{aligned}
(\mathbf{w}_{dat} \otimes \mathbf{w}_{ref}) &= (\mathbf{I}_{N_{dat}} \otimes \mathbf{w}_{ref})\mathbf{w}_{dat} \\
&= (\mathbf{w}_{dat} \otimes \mathbf{I}_{N_{ref}})\mathbf{w}_{ref}
\end{aligned} \tag{3.21}
$$

$$
\begin{aligned}
(\mathbf{w}_{dat} \otimes \mathbf{w}_{ref})^T &= \mathbf{w}_{dat}^T(\mathbf{I}_{N_{dat}} \otimes \mathbf{w}_{ref}^T) \\
&= \mathbf{w}_{ref}^T(\mathbf{w}_{dat}^T \otimes \mathbf{I}_{N_{ref}})
\end{aligned} \tag{3.22}
$$

$$
\begin{aligned}
(\mathbf{w}_{dat} \otimes \mathbf{w}_{ref})^T(\mathbf{w}_{dat} \otimes \mathbf{w}_{ref}) &= \\
= \mathbf{w}_{dat}^T(\mathbf{I}_{N_{dat}}\mathbf{I}_{N_{dat}} \otimes \mathbf{w}_{ref}^T\mathbf{w}_{ref})\mathbf{w}_{dat} \\
= \mathbf{w}_{ref}^T(\mathbf{w}_{dat}^T\mathbf{w}_{dat} \otimes \mathbf{I}_{N_{ref}}\mathbf{I}_{N_{ref}})\mathbf{w}_{ref}
\end{aligned} \tag{3.23}
$$

Then we equate the derivative with respect to $\mathbf{w}_{dat}$ to zero

$$
\begin{aligned}
\frac{\partial \sigma_e^2}{\partial \mathbf{w}_{dat}} &= 2((\mathbf{I}_{N_{dat}} \otimes \mathbf{w}_{ref}^T)\mathbf{H}^T\mathbf{H}(\mathbf{I}_{N_{dat}} \otimes \mathbf{w}_{ref}) \\
&\quad + (\mathbf{I}_{N_{dat}}\mathbf{I}_{N_{dat}} \otimes \mathbf{w}_{ref}^T\mathbf{w}_{ref})\sigma_\nu^2)\mathbf{w}_{dat} \\
&\quad - 2(\mathbf{I}_{N_{dat}} \otimes \mathbf{w}_{ref}^T)\mathbf{e}_1^T\mathbf{H}^T \\
&= 0.
\end{aligned} \tag{3.24}
$$

Therefore the solution is

$$
\begin{aligned}
\mathbf{w}_{dat} &= ((\mathbf{I}_{N_{dat}} \otimes \mathbf{w}_{ref}^T)\mathbf{H}^T\mathbf{H}(\mathbf{I}_{N_{dat}} \otimes \mathbf{w}_{ref}) \\
&\quad + (\mathbf{I}_{N_{dat}}\mathbf{I}_{N_{dat}} \otimes \mathbf{w}_{ref}^T\mathbf{w}_{ref})\sigma_\nu^2\mathbf{I})^{-1} \\
&\quad \cdot (\mathbf{I}_{N_{dat}} \otimes \mathbf{w}_{ref}^T)\mathbf{e}_1^T\mathbf{H}^T.
\end{aligned} \tag{3.25}
$$

We note that $\mathbf{e}_1^T\mathbf{H}^T = \mathbf{h}_1^{(1)}$ is a column vector containing the linear model coefficients of the desired bit of user one. Appropriate synchronization has been assumed. So we can re-write the combiner

$$
\begin{aligned}
\mathbf{w}_{dat} &= ((\mathbf{I}_{N_{dat}} \otimes \mathbf{w}_{ref}^T)\mathbf{H}^T\mathbf{H}(\mathbf{I}_{N_{dat}} \otimes \mathbf{w}_{ref}) \\
&\quad + (\mathbf{I}_{N_{dat}}\mathbf{I}_{N_{dat}} \otimes \mathbf{w}_{ref}^T\mathbf{w}_{ref})\sigma_\nu^2)^{-1} \\
&\quad \cdot (\mathbf{I}_{N_{dat}} \otimes \mathbf{w}_{ref}^T)(\mathbf{h}^{(1)})^T.
\end{aligned}
\tag{3.26}
$$

Then we equate the derivative with respect to $\mathbf{w}_{ref}$ to zero

$$
\begin{aligned}
\frac{\partial\sigma_e^2}{\partial\mathbf{w}_{ref}} &= 2((\mathbf{w}_{dat}^T \otimes \mathbf{I}_{N_{ref}})\mathbf{H}^T\mathbf{H}(\mathbf{w}_{dat} \otimes \mathbf{I}_{N_{ref}}) \\
&\quad + (\mathbf{w}_{dat}^T\mathbf{w}_{dat} \otimes \mathbf{I}_{N_{ref}}\mathbf{I}_{N_{ref}})\sigma_\nu^2)\mathbf{w}_{ref} \\
&\quad - 2(\mathbf{w}_{dat}^T \otimes \mathbf{I}_{N_{ref}})\mathbf{e}_1^T\mathbf{H}^T \\
&= 0.
\end{aligned}
\tag{3.27}
$$

Therefore the solution is

$$
\begin{aligned}
\mathbf{w}_{ref} &= ((\mathbf{w}_{dat}^T \otimes \mathbf{I}_{N_{ref}})\mathbf{H}^T\mathbf{H}(\mathbf{w}_{dat} \otimes \mathbf{I}_{N_{ref}}) \\
&\quad + (\mathbf{w}_{dat}^T\mathbf{w}_{dat} \otimes \mathbf{I}_{N_{ref}}\mathbf{I}_{N_{ref}})\sigma_\nu^2)^{-1} \\
&\quad \cdot (\mathbf{w}_{dat}^T \otimes \mathbf{I}_{N_{ref}})\mathbf{e}_1^T\mathbf{H}^T
\end{aligned}
\tag{3.28}
$$

We note that $\mathbf{e}_1^T\mathbf{H}^T = \mathbf{h}_1^{(1)}$ is a column vector containing the linear model coefficients of the desired bit of user one. Appropriate synchronization has been assumed. So we can re-write the combiner

$$
\begin{aligned}
\mathbf{w}_{ref} &= ((\mathbf{w}_{dat}^T \otimes \mathbf{I}_{N_{ref}})\mathbf{H}^T\mathbf{H}(\mathbf{w}_{dat} \otimes \mathbf{I}_{N_{ref}}) \\
&\quad + (\mathbf{w}_{dat}^T\mathbf{w}_{dat} \otimes \mathbf{I}_{N_{ref}}\mathbf{I}_{N_{ref}})\sigma_\nu^2)^{-1} \\
&\quad \cdot (\mathbf{w}_{dat}^T \otimes \mathbf{I}_{N_{ref}})(\mathbf{h}^{(1)})^T.
\end{aligned}
\tag{3.29}
$$

Unfortunately, both formulas depend on each other. Thus the pre-combining MMSE is done iteratively. We propose two initializations: using the chip code of the reference pulses and of the data pulses respectively, as summarized in Table 3.1.

It is desirable in any optimisation problem to have a single global minimum. In the case of the proposed pre-combining MMSE, this is found by constraining the

Table 3.1: Pre-combining MMSE detector

Initialization ONE	Initialization TWO
1. Choose initial values $\mathbf{w}_{ref}$ with $\mathbf{b}_{j_{\mathbf{r}}}$	1. Choose initial values $\mathbf{w}_{dat}$ with $\mathbf{b}_{j_{\mathbf{d}}}$
2. Determine $\mathbf{w}_{dat}$ by (3.23)	2. Determine $\mathbf{w}_{ref}$ by (3.29)
3. Determine $\mathbf{w}_{ref}$ by (3.29)	3. Determine $\mathbf{w}_{dat}$ by (3.23)
4. Do iterations for $\mathbf{w}_{dat}$ and $\mathbf{w}_{ref}$	4. Do iterations for $\mathbf{w}_{ref}$ and $\mathbf{w}_{dat}$

detector's weight vector ($\mathbf{w}_{ref}$ and $\mathbf{w}_{dat}$) to have a unity magnitude. This is achieved by introducing the normalisation process in each iteration according to:

$$\mathbf{w} = \frac{\mathbf{w}}{\|\mathbf{w}\|} = \frac{\mathbf{w}}{\sqrt{\mathbf{w}^T \mathbf{w}}} \qquad (3.30)$$
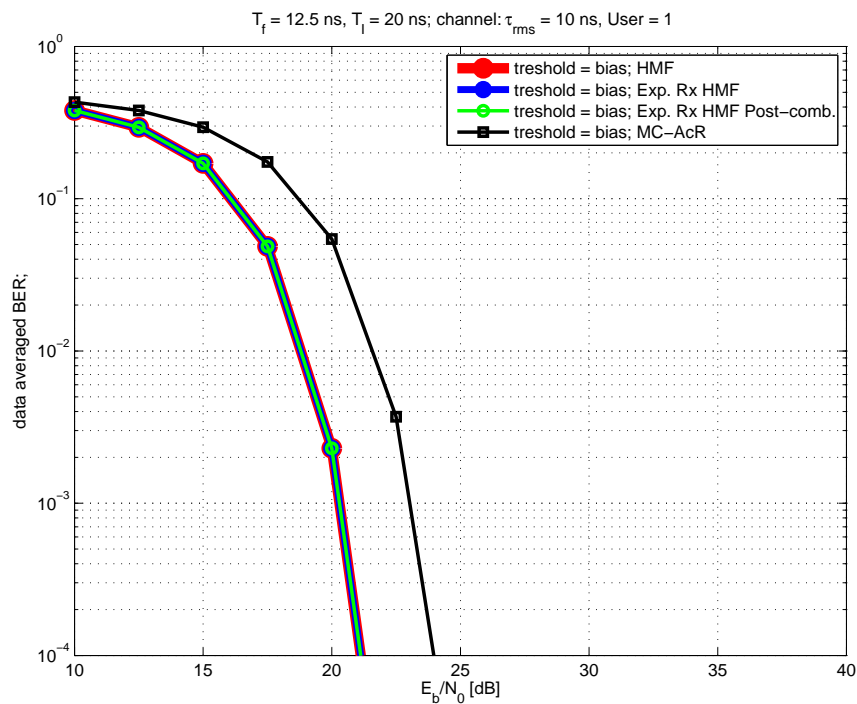
Figure 3.5: BER performance for single user (SU) at 10 Mbit/s, comparing the multi-channel AcR (MC-AcR) with post-combining in [1] (■) to various variants of the single correlator HMF.

3.5 Simulation Results

The following common system parameters are selected in all cases in order to obtain comparable results. The data rate has been set to medium bit-rates 10 Mbit/s ($T_{\mathrm{sym}} = 100$ ns). For simulation in Fig 3.5, an average pulse spacing of 12.5 ns has been used which increases the burst-duration to the total symbol interval for eight pulses per symbol. This scheme is referred to as the frame-differential (FD) TR scheme [22]. Then we reduce the average pulse spacing to 2 ns for simulation in Fig 3.6. This scheme represents the burst-oriented LDC transmission scheme with $N_p = 9pps$ which consists of 5 reference pulses N_{ref} and 4 data pulses N_{dat}. A sampling frequency of 20 GHz was chosen for the simulations and an integration interval of $T_{\mathrm{I}} = 20$ ns has been used. A non line-of-sight channel has been simulated, with an exponentially decaying power delay profile (PDP) at an RMS delay spread of $\tau_{\mathrm{rms}} = 10$ ns [34].

We apply a fixed set of codes in all 100 simulations performed for independent simulated channels. Random time-offsets between users have been introduced, i.e., the asynchronous case has been studied. Although not based on any analytical framework, these codes were selected for providing good multiple access capability.

Furthermore, the amplitude gains of all users were set equal to one. A non line-of-sight channel has been simulated, with an exponentially decaying power delay profile (PDP) at an RMS delay spread of $\tau_{\mathrm{rms}} = 10$ ns [22]. The channel simulator produces random ray arrival times corresponding to a Poisson process, with a mean arrival rate of $\lambda = 5$ rays per ns. The ray-amplitudes are Rayleigh distributed with random signs. A second-derivative Gaussian monocycle with $\tau_m = 0.2877$ ns, $w(t) = [1 - 4\pi(t/\tau_m)^2] \exp[-2\pi(t/\tau_m)^2]$, has been convolved with the such generated channel impulse responses, yielding $g^{(k)}(t)$. For fair comparison, the same channel impulse response realization have been applied to the MC-AcR and the HMF receiver.

The performance results for the conventional threshold detector of a conventional multi-channel AcR (MC-AcR) with post-combining in Chapter 2 and of the HMF receiver are first evaluated in a single user scenario in Fig 3.5. From the plot, it is clear that the performance for the HMF receiver and the expanded HMF receiver with post-combining have equal results as expected, because they have equivalent conceptual structures. They have about 2 dB advantage when BER=1e-3 over the MC-AcR because introducing despreading before the correlator reduces the error due to the nonlinear noise co-terms.

Performance results for eight-user scenarios are presented in Fig 3.6(a) for the conventional MC-AcR and in Fig 3.6(b) for the HMF receiver. Both figures compare results for the simple threshold detector to the detection schemes. While the linear MMSE combiners (post-combining computation of linear and non linear terms) sig-

T_f = 2 ns, N_p = 9 pulses/symb., T_l = 20 ns; channel: τ_{rms} = 10 ns, User = 8

(a)

T_f = 2 ns, N_p = 9 pulses/symb., T_l = 20 ns; channel: τ_{rms} = 10 ns, User = 8

(b)
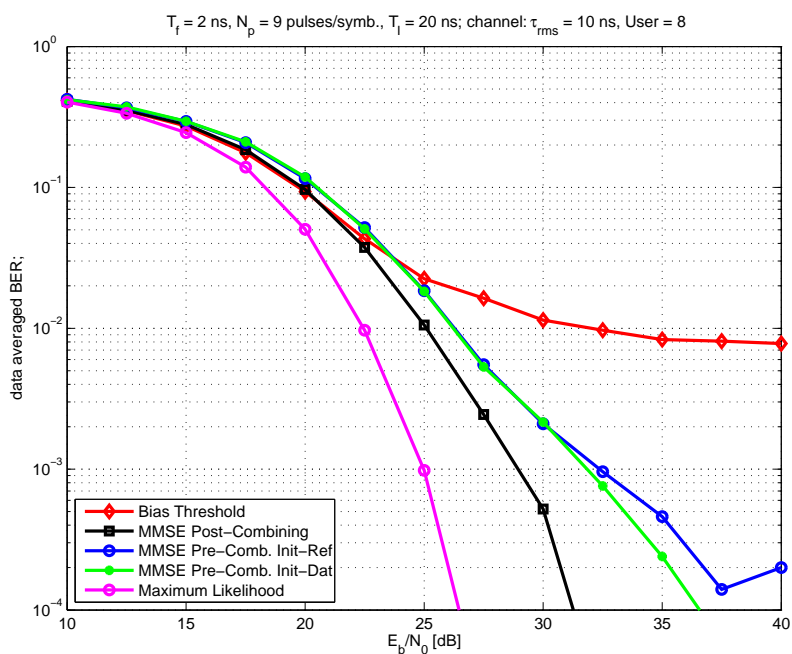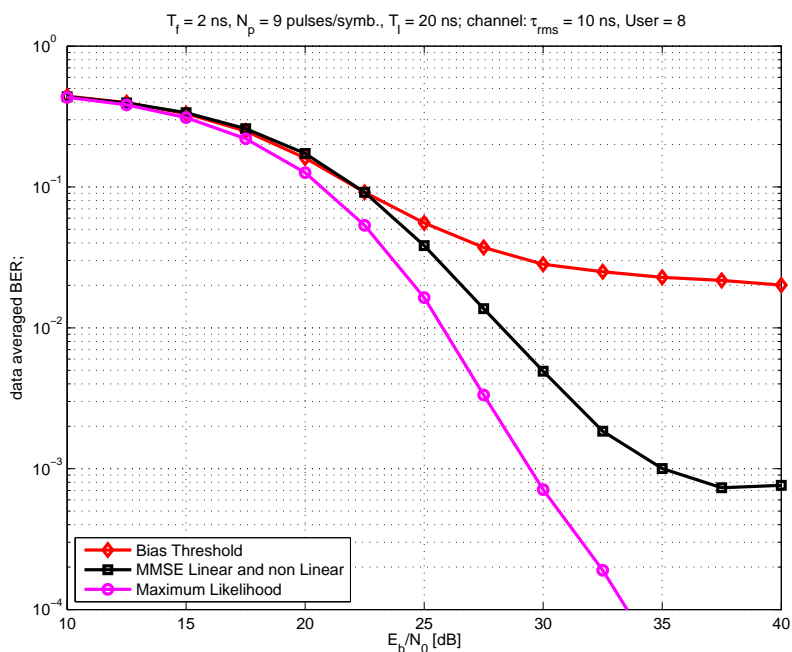
Figure 3.6: BER performance evaluation of an 8-user scenario at 10 Mbit/s, comparing the conventional detector to the joint ML detector and the MMSE detector; (a) the multi-channel AcR (MC-AcR) with post-combining computation of linear and non linear terms; (b) the expanded receiver frontend for the HMF in Section 3.3.1.

nificantly reduce the error floors, additional 3 dB of performance gain are achieved at BER of 0.01, employing the more complex (close to optimal) ML detectors. Comparing the MC-AcR and HMF results, Fig 3.6(a) vs. Fig 3.6(b), an advantage of about 3 dB is evident for the HMF structure, looking at the MMSE and ML detectors at BER of 0.01. This gain is remarkably similar to the gain found from Fig 3.5.

We would like to remind that the post-combining MMSE and ML solutions are only benchmark solutions for the HMF receiver structure. The actual, non-expanded HMF receiver of Fig 3.2 does not allow for the application of the post-combining MMSE and the ML detectors, if it is implemented in analog hardware. Assuming we can implement adjustable gain blocks in the pre-AcR matched filters, we obtain the pre-combining detector, for which the MMSE solution with the initializations using the chip code of the reference pulses and of the data pulses to finding the combining weights has been derived in Section 3.4.4. Fig 3.6(b) shows performance results for this pre-combining MMSE receiver. Apparently, this detector is also capable of significantly reducing the error floor, but it remains clearly behind the post-combining benchmark. This shortcoming is due to the reduced degrees of freedom in the combiner. Instead of a separate weight coefficient *for each combination* of pulses, only one coefficient per pulse is available in the pre-combining scheme.

When we compare the pre-combining HMF receiver with the post-combining MC-AcR receiver, which is a very well feasible structure, the gain of the HMF is reduced to less than 2 dB at a BER of 0.01.

Note that all detectors have assumed perfect knowledge of the coefficients of the equivalent system models. In practice, these model coefficients would need to be estimated, for instance from training data. We did not investigate the coefficient estimation problem, as our focus has been put on the comparison of the receiver structures.

3.6 Summary

In this chapter, we have considered the hybrid matched-filter (HMF) transmitted-reference system in single and multiuser scenarios. We have derived a multiuser equivalent system model accounting for MAI to obtain advanced detectors for the HMF receiver. The results demonstrate that the system performance improves by using the HMF for TR UWB over the conventional multichannel AcR. Results also show that the HMF receiver performs well in multipath and multiple access environments. Also the newly proposed pre-combining MMSE detector has been proven useful by computer simulation although it remains behind the benchmark solutions.

4 Performance Analysis of Dual Pulse TR UWB System

Multiple-access performance in conjuction with a TR receiver has been addressed in some papers. Time hopping (TH) [3, 50] is a widely adopted principle to allow multiple users to share the same UWB channel. In [51], the authors proposed optimal/suboptimal TR receiver structures, combined with TH as its multiple-access technique, such that averaging multiple reference signals obtains a favorable system performance in the multiuser scenario. In [52], the authors proposed a modified balanced TR system, using the frame-rate correlator as in the conventional TR UWB system, which is capable of eliminating the inter-pulse interference (IPI) with MAI capability, thus it offers an increased information rate.

In this chapter, we consider the conventional TR UWB scheme for dual-pulse systems in multi-user scenarios. We derive the equivalent system model for the TR UWB receiver in a similar form as presented in [22, 1]. The objective of this chapter is to study the statistical characterization of the MAI in terms of channel-averaged signal-to-interference ratio (SIR) and the influence of system parameters on the receiver. The authors in [24, 25, 26] have developed the theoretical framework of the statistical signal properties of the auto and cross-correlations functions of the received pulse in a UWB autocorrelation receiver (AcR) system. We directly apply their theoretical framework, which will enable us to analyze the channel-averaged output signal-to-interference ratio (SIR) for a TR UWB receiver in two asynchronous scenarios, based on random time-hopping (TH) codes [27]. Analytical results and numerical results are presented for illustration. We further show the impact of the chosen system parameters (e.g., symbol duration and delay hopping code) to better understand their influence on the multi-user performance.

4.1 System Model

In this section, a typical model of a multiple-access time-hopping (TH) TR UWB communications scheme is presented. One of the pulses in the frame serves as a reference with fixed polarity while the second pulse's polarity is modulated according to the data symbol and the spreading code. The transmissions from different users

are assumed to be asynchronous.

The transmitted signal of the kth transmitter's pulse train is described in the following model

$$s^{(k)}(t) = \sum_{i=-\infty}^{\infty} [w(t - iT_s - c_i^{(k)}T_c) + d_i^{(k)}b_i^{(k)}w(t - iT_s - c_i^{(k)}T_c - D^{(k)})] \qquad (4.1)$$

where the two transmitted pulses correspond to the reference and modulated data pulse. $D^{(k)}$ is the delay between the reference and the modulated data pulse of each user. In addition, T_s, T_c and $w(t)$ are the symbol period, the time period of a TH chip and the waveform of a transmitted UWB pulse with duration τ_w, respectively. $d_i^{(k)} \in \{\pm 1\}$, is the ith data bit to be transmitted from the kth transmitter, assumed to be equiprobable. The polarity code $\{b_i^{(k)}\}$ represents a user-specific pseudo-random sequence of values $\{\pm 1\}$ to randomize the polarities of the transmitted pulse. The integer TH sequence assigned to user k $\{c_i^{(k)}\}$ is uniformly distributed in $\{0, 1, \cdots, N_h - 1\}$, with N_h being the number of hops, which prevents catastrophic collision between different users. The symbol period T_s is assumed to be larger than the delay spread of the channel plus pulse duration so that there is no intersymbol interference (ISI).

4.2 Two Users Dual-Pulse TR Systems

We focus on a symbol period T_s. The analysis will proceed for two active users that are transmitting asynchronously on the channels. At the receiver side, after travelling through the multipath channel, the noise-free received waveform corresponding to the symbol $i = 0$ of the desired user $k = 1$ can be expressed as the superposition of two terms

$$r(t) = r_d(t) + r_I(t), \qquad (4.2)$$

where the desired signal is then given as

$$r_d(t) = [g^{(1)}(t - c^{(1)}T_c) + d^{(1)}b^{(1)}g^{(1)}(t - c^{(1)}T_c - D^{(1)})]$$

and the interference part can be written as

$$r_I(t) = [g^{(2)}(t - c^{(2)}T_c - \tau^{(2)}) + d^{(2)}b^{(2)}g^{(2)}(t - c^{(2)}T_c - D^{(2)} - \tau^{(2)})]$$

where $g^{(k)}(t) = h^{(k)}(t) * w(t)$ is the response of the channel to one transmitted monocycle at $t = 0$, $h^{(k)}(t)$ denotes the channel impulse response (CIR) of the UWB radio channel for user k [24], and $*$ is the convolution operator. We assume that $\tau^{(1)} = 0$, without loss of generality, and $\tau^{(2)}$ represents time asynchronism between

the transmitter clocks. Fig. 4.1 illustrates the typical symbol waveform for the dual-pulse TR UWB system. In a dual-pulse AcR, a single correlator is used, where a delayed replica of the received signal is correlated with the signal itself. The correlation lag $\overline{D}^{(1)}$ is matched to the delay of the transmitted signal of user 1. The correlator output without noise is then written as

$$y[i] = \int_{\hat{c}_i^{(1)}T_c}^{\hat{c}_i^{(1)}T_c+T_I} r(t) \; r(t+\overline{D}^{(1)}) \, dt, \tag{4.3}$$

where we may observe an impact of all the interfering pulses falling in the observation window $[\hat{c}_i^{(1)}T_c, \hat{c}_i^{(1)}T_c + T_I]$. $\hat{c}_i^{(1)}T_c$ and T_I are the starting point and the time interval of the integration, respectively. The receiver is assumed perfectly synchronized to the desired user, i.e., $\tau^{(1)}$ and $\hat{c}_i^{(1)}$ are known.

The channel ACF is expressed as

$$I_g^{(k,k')}(t_1, t_2; \tau) = \int_{t_1}^{t_2} g^{(k)}(t) \; g^{(k')}(t+\tau) \, dt, \tag{4.4}$$

representing the autocorrelation integrals for the data model accounting for users k and k' and interfering reference pulses and modulated data pulses.

The decision variable for detecting the ith bit of user 1, being the user of interest, is demodulated by a de-spreading code $\hat{b}^{(1)}$. Following similar steps for the derivation of a second-order Volterra model as fully derived in [22, 1], the decision variable $z[i]$ is compactly expressed in the following quadratic form

$$z[i] = \hat{b}_i^{(1)} \sum_{k=1}^{2} \sum_{k'=1}^{2} \mathbf{a}^{(k)}[i]^T \mathbf{Y}^{(k,k')} \mathbf{a}^{(k')}[i]. \tag{4.5}$$

The polarities of all pulses of all users having impact on received symbol i are represented by vectors $\mathbf{a}^{(k)}[i]$, taking into account the spreading code, the constant part and the data dependent part of all users interfering with the current symbol, as completely described in [22, 1]. The autocorrelation integrals for the data model are defined by the matrix $\mathbf{Y}^{(k,k')}$, expressing the interference among the pulses due to multiple existing users, with elements of $[\mathbf{Y}^{(k,k')}]_{m,n}$, where $k, k' \in \{1, 2\}$ denote the user indices and $m, n \in \{1, 2\}$ represent the indices of the reference and modulated data pulses.

The generic element of matrix $[\mathbf{Y}^{(k,k')}]_{m,n}$, which represents the auto-or cross-correlation of the received pulse and whose random nature is due to multipath propagation, can be derived as
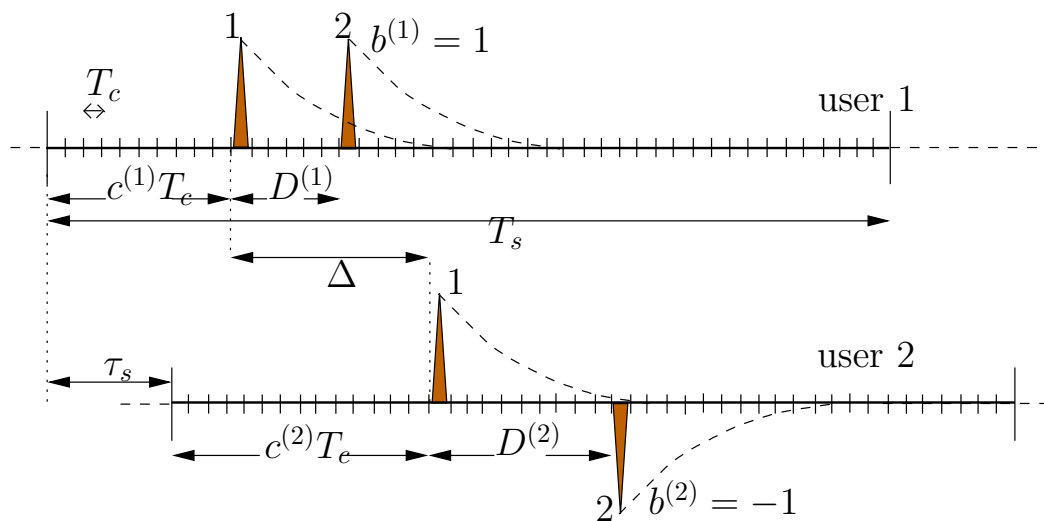
Figure 4.1: Illustration of symbol waveforms for a dual-pulse two users TR UWB system in one symbol duration. Δ denotes the time-of-arrival difference between the reference pulse of user 1 and a possibly interfering pulse of user 2. The reference and modulated data pulses are indexed as 1 and 2, respectively.

$$
\begin{aligned}
[\mathbf{Y}^{(k,k')}]_{m,n} &= \int_{\alpha}^{\alpha+T_I} g^{(k)}(t) \, g^{(k')}(t + \tau_{m,n}^{(k,k')}) \, dt \\
&= I_{g_{m,n}}^{(k,k')}(\alpha, \alpha + T_I; \tau_{m,n}^{(k,k')})
\end{aligned}
\tag{4.6}
$$

where

$$
\begin{aligned}
\alpha &= -(c^{(k)} - \hat{c}^{(1)})T_c - (m-1)D^{(k)} - \tau^{(k)} \\
\tau_{m,n}^{(k,k')} &= (c^{(k)} - c^{(k')})T_c - (n-1)D^{(k')} - \tau^{(k')} \\
&\quad + (m-1)D^{(k)} + \tau^{(k)} + \overline{D}^{(1)}.
\end{aligned}
$$

Basically, in the above TH structure, two pulses from user 2 can interfere with any of the pulses of user 1. The time delay of user 2 relative to user 1 lies within one symbol interval, so that $\tau^{(2)} - \tau^{(1)} = \tau_s$, $0 \leq \tau_s \leq T_s$. $(c^{(2)} - \hat{c}^{(1)})$ is equivalent to the

difference of two independent uniformly distributed random variables, and thus has triangular PDF. $\Delta = (c^{(2)} - c^{(1)})T_c + \tau_s$ is the time-of-arrival difference between the reference pulses of user 1 and user 2. It is uniform in $[\frac{-T_s}{2}, \frac{T_s}{2}]$ for cyclostationarity. This property will be used for averaging each Δ in the next section. Finally, the noise-free output of a memoryless multiuser equivalent system model of a single output variable $z[i]$ of two users can be expressed by the following more intuitive representation as the superposition of four terms [38]

$$z[i] = h_0 + h_1^{(1)} d^{(1)}[i] + h_1^{(2)} d^{(2)}[i] + h_2 d^{(1)}[i] d^{(2)}[i]. \tag{4.7}$$

The h_0 term represents the bias term, $h_1^{(1)}$ and $h_1^{(2)}$ denote the linear coefficients of the desired user 1 and user 2, respectively, and the qudratic coefficient denoted by h_2 exists in presence of MAI. All these terms can be modeled as random variables, due to the random nature of the radio channels. In a multiuser environment, the decision variable is not optimal due to the impact of MAI represented by the third and fourth terms in (4.7). Their distributions will be briefly introduced in Subsection 4.3.3. The coefficients of the equivalent system model are described as

$$
\begin{aligned}
h_0 = {} & (b^{(1)}.I_g^{(1,1)}\{0, T_I; \overline{D}^{(1)}\} \\
& + \; b^{(1)}.I_g^{(1,1)}\{-D^{(1)}, T_I - D^{(1)}; \overline{D}^{(1)}\} \\
& + \; b^{(1)}.I_g^{(1,2)}\{0, T_I; \overline{D}^{(1)} - \Delta\} \\
& + \; b^{(1)}.I_g^{(2,1)}\{\overline{D}^{(1)}, T_I + \overline{D}^{(1)}; \overline{D}^{(1)} + \Delta\} \\
& + \; b^{(1)}.I_g^{(2,2)}\{-\Delta, T_I - \Delta; \overline{D}^{(1)}\} \\
& + \; b^{(1)}.I_g^{(2,2)}\{-(\Delta + D^{(2)}), T_I - (\Delta + D^{(2)}); D^{(1)} + \overline{D}^{(1)}\}
\end{aligned}
\tag{4.8}
$$

This first term in (4.7) represents the bias term that is used for threshold detection. The second, third and fourth terms in (4.7) are then written as

$$
\begin{aligned}
h_1^{(1)} d^{(1)}[i] = (I_g^{(1,1)} & \{0, T_I; \overline{D}^{(1)} - D^{(1)}\} \\
+ \ & I_g^{(1,1)} \{-D^{(1)}, T_I - D^{(1)}; \overline{D}^{(1)} + D^{(1)}\} \\
+ \ & I_g^{(1,2)} \{-D^{(1)}, T_I - D^{(1)}; \overline{D}^{(1)} + D^{(1)} - \Delta\} \\
+ \ & I_g^{(2,1)} \{-D^{(1)} + \overline{D}^{(1)}, T_I - D^{(1)} + \overline{D}^{(1)}; -D^{(1)} + \overline{D}^{(1)} + \Delta\}) d^{(1)}[i]
\end{aligned}
$$
$$(4.9)$$

$$
\begin{aligned}
h_1^{(2)} d^{(2)}[i] = (b^{(1)} \cdot b^{(2)}. I_g^{(1,2)} & \{0, T_I; \overline{D}^{(1)} - D^{(2)} - \Delta\} \\
+ \ b^{(1)} \cdot b^{(2)}. I_g^{(2,1)} & \{\overline{D}^{(1)}, T_I + \overline{D}^{(1)}; D^{(2)} + \overline{D}^{(1)} + \Delta\} \\
+ \ b^{(1)} \cdot b^{(2)}. I_g^{(2,2)} & \{-\Delta, T_I - \Delta; \overline{D}^{(1)} - D^{(2)}\} \\
+ \ b^{(1)} \cdot b^{(2)}. I_g^{(2,2)} & \{-(\Delta + D^{(2)}), T_I - (\Delta + D^{(2)}); \overline{D}^{(1)} + D^{(2)}\}) d^{(2)}[i]
\end{aligned}
$$
$$(4.10)$$

$$
\begin{aligned}
h_2 d^{(1)}[i] d^{(2)}[i] = (b^{(2)} \cdot I_g^{(1,2)} & \{-D^{(1)}, T_I - D^{(1)}; D^{(1)} + \overline{D}^{(1)} - D^{(2)} - \Delta\} \\
+ \ b^{(2)}. I_g^{(2,1)} & \{-D^{(1)} + \overline{D}^{(1)}, T_I - D^{(1)} + \overline{D}^{(1)}; -D^{(1)} + \overline{D}^{(1)} + D^{(2)} + \Delta\}) \\
\times \ d^{(1)}[i] & d^{(2)}[i]
\end{aligned}
$$
$$(4.11)$$

where $\Delta = [c^{(2)} - \hat{c}^{(1)}]T_c + \tau^{(2)}$.

4.3 Performance Evaluation

In this section, we formulate the statistical characterization of the memoryless multiuser Volterra model coefficients based on the statistics of the ACF of the channel's response to a UWB pulse, to gain insight in the impact of MAI on TR UWB systems. A theoretical framework of the statistical models of the first and second moments of $I_g^{(k,k')}(t_1, t_2; \tau)$ (c.f.(4.6)) has been developed in [24, 25] and we directly apply the results to average over various sets of independent channel realizations.

The goal is to understand the overall statistical characterization of variations of the multiple-access memoryless Volterra model parameters for various sets of channel impulse responses and for realisations of the time-offset variable Δ. It will be evaluated in terms of the first and the second moments of the random terms $I_g^{(k,k')}(t_1, t_2; \tau)$ in (4.6) [24, 25].

4.3.1 Expected value of $h_1^{(1)}$

We analyze the cross product for the AcR of desired user 1 $h_1^{(1)}$ based on the elementary operation in (4.6). It can be derived as

$$
\begin{aligned}
h_1^{(1)} = \; & I_g^{(1,1)}\{0, T_I; \overline{D}^{(1)} - D^{(1)}\} \\
& + \; I_g^{(1,1)}\{-D^{(1)}, T_I - D^{(1)}; \overline{D}^{(1)} + D^{(1)}\} \\
& + \; I_g^{(1,2)}\{-D^{(1)}, T_I - D^{(1)}; \overline{D}^{(1)} + D^{(1)} - \Delta\} \\
& + \; I_g^{(2,1)}\{-\Delta, T_I - \Delta; \overline{D}^{(1)} - D^{(1)} + \Delta\}.
\end{aligned}
\tag{4.12}
$$

We have applied a result from [53, 25], introducing the mean of the received-pulse auto correlation function (RP-ACF). For the same user ($k = k'$) this can be written explicitly as

$$
\mathsf{E}\{I_g^{(k,k)}(a, b; \gamma)\} \approx \phi_w(\gamma) E_w^{(k)} \begin{cases} (1 - e^{\frac{-b}{\tau_r}}) & a \leqslant 0 \\ (e^{\frac{-a}{\tau_r}} - e^{\frac{-b}{\tau_r}}) & a > \tau_w \end{cases}
\tag{4.13}
$$

where $\phi_w(\varphi) = \int_0^{\tau_w} w(\psi) w(\psi + \varphi)\, d\psi$ is the pulse ACF, the prototype pulse is normalized to have unit energy i.e., $\phi_w(0) = 1$ and $E_w^{(1)}$ is defined as the average received pulse-energy of user 1. The expected value of the received-pulse cross correlation function (RP-CCF) for different users is given as

$$
\mathsf{E}\{I_g^{(k,k')}(a, b; \gamma)\} = \mathsf{E}\left\{\int_a^b g^{(k)}(t) g^{(k')}(t + \gamma)\, dt\right\} = 0
\tag{4.14}
$$

The expectation of the third and fourth terms of (4.12) will simply become zero. Substituting (4.13) and (4.14) into (4.12), we finally obtain

$$
\begin{aligned}
\mathsf{E}\{h_1^{(1)}\} \simeq \; & \phi_w(0) E_w^{(1)}[1 - e^{\frac{-T_I}{\tau_r}}] \\
& + \phi_w(D^{(1)} + \overline{D}^{(1)}) E_w^{(1)}[e^{\frac{D^{(1)}}{\tau_r}} - e^{\frac{(D^{(1)} - T_I)}{\tau_r}}]
\end{aligned}
\tag{4.15}
$$

4.3.2 Variances of $h_1^{(2)}$ and h_2

Again, based on (4.5) and (4.6), we can define the elements of the linear term $h_1^{(2)}$, given as

$$
\begin{aligned}
h_1^{(2)} = \hat{b}^{(1)} \cdot b^{(2)} \Big\{ & I_g^{(1,2)}\{0, T_I; \overline{D}^{(1)} - D^{(2)} - \Delta\} \\
& + \; I_g^{(2,1)}\{-\Delta - D^{(2)}, T_I - \Delta - D^{(2)}; \Delta + \overline{D}^{(1)} + D^{(2)}\} \\
& + \; I_g^{(2,2)}\{-\Delta, T_I - \Delta; \overline{D}^{(1)} - D^{(2)}\} \\
& + \; I_g^{(2,2)}\{-\Delta - D^{(2)}, T_I - \Delta - D^{(2)}; \overline{D}^{(1)} + D^{(2)}\} \Big\}.
\end{aligned}
\tag{4.16}
$$

$h_1^{(2)}$ can be decomposed into two terms $h_1^{(2)} = \mathtt{I_{1A}} + \mathtt{I_{1B}}$. $\mathtt{I_{1A}}$ accounts for the interference resulting from correlating different users, expressed by the first and second terms in (4.16), while $\mathtt{I_{1B}}$ accounts for the interference resulting from correlating the same user, expressed by the third and fourth terms in (4.16). The assumption of independence of channel realizations for different users enables us to evaluate the second order moment of $h_1^{(2)}$, which can be expressed as

$$\mathsf{E}\{h_1^{(2)^2}\} = \mathsf{E}_\Delta\{\mathtt{I_{1A}^2}\} + \mathsf{E}_\Delta\{\mathtt{I_{1B}^2}\} \tag{4.17}$$

Revisiting the results from [53, 25] for the channel AcR, the second moment for $\gamma > \tau_w$ can be calculated as

$$\mathsf{E}\{I_g^{(k,k')^2}(a,b;\gamma)\} \approx$$
$$\approx \frac{\mathsf{c}_1}{2\tau_r} e^{\frac{-\gamma}{\tau_r}} E_w^{(k)} E_w^{(k')} \times \begin{cases} (1 - e^{\frac{-2b}{\tau_r}}) & a \leqslant 0 \\ (e^{\frac{-2a}{\tau_r}} - e^{\frac{-2b}{\tau_r}}) & a > \tau_w \end{cases} \tag{4.18}$$

where $\mathsf{c}_1 = \int_{-\tau_w}^{\tau_w} \phi_w^2(\psi)\, d\psi$ is the correlation energy of the pulse ACF. Furthermore, the second moment for $\gamma = 0$ can be computed as

$$\mathsf{E}\{I_g^{(k,k')^2}(a,b;0)\} \approx$$
$$\approx \frac{\mathsf{c}_1 + \mathsf{c}_2}{\tau_r} E_w^{(k)} E_w^{(k')} \times \begin{cases} (1 - e^{\frac{-2b}{\tau_r}}) & a \leqslant 0 \\ (e^{\frac{-2a}{\tau_r}} - e^{\frac{-2b}{\tau_r}}) & a > \tau_w \end{cases} \tag{4.19}$$

where $\mathsf{c}_2 = \frac{1}{2\lambda}(1 + \frac{1}{m})$ is a term for a Poisson process of ray arrivals at λ rays per second and for Nakagami-m distributed ray amplitudes. The covariance is zero if the integration intervals are non-overlapping. If $|\gamma_1| = |\gamma_2| = \gamma$, the covariance becomes

$$\mathrm{cov}\{I_g^{(k,k')}(a_1,b_1;\gamma_1)I_g^{(k,k')}(a_2,b_2;\gamma_2)\} \approx$$
$$\approx \begin{cases} \mathrm{var}\{I_g^{(k,k')}(a_\alpha,b_\alpha;\gamma)\} & |\gamma_1| = |\gamma_2| = \gamma \\ 0 & \text{otherwise} \end{cases} \tag{4.20}$$

where $a_\alpha = \max(a_1, a_2)$ and $b_\alpha = \min(b_1, b_2)$.

It is evident that $\mathtt{I_{1A}}$ has zero mean, since the expected value of the RP-CCF becomes zero and the polarity codes of different users are random variables with equal probabilities.

Variances of $h_1^{(2)}$

For the channel realizations, we use the symmetry property $I(a,b;\tau) = I(a + \tau, b + \tau; -\tau)$ for $\tau < 0$. The first two terms of (4.16) denote the interference resulting from correlating different users. The second-order moment of $\mathtt{I_{1A}}$ can be evaluated as

$$\mathsf{E}_\Delta\{\mathtt{I}_{1A}^2\} = \mathsf{E}_\Delta\Big\{ \Big(\hat{b}^{(1)} \cdot b^{(2)} \Big\{ I_g^{(1,2)}\{0, T_I; \overline{D}^{(1)} - D^{(2)} - \Delta\}$$
$$+\ I_g^{(2,1)}\{-\Delta - D^{(2)}, T_I - \Delta - D^{(2)}; \Delta + \overline{D}^{(1)} + D^{(2)}\}\Big\}\Big)^2\Big\} \qquad (4.21)$$

Substituting (4.18), (4.19) and (4.20) into (4.21) and after averaging over Δ, we obtain

$$\mathsf{E}_\Delta\{\mathtt{I}_{1A}^2\} \approx \frac{E_w^{(1)} E_w^{(2)}}{\tau_r} \frac{c_1}{2} e^{\frac{-2(\overline{D}^{(1)} - D^{(2)})}{\tau_r}} \left(1 - e^{\frac{-2T_I}{\tau_r}}\right) e^{\frac{-(D^{(2)} - \overline{D}^{(1)})}{\tau_r}} \frac{\left(1 + e^{\frac{-T_s}{2}}\right)}{T_s} \int_{\frac{-T_s}{2}}^{\frac{-T_s}{2}} e^\Delta \, d\Delta$$

$$+\ \frac{E_w^{(1)} E_w^{(2)}}{\tau_r} \frac{c_1}{2} e^{\frac{-2\overline{D}^{(1)}}{\tau_r}} \left(1 - e^{\frac{-2T_I}{\tau_r}}\right) e^{\frac{-(D^{(2)} - \overline{D}^{(1)})}{\tau_r}} \frac{\left(1 + e^{\frac{-T_s}{2}}\right)}{T_s} \int_{\frac{-T_s}{2}}^{\frac{-T_s}{2}} e^\Delta \, d\Delta$$

$$\approx \frac{E_w^{(1)} E_w^{(2)}}{\tau_r} \frac{c_1}{2} (1 - e^{\frac{-2T_I}{\tau_r}}) (e^{\frac{T_s}{2\tau_r}} - e^{\frac{-T_s}{2\tau_r}}) e^{\frac{(\overline{D}^{(1)} + D^{(2)})}{\tau_r}} (e^{\frac{T_s}{2\tau_r}} - 1)^{-1}$$

$$+\ (e^{\frac{(D^{(2)} - \overline{D}^{(1)})}{\tau_r}} (1 + e^{\frac{-T_s}{\tau_r}}) + e^{\frac{-(3\overline{D}^{(1)} + D^{(2)})}{\tau_r}} (1 + e^{\frac{-T_s}{\tau_r}}))$$

$$\approx \frac{E_w^{(1)} E_w^{(2)}}{\tau_r} \frac{c_1}{2} (e^{\frac{2D^{(2)}}{\tau_r}} + e^{\frac{-2\overline{D}^{(1)}}{\tau_r}}) (1 - e^{\frac{-2T_I}{\tau_r}}) (e^{\frac{T_s}{2\tau_r}} - e^{\frac{-T_s}{2\tau_r}})$$

$$\times\ (e^{\frac{T_s}{2\tau_r}} - 1)^{-1} (1 + e^{\frac{-T_s}{2\tau_r}})$$

$$(4.22)$$

The following expression of the second moment of $\mathtt{I}_{1A}$ is then obtained as

$$\mathsf{E}_\Delta\{\mathtt{I}_{1A}^2\} \simeq \frac{E_w^{(1)} E_w^{(2)}}{T_s} c_3 \left(e^{\frac{2D^{(2)}}{\tau_r}} - e^{\frac{-2D^{(1)}}{\tau_r}}\right) \sinh(\frac{T_s}{2\tau_r}) \qquad (4.23)$$

where $c_3 = c_1 (e^{\frac{T_s}{2\tau_r}} - 1)^{-1} (1 + e^{\frac{-T_s}{\tau_r}} - e^{\frac{-2T_I}{\tau_r}} - e^{\frac{-(2T_I + T_s)}{\tau_r}})$.

The second-order moment of $\mathtt{I}_{1B}$, taking into account the interference resulting from correlating the same user, can be evaluated as

$$\mathsf{E}_\Delta\{\mathtt{I}_{1B}^2\} = \mathsf{E}_\Delta\Big\{ \Big(\hat{b}^{(1)} \cdot b^{(2)} \Big\{ I_g^{(2,2)}\{-\Delta, T_I - \Delta; \overline{D}^{(1)} - D^{(2)}\}$$
$$+\ I_g^{(2,2)}\{-\Delta - D^{(2)}, T_I - \Delta - D^{(2)}; \overline{D}^{(1)} + D^{(2)}\}\Big\}\Big)^2\Big\} \qquad (4.24)$$

Substituting (4.18), (4.19) and (4.20) into (4.24) and after averaging over Δ, we obtain

$$\mathsf{E}_\Delta\{\mathtt{I}_{1\mathtt{B}}^2\} \approx \frac{(E_w^{(2)})^2}{\tau_r}\frac{c_1}{2}(1 - e^{\frac{-2T_I}{\tau_r}})(e^{\frac{T_s}{2\tau_r}} - e^{\frac{-T_s}{2\tau_r}})e^{\frac{\overline{D}^{(1)}+D^{(2)}}{\tau_r}}(e^{\frac{(\overline{D}^{(1)}+D^{(2)})}{2\tau_r}} - 1)^{-1}$$

$$\times \ (e^{\frac{(\overline{D}^{(1)}-D^{(2)})}{\tau_r}} - e^{\frac{-(\overline{D}^{(1)}-D^{(2)})}{2\tau_r}})$$

$$\approx \frac{(E_w^{(2)})^2}{T_s}\frac{c_1}{2}(e^{\frac{T_s}{2\tau_r}} - 1)^{-1}(1 - e^{\frac{-2D^{(2)}}{\tau_r}} - e^{\frac{-2T_I}{\tau_r}} - e^{\frac{-2(T_I+D^{(2)})}{\tau_r}})(e^{\frac{T_s}{2\tau_r}} - e^{\frac{-T_s}{2\tau_r}})$$

$$(4.25)$$

Similarly, one finds that $\mathtt{I}_{1\mathtt{B}}$ has zero mean. The second moment of $\mathtt{I}_{1\mathtt{B}}$, can be derived as shown in

$$\mathsf{E}_\Delta\{\mathtt{I}_{1\mathtt{B}}^2\} \simeq \frac{(E_w^{(2)})^2}{T_s}\ c_4\ \sinh(\frac{T_s}{2\tau_r}) \tag{4.26}$$

where $c_4 = c_1(e^{\frac{T_s}{2\tau_r}} - 1)^{-1}(1 - e^{\frac{-2D^{(2)}}{\tau_r}} - e^{\frac{-2T_I}{\tau_r}} - e^{\frac{-2(T_I+D^{(2)})}{\tau_r}})$ and $E_w^{(2)}$ is the average received pulse-energy of user two.

Variances of h_2

We can evaluate the second-order moments of h_2 as

$$\mathsf{E}_\Delta\{h_2\} = \Big\{ \Big(b^{(2)} \cdot I_g^{(1,2)}\{-D^{(1)}, T_I - D^{(1)};$$

$$D^{(1)} + \overline{D}^{(1)} - D^{(2)} - \Delta\}$$

$$+ \ b^{(2)} \cdot I_g^{(2,1)}\{-D^{(1)} + \overline{D}^{(1)}, T_I - D^{(1)} + \overline{D}^{(1)};$$

$$- D^{(1)} + \overline{D}^{(1)} + D^{(2)} + \Delta\}\Big)^2\Big\} \tag{4.27}$$

$$\approx \frac{E_w^{(1)}E_w^{(2)}}{\tau_r}\frac{c_1}{2}e^{(\frac{D^{(1)}+D^{(2)}}{\tau_r})}(1 - e^{\frac{-2T_I}{\tau_r}})(e^{\frac{T_s}{2\tau_r}} - e^{\frac{-T_s}{2\tau_r}})$$

$$\times \ (e^{\frac{T_s}{2\tau_r}} - 1)^{-1}\ (1 + e^{\frac{-T_s}{2\tau_r}})$$

From (4.6), applying similar expressions (4.18), (4.19) and (4.20), further averaging this result over the Δ, we obtain the following variance of $\mathsf{E}_\Delta\{h_2^2\}$ as

$$\mathsf{E}_\Delta\{h_2^2\} \simeq \frac{E_w^{(1)}E_w^{(2)}}{T_s}\ c_3\ e^{(\frac{D^{(1)}+D^{(2)}}{\tau_r})}\ \sinh(\frac{T_s}{2\tau_r}) \tag{4.28}$$

We can straightforwardly extend the obtained results of mean and variances of $h_1^{(1)}$, $h_1^{(2)}$ and h_2 from the case of two users to multiple users case by following a

similar derivation and summing up all terms in (4.15),(4.23),(4.26),(4.28). In the next section, we compare the analytical results with the simulated system model.

4.3.3 Distributions of $h_1^{(1)}$, $h_1^{(2)}$ and h_2

In this section, we discuss the probability density function (PDF) of the model coefficients in (4.7) for the desired signal $(h_1^{(1)})$, the linear MAI component $(h_1^{(2)})$ and the quadratic MAI component (h_2), respectively. The distribution of the model coefficients is useful to obtain measures of performance such as average SIR and average BER. We assume that the interfering users have equal received powers.

The distribution of a set of $h_1^{(1)}$ over channel impulse responses has been generated by computer simulations. It demonstrates a good fit to a lognormal PDF, which is specified by its mean M and standard deviation S in the logarithmic dB scale. These parameters are related to the actual mean μ and standard deviation σ of a lognormal PDF as [54]

$$M[dB] = \frac{10}{\ln(10)} \ln\left(-\frac{\mu^2}{\sqrt{\mu^2 + \sigma^2}}\right)$$
$$S[dB] = \frac{10}{\ln(10)} \sqrt{\left(\ln\frac{\mu^2}{\sigma^2} + 1\right)}$$

A computer simulation has been carried out to validate the accuracy of the analytical results. Fig. 4.2(a) depicts a comparison between the PDF obtained by simulations of a dual-pulse two user scenario and compares it with an approximated PDF. The following parameters of the transmission scheme have been used: $T_s = 300$ ns, $T_c = 0.25$ ns, $\tau_w = 0.25$ ns, $D^{(1)} = 10.25$ ns and $D^{(2)} = 10.5$ ns, with channel parameters $\tau_r = 10$ ns, $\lambda = 5$ rays/ns. In the simulations the pulse $w(t)$ is chosen as the second-derivative of a Gaussian monocycle pulse with effective duration $\tau_w = 0.25$ ns. The lognormal PDF modeling the distribution is shown in dB-values and fitted to a Gaussian PDF over a set of 5000 channel realizations. Moreover, an analytic Gaussian PDF has been derived employing the given analytical results in Subsections 4.3.1 and 4.3.2 for actual mean μ and standard deviation σ. It is shown that the fitted and analytic Gaussian PDFs demonstrate a good fit to represent the desired component of user one. In [55], the authors proposed an approach to calculate an analytical closed-form expression of lognormal PDF for UWB AcR over Nakagami-fading channels.

Fig. 4.2(b) and Fig. 4.2(c) show the distributions of $h_1^{(2)}$ and h_2 generated by computer simulation with parameters as in Fig. 4.2(a). Both are approximated by the Laplacian PDF
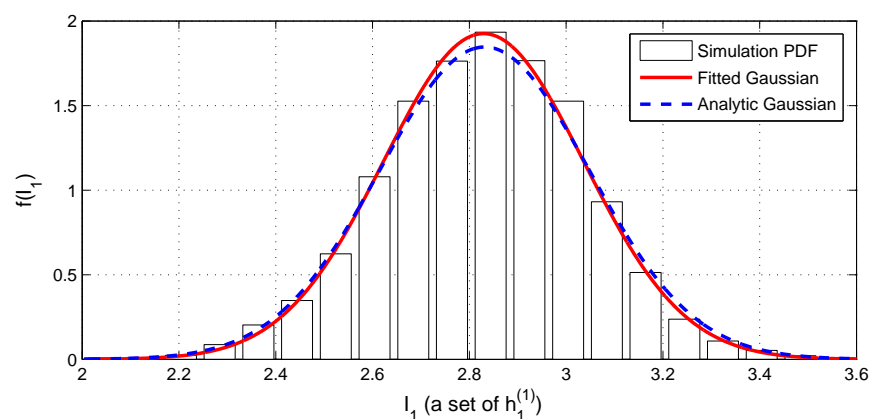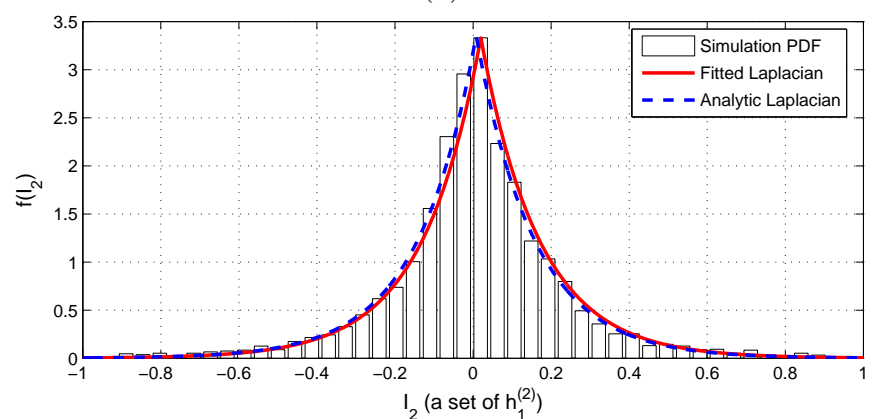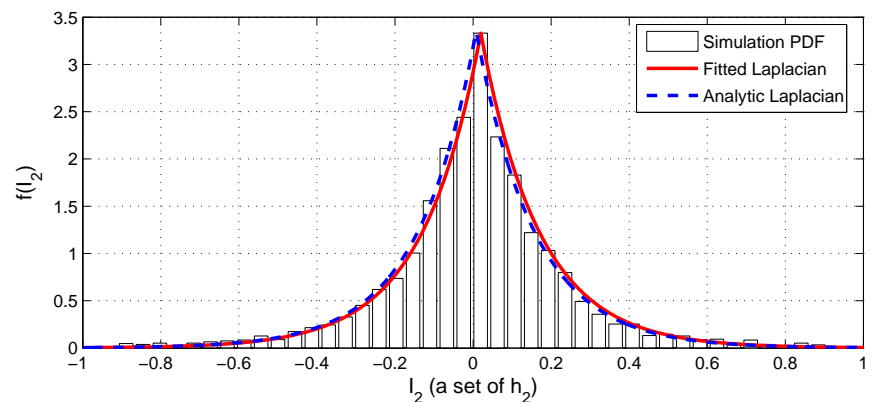
Figure 4.2: Comparison between PDF obtained by simulations of a dual-pulse two users and approximated PDF. (a) A set of $h_1^{(1)}$ approximated by a log-normal distribution in dB-values as Gaussian PDF, fitted to a Gaussian PDF and analytic Gaussian PDF in dB-values; (b) A set of $h_1^{(2)}$ approximated by a Laplace distribution (4.29); (c) A set of h_2 approximated by a Laplace distribution (4.29).

$$f(I_2) = \frac{1}{2s}\exp\left(-\frac{|I_2|}{s}\right) \tag{4.29}$$

where I_2 is a set realization of $h_1^{(2)}$ or h_2 over independent channel realizations, and $2s^2 = \mathsf{E}\{I_2^2\}$ is the variance of I_2, which has been analytically computed in (4.23)-(4.28). We verify the suitability of the Laplace PDF for modeling the distribution of $h_1^{(2)}$ and h_2, comparing the simulated Laplace PDF, the fitted Laplacian PDF over a sets of channel impulse responses and the analytic Laplacian PDF employing the actual mean μ and standard deviation σ, which have been evaluated using the results in Subsection 4.3.1 and 4.3.2. It is shown that the fitted and analytic Laplacian PDFs demonstrate fit to represent $h_1^{(2)}$. The same results hold for the simulation data, fitted Laplacian PDF and analytic Laplace PDF of h_2.

4.3.4 Receiver performance

For the case of no ISI and no noise between reference and data pulses, a simpler expression of the decision variable can be obtained. In this section, we perform the derivation of the SIR in order to study the properties of the channel and system parameters and verify the theoretical analysis. The expression of the received signal $z[i] - h_0$ for the multiuser case without noise can be written as

$$\begin{aligned}
z[i] &= h_0 + \mathbf{h}_1^T \mathbf{d}[i] + \mathbf{h}_2^T(\mathbf{d}[i] \widetilde{\otimes} \mathbf{d}[i]) \\
&= h_0 + h_1^{(1)} d^{(1)}[i] + [\overline{\mathbf{h}}_1^T \ \mathbf{h}_2^T] \begin{bmatrix} \overline{\mathbf{d}}[i] \\ \mathbf{d}[i] \widetilde{\otimes} \mathbf{d}[i] \end{bmatrix} \\
&= h_0 + h_1^{(1)} d^{(1)}[i] + \overline{\mathbf{h}}^T \begin{bmatrix} \overline{\mathbf{d}}[i] \\ \mathbf{d}[i] \widetilde{\otimes} \mathbf{d}[i] \end{bmatrix}
\end{aligned} \tag{4.30}$$

where $\mathbf{d}[i] = [d^{(1)}[i], \cdots, d^{(N_u)}[i]]^T$, $\overline{\mathbf{d}}[i] = [d^{(2)}[i], \cdots, d^{(N_k)}[i]]^T$, $\overline{\mathbf{h}}_1 = [h_1^{(2)}[i], \cdots, h_1^{(N_u)}[i]]^T$, $\mathbf{h}_2$ denotes the quadratic terms, $\overline{\mathbf{h}}^T = [\overline{\mathbf{h}}_1^T \ \mathbf{h}_2^T]$ and $\widetilde{\otimes}$ is a reduced version of the Kronecker product for binary vectors, omitting all redundant duplicate products and trivial squares as defined by

$$\mathbf{d} \widetilde{\otimes} \mathbf{d} = [d^{(1)}d^{(2)}, \cdots, d^{(1)}d^{(K)}, d^{(2)}d^{(3)}, \cdots, d^{(2)}d^{(K)}, d^{(3)}d^{(4)}, \cdots, d^{(K-1)}d^{(K)}] \tag{4.31}$$

The system performance in terms of the channel-averaged SIR of $z[i] - h_0$ can be

evaluated as

$$
\begin{aligned}
SIR\,|_{h_1,h_2} &\triangleq \mathsf{E}\{SIR\} \\[2mm]
&= \frac{(h_1^{(1)})^2 \cdot \mathsf{E}\{(d^{(1)}[i])^2\}}{\mathsf{E}\{(\overline{\mathbf{h}}^T \begin{bmatrix} \overline{\mathbf{d}}[i] \\ \mathbf{d}[i]\,\widetilde{\otimes}\,\mathbf{d}[i] \end{bmatrix})^2\}} \\[2mm]
&= \frac{(h_1^{(1)})^2 \cdot \mathsf{E}\{(d^{(1)})^2\}}{\mathsf{E}\{\overline{\mathbf{h}}^T \begin{bmatrix} \overline{\mathbf{d}} \\ \mathbf{d}\,\widetilde{\otimes}\,\mathbf{d} \end{bmatrix} \begin{bmatrix} \overline{\mathbf{d}} \\ \mathbf{d}\,\widetilde{\otimes}\,\mathbf{d} \end{bmatrix}^T \overline{\mathbf{h}}\}} \\[2mm]
&= \frac{(h_1^{(1)})^2 \cdot 1}{\overline{\mathbf{h}}^T\,\mathsf{E}\{\begin{bmatrix} \overline{\mathbf{d}} \\ \mathbf{d}\,\widetilde{\otimes}\,\mathbf{d} \end{bmatrix} \begin{bmatrix} \overline{\mathbf{d}} \\ \mathbf{d}\,\widetilde{\otimes}\,\mathbf{d} \end{bmatrix}^T\}\,\overline{\mathbf{h}}} \\[2mm]
&= \frac{(h_1^{(1)})^2}{\overline{\mathbf{h}}^T \cdot \mathbf{I} \cdot \overline{\mathbf{h}}} \\[2mm]
&= \frac{(h_1^{(1)})^2}{\|\overline{\mathbf{h}}\|^2}
\end{aligned}
\tag{4.32}
$$

We then derive the SIR of the two-user case where

$$
\begin{aligned}
\overline{SIR} &= \frac{\mathsf{E}\{(h_1^{(1)})^2\}}{\mathsf{E}\{\|\overline{\mathbf{h}}\|^2\}} \\[2mm]
&= \frac{|\,\mathsf{E}\{h_1^{(1)}\}\,|^2}{\mathsf{E}_\Delta\{\mathrm{I}_{1A}^2\} + \mathsf{E}_\Delta\{\mathrm{I}_{1B}^2\} + \mathsf{E}_\Delta\{h_2^2\}}
\end{aligned}
\tag{4.33}
$$

which represents the conditional channel-averaged signal-to-interference ratio (SIR) expression given the specific channel realizations of h_1 and h_2. Note that all terms in the numerator and denominator of (4.33) have been derived in the previous subsection.

4.4 Numerical Results

To validate the analytical results with the simulated dual-pulse TR UWB system, we use the second-derivative Gaussian monocycle pulse with normalized energy. In Fig. 4.3, the simulations are performed for a two-users asynchronous case for 5000 channel realizations with parameters $T_I = 20$ ns, $T_c = 0.25$ ns, $\tau_m = 0.25$ ns, $D^{(1)} = 10.25$ ns and $D^{(2)} = 10.5$ ns. A sampling frequency of 20 GHz was chosen for the simulation. The channel model has an exponentially decaying power delay profile

characterized by $\tau_r = 10$ ns and channel impulse response according to a Poisson process of ray-arrivals at $\lambda = 5$ rays/ns with Rayleigh-distributed ray-magnitudes, i.e., the Nakagami parameter $m = 1$. We plotted the variance of $h_1^{(2)}$ and h_2 for different values of $\frac{T_s}{\tau_r}$. The normalized variance has been introduced, i.e., $\text{vâr}(I_2) = \frac{\mathsf{E}_\Delta\{h_2^2\}}{|\mathsf{E}\{h_1^{(1)}\}|^2}$. Both simulation and analytical results are shown. This confirms the accuracy of the analysis, and the influence of the symbol rate $1/T_s$ on the variance of $h_1^{(2)}$ and h_2. It follows that the variance can be reduced, i.e., the effect of MAI can be considerably mitigated by reducing the symbol rate.
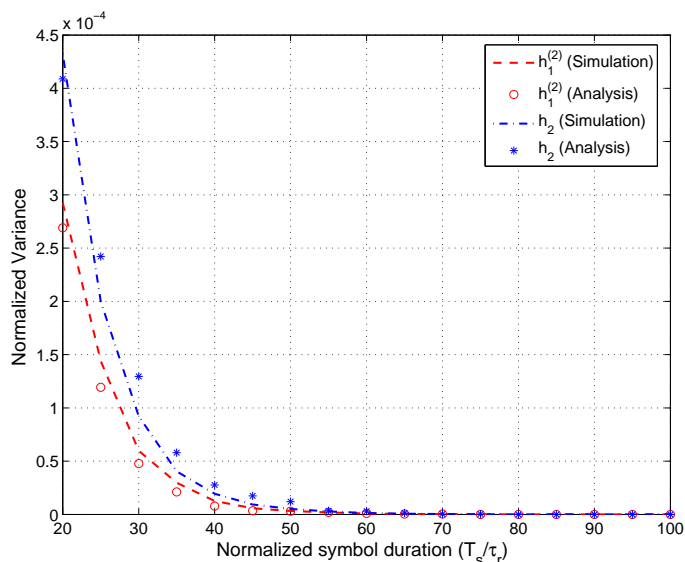
Figure 4.3: Variance of $h_1^{(2)}$ and h_2 for two users. Comparison between the simulated and analytical results for different values of normalized symbol duration $\frac{T_s}{\tau_r}$, with parameters $T_I = 20$ ns, $T_c = 0.25$ ns, $\tau_w = 0.25$ ns, $D^{(1)} = 10.25$ ns and $D^{(2)} = 10.5$ ns; channel model: $\tau_r = 10$ ns, $\lambda = 5$ rays/ns.

Fig. 4.4 shows the comparison of the SIR performance of two asynchronous users for different values of delay for two different systems. The bandwidth of the transmitted signal is determined by the effective duration of τ_w of the second-derivative Gaussian monocycle. Two 5 GHz systems ($\tau_w = 0.25$ ns): $D^{(1)} = 0.25$ ns and $D^{(2)} = 0.25$ ns, and $D^{(1)} = 10.25$ ns and $D^{(2)} = 10.50$ ns and one 500 MHz system ($\tau_w = 2.5$ ns): $D^{(1)} = 20$ ns and $D^{(2)} = 22.5$ ns, have been compared. We notice that $c_1 \approx \frac{\tau_w}{2}$ in (4.23),(4.26),(4.28) [53] for a second-derivative Gaussian pulse with effective length τ_w. It is shown that the system using the delays excess $\tau_r = 10$ ns outperforms the system using a delay less than τ_r (for the 5 GHz system). This par-
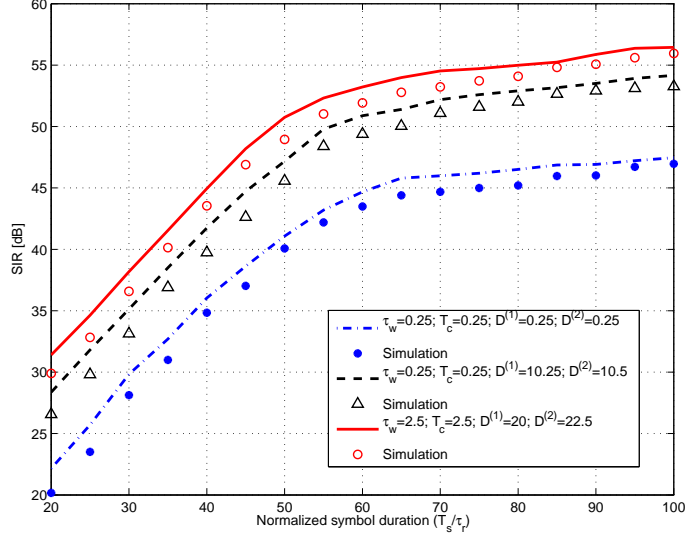
Figure 4.4: SIR receiver performance of two users. Comparison between the simulated and analytical results for different values of delay hopping code D and different values of normalized symbol duration $\frac{T_s}{\tau_r}$, channel model: $\tau_r = 10$ ns, $\lambda = 5$ rays/ns.

ticularly holds in a special worst-case scenario of equal short delays. This is because the system with short delay suffers from inter-pulse interference (IPI) among users. The performance results indicate to increase the delay to be larger than the channel delay spread τ_r to achieve better SIR performance, with a trade-off in hardware and implementation complexity due to a long delay.

Fig. 4.5 gives an understanding of the impact of MAI on the SIR system performance with well chosen design parameters. The SIR is shown for a 5 GHz system with $\tau_w = 0.25$ ns, $D^{(1)} = 10.25$ ns and delay of $D^{(k)}$ with increments of 0.25 ns for $2 \leq k \leq 30$. The obtained results of mean and variances of $h_1^{(1)}$, $h_1^{(2)}$ and h_2 from the two-user case can be extended to the multiple user case by following the procedure of Section 4.3.1 and 4.3.2 and summing up all possible terms (c.f. (4.15),(4.23),(4.26),(4.28)). As expected, the SIR performance drops for an increased number of users.

4.5 Summary

We studied the performance of a dual-pulse TR UWB multiple access system with a memoryless multiuser AcR Volterra equivalent system model. An analytical expres-
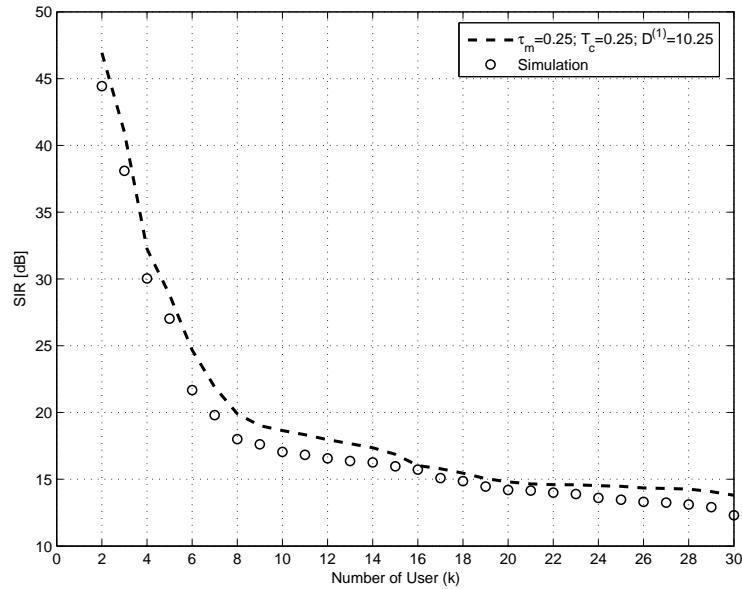
Figure 4.5: SIR receiver performance as a function of different number of users. Comparison between the simulated and analytical results for a value of delay hopping code D.

sion of channel-averaged SIR has been obtained by statistical characterization as a function of system and channel parameters. In the numerical results, the receiver performance of SIR is validated by simulation. The numerical results further show the constraint relationship between the bit rate and the chosen delay hopping code with the impact of MAI in dual-pulse TR UWB. In future work, the presented results can be applied to evaluate and possibly optimize certain system design choices under various design constraints.

5 Energy Detection UWB Systems in Presence of Multiuser Interference

Noncoherent receivers are attractive for pulsed UWB systems due to the implementation simplicity [56, 16, 57, 58, 59]. Energy detection receivers are appealing to IEEE 802.15.4a low data rate (LDR) networks because of their low complexity [60, 61, 62]. With a reasonable energy consumption, these receivers can exploit the ranging capabilities and multipath resistance of impulse-radio UWB (IR-UWB) [16, 17]. This receiver is a promising candidate for low-cost low-power UWB receiver implementation, which relies on LDR wireless capabilities. They make no attempts to gather information on the channel response. For example, assume binary pulse position modulation (2-PPM) with rate $1/T$. Symbol zero corresponds to transmitting a pulse in the first half of the interval $(0, T)$ while symbol one corresponds to transmitting a pulse in the second half. Its data decisions are based only on signal energy measurements. The receiver measures the signal energies on both halves and selects the symbol with the largest energy. However, the performance of energy-detection receivers can be severely degraded by multiple-access interference (MAI). The simplicity of this approach comes at the cost of a lower immunity to interference coming from other users or other systems. This energy-capture scheme appears as a valid solution in terms of complexity, cost and power consumption.

In some literature, the weighted receivers for transmitted reference and noncoherent receivers have been investigated [7, 63]. In [63], the weighted autocorrelation receiver (AcR) has been studied taking inter-symbol interference (ISI) into account. The linear weighting coefficients of the fractionally sampled receiver are computed in a closed form using the minimum mean-square error (MMSE) and maximum ratio combining (MRC) criteria. A simple yet flexible receiver is proposed based on a weighted receiver [7] for energy detection. However, in spite of the low duty cycle usually exhibited by UWB signals, some of the envisioned application scenarios imply that multiple competing transmissions produce harmful collisions. This chapter will be devoted to such issues with the aim to properly consider the effects and to cope with multiple-access interference (MAI) at the physical layer (PHY) level in IR-UWB systems for an energy detection receiver. In presence of multiple users, single-user detection is typically suboptimal and special effort is needed to cope with MAI effects utilizing weighting coefficients. The weighting coefficients for the weighted energy

detection receiver will be derived based on maximization of a signal-to-interference metric in a single and multiuser scenario [28].

5.1 Description of the System and Definition of the Terms

We consider a typical IEEE 802.15.4a transmitted signal for the time-hopping (TH) asynchronous Burst Position Modulation (BPM) energy detector communications system which employs the time-hopping (TH) scheme [64]. The transmitted signal consists of N_c time-shifted low duty cycle pulses. Assuming N_u users are active in the network, these users transmit information asynchronously through different propagation channels. A typical TH UWB BPM signal is of the form

$$
\begin{aligned}
s^{(k)}(t) &= \sum_{i=-\infty}^{\infty} a_{1i}^{(k)} \sum_{j=0}^{N_c-1} c_j^{(k)} w(t - iT_s - h_i^{(k)}T_B - jT_c - a_{0i}^{(k)}\Delta_{bpm}) \\
&= \sum_{i=-\infty}^{\infty} a_{1i}^{(k)} \sum_{j=0}^{N_c-1} c_j^{(k)} w(t - iT_s - (h_i^{(k)}N_c + j)T_c - a_{0i}^{(k)}\Delta_{bpm})
\end{aligned}
\tag{5.1}
$$

where t is time, $s^{(k)}(t)$ is the kth user's signal conveying the ith data bit, and $w(t)$ is the unit-energy transmitted pulse waveform with the signal pulse width, normalized so that $\int_{-\infty}^{\infty} w^2(t)dt = 1$. The parameters employed in this UWB model are described as follows:

- N_c is the number of pulses required to convey each information bit, called the length of the repetition code in one burst period.

- $c_j^{(k)}$ is the user-specific "scrambling code" of values $\{-1, 1\}$ with equal probabilities.

- T_s is the symbol duration.

- T_c is the duration of the time slot, *i.e.* the so-called chip time interval.

- Δ_{bpm} is Burst Position Modulation (BPM) which is set as $N_h T_B + T_g$, to avoid inter-symbol interference (ISI). We therefore neglect the effect of ISI in this study. T_g denotes the guard time which is set to be half of Δ_{bpm}.

- $h_i^{(k)}$ represents the TH burst position for the kth source. It is pseudo-random with each element taking an integer value, i.e., $h_i^{(k)} \in \{0, 1, \cdots, N_h - 1\}$ with equal probability, where N_h is the number of hop-positions.

- T_B is the burst duration which is further defined as $T_B = N_c T_c$.

- $a_{0i}^{(k)}$ represents the ith binary data bit transmitted by the kth source, and different bits are assumed to be equiprobable, where $a_{0i}^{(k)} \in \{0, 1\}$. The data bits of each user are assumed to be an independent and identically distributed (i.i.d) random sequence.

- $a_{1i}^{(k)}$ represents BPSK symbol values $\{-1, 1\}$ with equal probabilities that randomizes the polarity of the transmitted pulses to smoothen the power spectrum of the signal.

5.2 Conventional Energy Detection Receiver

Fig. 5.1 shows the architecture of the energy receiver for a low-cost low-power implementation of a UWB energy detection system. The received signal of the antenna is passed through a filter of impulse response $f_{rx}(t)$, a square law device, the integrators and dumps and a decision device.
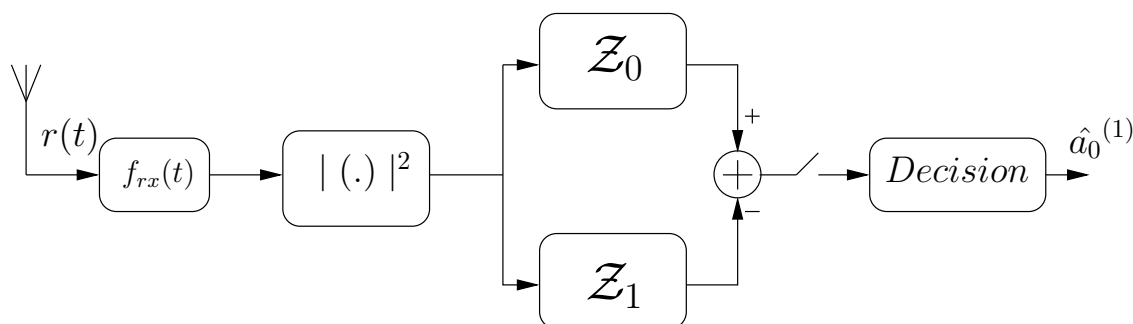
Figure 5.1: Block diagram of the energy receiver.

After transmission through the channel and, assuming the desired signal is from transmitter without loss of generality, the composite received signal $r(t)$ of the energy detection UWB BPM receiver corresponding to the bit $i = 0$, can be divided into three portions which are signals from the transmitter $k = 1$ as $s(t)$, signals from the undesired transmitter $v_m(t)$, and the receiver noise $n(t)$.

$$\hat{r}(t) = s(t) + v_m(t) + n(t) \tag{5.2}$$

where

$$s^{(1)}(t) = a_1^{(1)} \sum_{j=0}^{N_c-1} c_j^{(1)} g^{(1)}(t - (h^{(1)}N_c + j)T_c - a_0^{(1)}\Delta_{bpm}) \tag{5.3}$$

$$v_m(t) = \sum_{k=2}^{N_u} a_1^{(k)} \sum_{j=0}^{N_c-1} c_j^{(k)} g^{(k)}(t - (h^{(k)} N_c + j)T_c - a_0^{(k)} \Delta_{bpm} - \tau^{(k)}) \qquad (5.4)$$

and $g^{(k)}(t) = h^{(k)}(t) * w(t) * f_{rx}(t)$ is the response of the channel to one transmitted monocycle at $t = 0$. $f_{rx}(t)$ is the impulse response of the front-end filter of the receiver and $*$ denotes linear convolution. $h(t)$ denotes the channel impulse response (CIR) of the UWB radio channel. We have assumed $\tau^{(1)} = 0$ without loss of generality because of the perfect synchronization to transmitter 1. The other users' asynchronous transmission delays relative to the first user, namely $\tau^{(k)}$, are i.i.d. random variables and uniformly distributed over $[0, T_s)$. $n(t)$ is additive white Gaussian noise (AWGN) with two-sided power spectral density of $\frac{N_0}{2}$. It is assumed that both the desired user and all the interfering users experience independent channel realizations, and parameters of the interferers may not be necessarily identical to those of the desired user. We notice that, due to the guard intervals, only one pulse burst of each user's signal will be overlapping within the integration window $[0, T_I)$.

The symbol $a_0^{(k)}$ is mapped by the BPM transmitter and the propagation channel to the received signal $r(t)$, which depends on the transmitted symbol, on the modulation details, on the scrambling code and on the actual received pulse or channel impulse response realization. The receiver captures two samples $\mathcal{Z}_0$ and $\mathcal{Z}_1$ at the distance of Δ_{bpm} seconds. In a conventional energy detection receiver, it is assumed that $\mathcal{Z}_0$ and $\mathcal{Z}_1$ are statistically independent, the decision variable $\mathcal{Z}$ [16, 25] for the ith bit under the assumption of perfect synchronization for the desired user's signal is defined as

$$\begin{aligned}
\mathcal{Z} &= \mathcal{Z}_0 - \mathcal{Z}_1 \\
&= \int_{h^{(1)}T_B}^{h^{(1)}T_B+T_I} r^2(t)\ dt - \int_{\Delta_{bpm}+h^{(1)}T_B}^{\Delta_{bpm}+h^{(1)}T_B+T_I} r^2(t)\ dt \\
&= \int_{h^{(1)}N_cT_c}^{h^{(1)}N_cT_c+T_I} r^2(t)\ dt - \int_{\Delta_{bpm}+h^{(1)}N_cT_c}^{\Delta_{bpm}+h^{(1)}N_cT_c+T_I} r^2(t)\ dt
\end{aligned} \qquad (5.5)$$

We assume that the transmitted symbol is 0, i.e., $a_0^{(1)} = 0$ which produces $\hat{a}_0^{(1)} = 0$ for $\mathcal{Z} \geq 0$ and $\hat{a}_0^{(1)} = 1$ for $\mathcal{Z} < 0$.

Substitute (5.2) into (5.5) leads to 9 components shown in table 5.1 and 5.2. Table 5.1 shows that two noise/interference variables in symmetric positions of the diagonal occur for the same reason in the first sample of $\mathcal{Z}_0$. The signal from transmitter 1 and the interfering transmitter's signals produce $\mathcal{Z}_{0,am}$ and $\mathcal{Z}_{0,ma}$. Both $\mathcal{Z}_{0,an}$ and $\mathcal{Z}_{0,na}$ are the correlation result of the signal from transmitter one and the receiver noise. The interfering transmitter's signals and the receiver noise generate $\mathcal{Z}_{0,mn}$ and $\mathcal{Z}_{0,nm}$. Hence two noise/interference variables which are symmetric have the same variance. We propose to analyze these terms in the following section in order

to evaluate the performance of the proposed weighted coefficient receiver for energy detection in a multiple access environment. Using a similar definition for the second sample of $\mathcal{Z}_0$ we can define the table 5.2.

	$s(t)$	$v_m(t)$	$n(t)$
$s(t)$	$\mathcal{Z}_{0,a}$	$\mathcal{Z}_{0,am}$	$\mathcal{Z}_{0,an}$
$v_m(t)$	$\mathcal{Z}_{0,ma}$	$\mathcal{Z}_{0,mm}$	$\mathcal{Z}_{0,mn}$
$n(t)$	$\mathcal{Z}_{0,na}$	$\mathcal{Z}_{0,nm}$	$\mathcal{Z}_{0,nn}$

Table 5.1: Signal, MAI, and noise in a decision statistic of an energy detection receiver in the first sample of $\mathcal{Z}_0$ in a multiple access environment.

	$s(t)$	$v_m(t)$	$n(t)$
$s(t)$	$\mathcal{Z}_{1,a}$	$\mathcal{Z}_{1,am}$	$\mathcal{Z}_{1,an}$
$v_m(t)$	$\mathcal{Z}_{1,ma}$	$\mathcal{Z}_{1,mm}$	$\mathcal{Z}_{1,mn}$
$n(t)$	$\mathcal{Z}_{1,na}$	$\mathcal{Z}_{1,nm}$	$\mathcal{Z}_{1,nn}$

Table 5.2: Signal, MAI, and noise in a decision statistic of an energy detection receiver in the second sample of $\mathcal{Z}_1$ in a multiple access environment.

5.3 Weighted Energy Detection Receiver for Multiple Access

In this section, we evaluate the multiple-access performance analysis for the energy detection receiver with a weighted receiver, which multiplies some weighting function on the output of decision variable $\mathcal{Z}$, to alleviate the multiple-access and noise effects in noncoherent energy detection. Firstly, we discuss and derive a weighted receiver to alleviate the noise effect in noncoherent energy detection taking into account the property of the instantaneous channel impulse response (CIR) in a similar fashion as [7] but for the multi-user scenario. The main difference with that work is that the BPM signal model follows the waveform for the IEEE 802.15.4a standard. The goal of this section is to provide details for the weighting coefficient for a noncoherent receiver that requires the knowledge of the instantaneous power delay profile (IPDP) [65, 66] of the channel realization and to compare it to the conventional noncoherent receiver without weighting coefficient implementation. In the sequel, we assume that only the

IPDP for all users are available at the receiver side, then $g^{(k)}(t) = q^{(k)}(t) \times \zeta^{(k)}(t)$, where $q^{(k)}(t)$ and $\zeta^{(k)}(t)$ denote the magnitudes of the channel impulse response (i.e., the IPDP is defined as $[q^{(k)}(t)]^2$) and the signs of $g^{(k)}(t)$, respectively.

Channels are assumed invariant over one symbol interval and, without loss of generality, the the decision statistic is evaluated as

$$
\begin{aligned}
\mathcal{Z} = \mathcal{Z}_0 - \mathcal{Z}_1 &= \sum_{l=0}^{L-1} w_l \left(\mathcal{Z}_0^l - \mathcal{Z}_1^l \right) \\
&= \sum_{l=0}^{L-1} w_l \int_{(h^{(1)}N_c+l)T_c}^{(h^{(1)}N_c+l)T_c+T_I} r^2(t) \ dt - \sum_{l=0}^{L-1} w_l \int_{\Delta_{bpm}+(h^{(1)}N_c+l)T_c}^{\Delta_{bpm}+(h^{(1)}N_c+l)T_c+T_I} r^2(t) \ dt \quad (5.6) \\
&= \sum_{l=0}^{L-1} w_l \int_{(h^{(1)}N_c+l)T_c}^{(h^{(1)}N_c+l+1)T_c} r^2(t) \ dt - \sum_{l=0}^{L-1} w_l \int_{\Delta_{bpm}+(h^{(1)}N_c+l)T_c}^{\Delta_{bpm}+(h^{(1)}N_c+l+1)T_c} r^2(t) \ dt
\end{aligned}
$$

where L is the number of integration sub-intervals, which corresponds to the number of pulses transmitted per symbol and the integration interval T_I is chosen as T_c, and the starting time of the sub-interval integral is denoted by $t_l = lT_c$, $\{l = 0, 1, \cdots N_c - 1\}$.

The optimal weight vector used for combining the energy detection receiver and for estimating the desired user data is the one that minimizes the BER of the receiver. Hence, the optimal detector applies a weighting function with coefficients w_l prior to comparing the energies in the first and second half of a data symbol. To generate the decision statistic for a_0, each of $2L$ sub-interval integration outputs $\mathcal{Z}_0^l$ and $\mathcal{Z}_1^l$ is multiplied by a weighting coefficients w_l and then combined linearly.

We assume the sub-integration outputs of (5.5) are uncorrelated for $l \neq l'$ because of the polarity codes. After summing the L weighted outputs, the desired user transmitted bits are estimated according to the above detection scheme. To evaluate the bit-error rate (BER) performance of the energy detection receiver, we investigate the desired signal as well as the second-order moments of the noise and all interference terms. It has been suggested that a Gaussian approximation can be used, since the MAI and noise can be decomposed in a sum of independent random variables. Hence the central limit theorem (CLT) can be applied. Then, we use the Q-function to evaluate the BER conditioned on the magnitude channel realization for all users and then take the average of Q-function over many channel realizations to finally obtain the optimal weighting coefficients.

$$
\mathrm{P}_e = Q(\frac{\mu_z}{\sigma_z}) \tag{5.7}
$$

where the mean of $\mu_z = \mathsf{E}\{\mathcal{Z}|a^{(1)} = 0\}$ and the variance of $\sigma_z^2 = \mathrm{var}\{\mathcal{Z}|a^{(1)} = 0\}$. The symbol $Q[.]$ denotes the Q-function defined as $Q[z] = \int_z^\infty \frac{1}{\sqrt{2\pi}} \exp(-\frac{y^2}{2}) \ dy$.

The BER is minimized with $Q(\frac{\mu_z}{\sigma_z}) = Q(\frac{\mathbf{w}^T \mathbf{h}}{\sqrt{\mathbf{w}^T \Sigma \mathbf{w}}})$ when the metric function $J(w)$ is maximized using the derivative condition

$$\frac{dJ(w)}{dw} = \frac{d}{dw}\left(\frac{\mathbf{w}^T \mathbf{h}}{\sqrt{\mathbf{w}^T \Sigma \mathbf{w}}}\right) = 0. \tag{5.8}$$

The way to find the weighting coefficients is based on maximation of the metric function as derived in Appendix A.1. The detector weight vector is defined as $\mathbf{w}$. The vector of the signal energy signal is defined as $\mathbf{h}$. Σ represents the matrix of collection variances and integrations.

5.4 Selection of Weighting Coefficients

The selection of weighting coefficients can be calculated by using the means and variances of $\mathcal{Z}$ conditioned on $a_0^{(1)} = 0$, respectively, as

$$\mu_z = \sum_{l=1}^{L} w_l \mu_l = \sum_{l=1}^{L} w_l(\mu_{0,l} - \mu_{1,l})$$

$$\sigma_z^2 = \sum_{l=1}^{L} w_l^{(2)} \sigma_l^2 = \sum_{l=1}^{L} w_l(\sigma_{0,l}^2 + \sigma_{1,l}^2) \tag{5.9}$$

where $\mu_{0,l}$ and $\mu_{1,l}$ are the means of the first and second sample of $\mathcal{Z}_1$, respectively. $\sigma_{0,l}^2$ and $\sigma_{1,l}^2$ are the variances of the first and second sample of $\mathcal{Z}_1$, respectively.

Assuming perfect estimation of the scrambling codes, the information about the codes is available at the receiver. The IPDP of all users is fully available at the receiver. That is, the receiver is perfectly locked to the signal from the user $k = 1$. Thus, letting the decision variable for the multiuser case in the first sample of $\mathcal{Z}_0$ be conditioned on $a_0^{(1)} = 0$, is obtained as

$$\mathcal{Z}_0 = \sum_{l=0}^{L-1} w_l \int_{(h^{(1)}N_c+l)T_c}^{(h^{(1)}N_c+l+1)T_c} \left\{ a_1^{(k)} \sum_{n=0}^{N_c-1} c_n^{(k)} q^{(k)}(t - h^{(1)}T_B - nT_c - a_0^{(1)}\Delta_{bpm}) \right.$$

$$\times \, a_1^{(k)} \sum_{m=0}^{N_c-1} c_m^{(k)} q^{(k)}(t - h^{(1)}T_B - mT_c - a_0^{(1)}\Delta_{bpm}) \right\} dt$$

$$= \sum_{l=0}^{L-1} w_l \left[\mathcal{Z}_{0,a}^l + 2\mathcal{Z}_{0,am}^l + 2\mathcal{Z}_{0,an}^l + 2\mathcal{Z}_{0,mn}^l + \mathcal{Z}_{0,mm}^l + \mathcal{Z}_{0,nn}^l \right] \tag{5.10}$$

where $\mathcal{Z}_{0,a}^l$, $\mathcal{Z}_{0,am}^l$, $\mathcal{Z}_{0,an}^l$, $\mathcal{Z}_{0,mn}^l$, $\mathcal{Z}_{0,mm}^l$, and $\mathcal{Z}_{0,nn}^l$ represent the desired signal, cross-terms signal by MAI, signal by noise, MAI by noise, MAI by MAI, and the quadratic noise term, respectively. The decision statistic in the second sample of $\mathcal{Z}_1$ for a single user can be written as

$$
\begin{aligned}
\mathcal{Z}_1 &= \sum_{l=0}^{L-1} w_l \int_{\Delta_{bpm}+(h^{(1)}N_c+l)T_c}^{\Delta_{bpm}+(h^{(1)}N_c+l+1)T_c} \left\{ a_1^{(k)} \sum_{n=0}^{N_c-1} c_n^{(k)} q^{(k)}(t - h^{(1)}T_B - nT_c - a_0^{(1)}\Delta_{bpm}) \right. \\
&\quad \left. \times\; a_1^{(k)} \sum_{m=0}^{N_c-1} c_m^{(k)} q^{(k)}(t - h^{(1)}T_B - mT_c - a_0^{(1)}\Delta_{bpm}) \right\} dt \\
&= \sum_{l=0}^{L-1} w_l \left[\mathcal{Z}_{1,mm}^l + 2\mathcal{Z}_{1,mn}^l + \mathcal{Z}_{1,nn}^l \right]
\end{aligned}
$$

$$(5.11)$$

where $\mathcal{Z}_{1,mm}^l$, $\mathcal{Z}_{1,mn}^l$, and $\mathcal{Z}_{1,nn}^l$ represent co-terms MAI by MAI, cross-terms MAI by noise and quadratic noise term, respectively.

In the next subsection, we will derive the collection terms of means and variances in the first sample of $\mathcal{Z}_0$ in a multiple access environment. Using a similar approach we can simply derive the collection terms of means and variances in the second sample of $\mathcal{Z}_1$.

5.4.1 Desired Signal Term

Assuming bit $a_0^{(1)} = 0$ is transmitted, the contribution to the decision statistic depending on the useful signal of interest $\mathcal{Z}_{0,a}^l$ is given as

$$
\begin{aligned}
\mathcal{Z}_{0,a}^l &= \int_{(h^{(1)}N_c+l)T_c}^{(h^{(1)}N_c+l+1)T_c} \left\{ a_1^{(1)} \sum_{n=0}^{N_c-1} c_n^{(1)} q^{(1)}(t - h^{(1)}T_B - nT_c) \right. \\
&\quad \left. \times\; a_1^{(1)} \sum_{m=0}^{N_c-1} c_m^{(1)} q^{(1)}(t - h^{(1)}T_B - mT_c) \right\} dt \\
&= (a_1^{(1)})^2 \sum_{n=0}^{N_c-1} \sum_{m=0}^{N_c-1} c_n^{(1)} c_m^{(1)} \int_{(h^{(1)}N_c+l)T_c}^{(h^{(1)}N_c+l+1)T_c} q^{(1)}(t - (h^{(1)}N_c + n)T_c) \\
&\quad \times\; q^{(1)}(t - (h^{(1)}N_c + m)T_c) \; dt
\end{aligned}
$$

$$(5.12)$$

It is also to be noted that we use the definition of the ACF of the received pulse (RP-ACF) defined as $I_{qq}(a, T_I; \tau) = \int_a^{a+T_I} q(t) \, q(t+\tau) \, dt$. Then the RP-ACF matrix

of $\mathbf{R}_q^l$ is further represented as

$$
\begin{aligned}
\mathbf{R}_q^l &= \int_{(h^{(1)}N_c+l)T_c}^{(h^{(1)}N_c+l+1)T_c} q(t-(h^{(1)}N_c+n)T_c)\ q(t-(h^{(1)}N_c+m)T_c)\ dt \\
&= I_q^l((l-n)T_c, T_I; (n-m)T_c)
\end{aligned}
\tag{5.13}
$$

After some necessary mathematical substitution as shown in [25], the desired signal can be written as

$$
\begin{aligned}
\mathcal{Z}_{0,a}^l &= (a_1^{(1)})^2 \sum_{n=0}^{N_c-1}\sum_{m=0}^{N_c-1} c_n^{(1)} c_m^{(1)}\ I_q^l((l-n)T_c, T_I; (n-m)T_c) \\
&= s_0 \mathbf{c}^T \mathbf{R}_q^l \mathbf{c} \\
&= E_b(a_1^{(1)})^2 \frac{1}{E_b} \sum_{\mu=-N_c+1}^{N_c-1}\sum_{m=0}^{N_c-1} c_m^{(1)} c_{m-\mu}^{(1)}\ I_q^l([l-m-\mu]T_c, T_I; \mu T_c) \\
&= s_0 E_b p^l
\end{aligned}
\tag{5.14}
$$

where $s_0 = (a_1^{(1)})^2$ and $p^l = \frac{1}{E_b}\sum_{\mu=-N_c+1}^{N_c-1}\sum_{m=0}^{N_c-1} c_m^{(1)} c_{m-\mu}^{(1)}\ I_q^l([l-m-\mu]T_c, T_I; \mu T_c) = (\mathbf{r}_q^l)^T \mathbf{r}_c$ with $\mathbf{r}_q^l = I_q^l(lT_c, T_I; \mu T_c)$ is the channel autocorrelation sequence. The scrambling code sequence is represented as $\mathbf{c} = [c_0, c_1, \cdots, c_{N_c-1}]^T$ and the autocorrelation vector $\mathbf{r}_c$ of the code sequence is written as $[\mathbf{r}_c]_\mu = \sum_{\mu=-N_c+1}^{N_c-1}\sum_{m=0}^{N_c-1} c_m^{(1)} c_{m-\mu}^{(1)}$ with dimension $2N_c - 1$. In evaluating the mean of the desired signal $\mathcal{Z}_{0,a}^l$ with respect to averaging over the code vector $\mathbf{c}$, we consider the following expression, whose contribution to the lth sub-integration interval can be written as

$$
\begin{aligned}
\mathsf{E}_\mathbf{c}\{\mathcal{Z}_{0,a}^l\} = \mathsf{E}\Big\{ &\sum_{n=0}^{N_c-1}\sum_{m=0}^{N_c-1} c_n^{(1)} c_m^{(1)} \int_{(h^{(1)}N_c+l)T_c}^{(h^{(1)}N_c+l)T_c+T_I} q(t-(h^{(1)}N_c+n)T_c) \\
&\times\ q(t-(h^{(1)}N_c+m)T_c)\ dt \Big\}
\end{aligned}
\tag{5.15}
$$

where $E\{c_n^{(1)}c_m^{(1)}\} = 1$ for $n = m$ and $E\{c_n^{(1)}c_m^{(1)}\} = 0$ for $n \neq m$. We can rewrite

$$
\begin{aligned}
E_{\mathbf{c}}\{\mathcal{Z}_{0,a}^l\} &= \sum_{m=0}^{N_c-1} \int_{(h^{(1)}N_c+l)T_c}^{(h^{(1)}N_c+l)T_c+T_I} q^2(t - (h^{(1)}N_c + m)T_c)dt \\
&= \sum_{m=0}^{N_c-1} \int_{lT_c}^{lT_c+T_I} q^2(\xi - mT_c)d\xi \\
&= \sum_{m=0}^{N_c-1} \int_{0}^{0+T_I} q^2(\xi + [l - m]T_c)d\xi \\
&= \sum_{m=0}^{N_c-1} I_q([l - m]T_c, T_I; 0)
\end{aligned}
\tag{5.16}
$$

where $\xi = t - h^{(1)}N_cT_c$. It follows that we need to evaluate the variance of the desired signal with respect to averaging over the code vector $\mathbf{c}$. This can be written as

$$
\text{var}_{\mathbf{c}}\{|\mathcal{Z}_{0,a}^l|\} = E_{\mathbf{c}}\{|\mathcal{Z}_{0,a}^l|^2\} - |E_{\mathbf{c}}\{\mathcal{Z}_{0,a}^l\}|^2
\tag{5.17}
$$

$$
\begin{aligned}
E_{\mathbf{c}}\{|\mathcal{Z}_{0,a}^l|^2\} &= E_{\mathbf{c}}\Bigg\{ \sum_{n=0}^{N_c-1}\sum_{m=0}^{N_c-1} c_n^{(1)}c_m^{(1)} \, I_q^l((l - n)T_c, T_I; (n - m)T_c) \\
&\quad \times \sum_{n'=0}^{N_c-1}\sum_{m'=0}^{N_c-1} c_{n'}^{(1)}c_{m'}^{(1)} \, I_q^l((l - n')T_c, T_I; (n' - m')T_c) \Bigg\} \\
&= E_{\mathbf{c}}\Bigg\{ \sum_{\mu=-N_c+1}^{N_c-1}\sum_{m=0}^{N_c-1} c_m^{(1)}c_{m-\mu}^{(1)} \, I_q^l([l - m - \mu]T_c, T_I; \mu T_c) \\
&\quad \times \sum_{\mu'=-N_c+1}^{N_c-1}\sum_{m'=0}^{N_c-1} c_{m'}^{(1)}c_{m'-\mu'}^{(1)} \, I_q^l([l - m' - \mu']T_c, T_I; \mu' T_c) \Bigg\}
\end{aligned}
\tag{5.18}
$$

where $E\{c_m c_{m-\mu} c_{m'} c_{m'-\mu'}\} = 1$ if $\mu = 0$ and $\mu' = 0$ or if $m = m'$ and $\mu = \mu'$. We can rewrite $E_{\mathbf{c}}\{|\mathcal{Z}_{0,a}^l|^2\}$ as

$$
\begin{aligned}
E_{\mathbf{c}}\{|\mathcal{Z}_{0,a}^l|^2\} &= \sum_{m=0}^{N_c-1}\sum_{m'=0}^{N_c-1} I_q([l - m]T_c, T_I; 0)I_q([l - m']T_c, T_I; 0) \\
&\quad + \sum_{m=0}^{N_c-1}\sum_{\substack{\mu=-N_c+1 \\ \mu \neq 0}}^{N_c-1} I_q^2([l - m - \mu]T_c, T_I; \mu T_c)
\end{aligned}
\tag{5.19}
$$

Then, the variance of the desired signal term at the output of the receiver can be rewritten as

$$\text{var}_{\mathbf{c}}\{|\mathcal{Z}_{0,a}^l|\} = \sum_{m=0}^{N_c-1} \sum_{\substack{\mu=-N_c+1 \\ \mu\neq 0}}^{N_c-1} I_q^2([l-m-\mu]T_c, T_I; \mu T_c) \tag{5.20}$$

5.4.2 Signal by Noise Terms

Next, following a similar approach as in (5.12), we define the cross terms signal-times-noise $\mathcal{Z}_{0,an}^l$ and $\mathcal{Z}_{0,na}^l$ which are symmetric and have the same variance, thus the computation can be used twice. $I_{qn}(a, T_I; \tau) = \int_a^{a+T_I} q(t)\, n(t+\tau)\, dt.$

$$\mathcal{Z}_{0,an}^l = \int_{(h^{(1)}N_c+l)T_c}^{(h^{(1)}N_c+l)T_c+T_I} a_1^{(1)} \sum_{n=0}^{N_c-1} c_n^{(1)} q(t - h^{(1)}T_B - nT_c)\, n(t) \tag{5.21}$$

For simplicity, $\mathsf{E}\{\mathcal{Z}_{0,an}^l\} = 0$ is given because $n(t)$ is zero-mean.

We need to evaluate the second-order moment of the cross terms with respect to averaging over the code vector $\mathbf{c}$ and noise. By following a similar step as derived in subsection (5.4.1), we obtain the variance of $\mathcal{Z}_{0,an}^l$, $\text{var}_{\mathbf{c}}\{|\mathcal{Z}_{0,an}^l|\} = \mathsf{E}_{\mathbf{c}}\{|\mathcal{Z}_{0,an}^l|^2\}$ as

$$\mathsf{E}_{\mathbf{c}}\{|\mathcal{Z}_{0,an}^l|^2\} = \mathsf{E}\left\{ \left[\int_{(h^{(1)}N_c+l)T_c}^{(h^{(1)}N_c+l)T_c+T_I} a_1^{(1)} \sum_{n=0}^{N_c-1} c_n^{(1)} q(t - h^{(1)}T_B - nT_c)\, n(t)dt \right]^2 \right\}$$

$$+ \mathsf{E}\left\{ \left[\int_{(h^{(1)}N_c+l)T_c}^{(h^{(1)}N_c+l)T_c+T_I} a_1^{(1)} \sum_{m=0}^{N_c-1} c_m^{(1)} q(t - h^{(1)}T_B - mT_c)\, n(t)dt \right]^2 \right\}$$

$$+ 2\mathsf{E}\left\{ \left[\int_{(h^{(1)}N_c+l)T_c}^{(h^{(1)}N_c+l)T_c+T_I} \int_{(h^{(1)}N_c+l)T_c}^{(h^{(1)}N_c+l)T_c+T_I} a_1^{(1)} a_1^{(1)} \sum_{n=0}^{N_c-1} \sum_{m=0}^{N_c-1} c_n^{(1)} c_m^{(1)} \right.\right.$$

$$\left.\left. \times q(t - h^{(1)}T_B - nT_c) q(t' - h^{(1)}T_B - mT_c)\; n(t)n(t')dtdt' \right] \right\}$$

$$= N_0 \sum_{m=0}^{N_c-1} I_q([l-m]T_c, T_I; 0)$$

$$+ N_0 \left\{ \sum_{m=0}^{N_c-1} \sum_{m'=0}^{N_c-1} I_q([l-m]T_c, T_I; 0) I_q([l-m']T_c, T_I; 0) \right.$$

$$\left. + \sum_{m=0}^{N_c-1} \sum_{\substack{\mu=-N_c+1 \\ \mu\neq 0}}^{N_c-1} I_q^2([l-m-\mu]T_c, T_I; \mu T_c) \right\}$$

$$\tag{5.22}$$

5.4.3 The MAI and Noise Terms

Next, we consider the second-order moment of the MAI-times-noise terms following a similar approach as in (5.12). Regarding to the time asynchronous transmission delay, namely $\tau^{(k)}$ is uniformly distributed over $[0, T_s)$. We define the cross terms MAI-times-noise $\mathcal{Z}_{0,mn}^l$ and $\mathcal{Z}_{0,nm}^l$ as

$$
\mathcal{Z}_{0,mn}^l = \int_{(h^{(1)}N_c+l)T_c}^{(h^{(1)}N_c+l)T_c+T_I} \sum_{k=2}^{N_u} a_1^{(k)} \sum_{n=0}^{N_c-1} c_n^{(k)} q^{(k)}(t - h^{(k)}N_cT_c - nT_c - \tau^{(k)})\ n(t)\ dt
$$

(5.23)

The variance of $\mathcal{Z}_{0,mn}^l$ and $\mathcal{Z}_{0,nm}^l$ is a function of $q^{(k)}(t)$ because these variables are correlation results of signals from interfering transmitters and the receiver noise. The evaluation of mean and second order moment of (5.23) is similar to the terms of (5.26). We can obtain the mean of $\mathcal{Z}_{0,mn}^l$ as

$$
\mathsf{E}\{\mathcal{Z}_{0,mn}^l\} = 0.
$$

(5.24)

For clarity, we shall denote by $\mathsf{E_c}\{.\}$, $\mathsf{E}_h\{.\}$ and $\mathsf{E}_\tau\{.\}$ the expectations with respect to the distribution of the random code, the distribution of the time hopping code and the scrambling distribution of the delay. We need to evaluate the second-order moment of the cross terms MAI-times-noise $\mathcal{Z}_{0,mn}^l$ with respect to averaging over the code vector $\mathbf{c}$, all users' hopping positions h, asynchronous delay τ and noise, whose expression can be written as

$$
\begin{aligned}
\mathsf{E}_{\mathbf{c},h,\tau}\{|\mathcal{Z}_{0,mn}^l|^2\} = &\ \mathsf{E}\Big\{\Big[\int_{(h^{(k)}N_c+l)T_c}^{(h^{(k)}N_c+l)T_c+T_I} \sum_{k=2}^{N_u} a_1^{(k)} \sum_{n=0}^{N_c-1} c_n^{(k)} \\
&\quad \times\ q^{(k)}(t - h^{(k)}T_B - nT_c - \tau^{(k)})\ n(t)dt\Big]^2\Big\} \\
&+ \mathsf{E}\Big\{\Big[\int_{(h^{(k)}N_c+l)T_c}^{(h^{(k)}N_c+l)T_c+T_I} \sum_{k=2}^{N_u} a_1^{(k)} \sum_{m=0}^{N_c-1} c_m^{(k)} \\
&\quad \times\ q^{(k)}(t - h^{(k)}T_B - mT_c - \tau^{(k)})\ n(t)dt\Big]^2\Big\} \\
&+ 2\mathsf{E}\Big\{\Big[\int_{(h^{(1)}N_c+l)T_c}^{(h^{(k)}N_c+l)T_c+T_I} \int_{(h^{(k)}N_c+l)T_c}^{(h^{(k)}N_c+l)T_c+T_I} \sum_{k=2}^{N_u} a_1^{(k)} a_1^{(k)} \sum_{n=0}^{N_c-1} \sum_{m=0}^{N_c-1} c_n^{(k)} c_m^{(k)} \\
&\quad \times q^{(k)}(t - h^{(k)}T_B - nT_c - \tau^{(k)})q^{(k)}(t' - h^{(k)}T_B - mT_c - \tau^{(k)}) \\
&\quad \times\ n(t)n(t')dtdt'\Big]\Big\}
\end{aligned}
$$

(5.25)

We need to evaluate the second-order moment of the cross terms with respect to averaging over the code vector $\mathbf{c}$, hopping positions h and noise. By following a similar step as derived in subsection 5.4.1, we obtain the variance of $\mathcal{Z}_{0,mn}^l$, $\mathrm{var}_{\mathbf{c},h,\tau}\{|\mathcal{Z}_{0,mn}^l|\} = \mathsf{E}_{\mathbf{c},h,\tau}\{|\mathcal{Z}_{0,mn}^l|^2\}$ as

$$
\begin{aligned}
\mathsf{E}_{\mathbf{c},h,\tau}\{|\mathcal{Z}_{0,mn}^l|^2\} = {} & \frac{N_0}{T_s} \sum_{k=2}^{N_u} \int_{-\infty}^{\infty} \sum_{m=0}^{N_c-1} I_{q^{(k)}}([l-m]T_c - \tau^{(k)}, T_I; 0)d\tau \\
& + \frac{N_0}{T_s} \sum_{k=2}^{N_u} \int_{-\infty}^{\infty} \Big\{ \sum_{m=0}^{N_c-1}\sum_{m'=0}^{N_c-1} I_{q^{(k)}}([l-m]T_c, T_I; -\tau^{(k)}) \\
& \times \quad I_{q^{(k)}}([l-m']T_c, T_I; -\tau^{(k)}) \\
& + \sum_{m=0}^{N_c-1}\sum_{\substack{\mu=-N_c+1\\\mu\neq 0}}^{N_c-1} I_{q^{(k)}}^2([l-m-\mu]T_c, T_I; \mu T_c - \tau^{(k)}) \Big\} d\tau
\end{aligned}
\tag{5.26}
$$

5.4.4 Signal and the MAI Terms

The cross terms signal-times-MAI ($\mathcal{Z}_{0,ma}^l$ and $\mathcal{Z}_{0,am}^l$) are written as

$$
\begin{aligned}
\mathcal{Z}_{0,ma}^l = {} & \int_{(h^{(1)}N_c+l)T_c}^{(h^{(1)}N_c+l)T_c+T_I} \sum_{k=2}^{N_u} \Big\{ a_1^{(1)} a_1^{(k)} \sum_{n=0}^{N_c-1}\sum_{m=0}^{N_c-1} c_n^{(k)} c_m^{(1)} \\
& \times \quad q^{(k)}(t - h_i^{(k)}T_B - nT_c - a_0^{(k)}\Delta_{bpm} - \tau^{(k)}) \\
& \times \quad q(t - h^{(1)}T_B - mT_c - a_0^{(1)}\Delta_{bpm}) \\
& + a_1^{(1)} a_1^{(k)} \sum_{n=0}^{N_c-1}\sum_{m=0}^{N_c-1} c_n^{(1)} c_m^{(k)} q(t - h^{(1)}T_B - nT_c - a_0^{(1)}\Delta_{bpm}) \\
& \times \quad q^{(k)}(t - h_i^{(k)}T_B - mT_c - a_0^{(k)}\Delta_{bpm} - \tau^{(k)}) \Big\} \, dt \\
= {} & \sum_{k=2}^{N_u} 2a_1^{(1)} a_1^{(k)} \sum_{n=0}^{N_c-1}\sum_{m=0}^{N_c-1} c_n^{(1)} c_m^{(k)} \Big\{ I_{q^{(k)}q}((l-n)T_c, T_I; \\
& \qquad\qquad (h^{(1)} - h^{(k)})T_B + (n-m)T_c - a_0^{(k)}\Delta_{bpm} - \tau^{(k)}) \Big\} \\
= {} & \sum_{k=2}^{N_u} 2a_1^{(1)} a_1^{(k)} \sum_{\mu=-N_c+1}^{N_c-1}\sum_{m=0}^{N_c-1} c_m^{(1)} c_{m-\mu}^{(k)} \Big\{ I_{q^{(k)}q}([l-m-\mu]T_c, T_I; \\
& \qquad\qquad (h^{(1)} - h^{(k)})T_B + \mu T_c - a_0^{(k)}\Delta_{bpm} - \tau^{(k)}) \Big\}.
\end{aligned}
\tag{5.27}
$$

The following assumptions are used that polarity codes $a_1^{(k)}$, the code vector $\mathbf{c}$ and data bits $a_0^{(k)}$ are independent random variables and equiprobably take on $\{-1, +1\}$. Given all the scrambling code vector $\mathbf{c}$ of user 1 and the interferences, it can be shown that the mean of (5.28) is zero.

$$
\begin{aligned}
\mathsf{E}\{\mathcal{Z}_{0,ma}^l\} = \sum_{k=2}^{N_u} \mathsf{E}\Big\{ 2a_1^{(1)} a_1^{(k)} \sum_{\mu=-N_c+1}^{N_c-1} \sum_{m=0}^{N_c-1} c_m^{(1)} c_{m-\mu}^{(k)} \Big\{ I_{q^{(k)}q}([l-m-\mu]T_c, T_I; \\
(h^{(1)} - h^{(k)})T_B + \mu T_c - a_0^{(k)}\Delta_{bpm} - \tau^{(k)}) \Big\} \Big\}
\end{aligned}
$$

$$
= 0.
$$

(5.28)

In evaluating the second-order moments of the interference terms $\mathcal{Z}_{0,ma}^l$ and $\mathcal{Z}_{0,am}^l$, we assume other users' asynchronous transmission delays, namely $\tau^{(k)}$ are uniformly distributed over $[0, T_s)$. By following a similar step as used in subsection (5.4.1), we obtain the variance of $\mathcal{Z}_{0,ma}^l$, $\text{var}_{\mathbf{c},h,\tau}\{|\mathcal{Z}_{0,ma}^l|\} = \mathsf{E}_{\mathbf{c},h,\tau}\{|\mathcal{Z}_{0,ma}^l|^2\}$ as

$$
\begin{aligned}
\mathsf{E}_{\mathbf{c},h,\tau}\{|\mathcal{Z}_{0,ma}^l|^2\} = \frac{2}{T_s} \sum_{k=2}^{N_u} \int_{-\infty}^{\infty} \Big[\sum_{m=0}^{N_c-1} \sum_{m'=0}^{N_c-1} I_{q^{(1)}q^{(k)}}([l-m]T_c, T_I; -\tau^{(k)}) \\
\times I_{q^{(1)}q^{(k)}}([l-m']T_c, T_I; -\tau^{(k)}) \Big] d\tau \\
+ \frac{2}{T_s} \sum_{k=2}^{N_u} \int_{-\infty}^{\infty} \Big[\sum_{m=0}^{N_c-1} \sum_{\substack{\mu=-N_c+1 \\ \mu \neq 0}}^{N_c-1} I_{q^{(1)}q^{(k)}}^2([l-m-\mu]T_c, T_I; \mu T_c - \tau^{(k)}) \Big] d\tau
\end{aligned}
$$

(5.29)

5.4.5 The MAI Interference Terms

The expression of cross terms MAI-times-MAI ($\mathcal{Z}_{0,mm}^l$) is written as

$$
\begin{aligned}
\mathcal{Z}_{0,mm}^l = \int_{(h^{(1)}N_c+l)T_c}^{(h^{(1)}N_c+l)T_c+T_I} \Big\{ \sum_{k=2}^{N_u} a_1^{(k)} \sum_{n=0}^{N_c-1} c_n^{(k)} q^{(k)}(t - h^{(k)}T_B - nT_c - a_0^{(k)}\Delta_{bpm} - \tau^{(k)}) \\
\times \sum_{k=2}^{N_u} a_1^{(k)} \sum_{m=0}^{N_c-1} c_m^{(k)} q^{(k)}(t - h^{(k)}T_B - mT_c - a_0^{(k)}\Delta_{bpm} - \tau^{(k)}) \Big\} dt
\end{aligned}
$$

(5.30)

where $\mathcal{Z}_{0,mm}^l$ can be written as the superposition of two terms as $\mathcal{Z}_{0,mm}^l := \mathcal{Z}_{0,mm,A}^l + \mathcal{Z}_{0,mm,B}^l$ where $\mathcal{Z}_{0,mm,A}^l$ represents the total interference from correlating the signals

of the same interferer (self MAI-by-MAI); while $\mathcal{Z}^l_{0,mm,B}$ accounts for the total interference from correlating the signals of different interferers, referred to as cross MAI-by-MAI. $\mathcal{Z}^l_{0,mm,A}$ and $\mathcal{Z}^l_{0,mm,B}$ can be written as

$$
\begin{aligned}
\mathcal{Z}^l_{0,mm,A} &= \int_{(h^{(1)}N_c+l)T_c}^{(h^{(1)}N_c+l)T_c+T_I} \left\{ \sum_{k=2}^{N_u} a_1^{(k)} \sum_{n=0}^{N_c-1} c_n^{(k)} q^{(k)}(t - h^{(k)}T_B - nT_c - a_0^{(k)}\Delta_{bpm} - \tau^{(k)}) \right.\\
&\quad \left. \times \sum_{k'=2}^{N_u} a_1^{(k)} \sum_{m=0}^{N_c-1} c_m^{(k)} q^{(k')}(t - h^{(k')}T_B - mT_c - a_0^{(k')}\Delta_{bpm} - \tau^{(k')}) \right\} dt,
\end{aligned}
$$

$$(5.31)$$

$$
\begin{aligned}
\mathcal{Z}^l_{0,mm,B} &= \int_{(h^{(1)}N_c+l)T_c}^{(h^{(1)}N_c+l)T_c+T_I} \left\{ \sum_{k=2}^{N_u} a_1^{(k)} \sum_{n=0}^{N_c-1} c_n^{(k)} q^{(k)}(t - h^{(k)}T_B - nT_c - a_0^{(k)}\Delta_{bpm} - \tau^{(k)}) \right.\\
&\quad \left. \times \sum_{\substack{k,k'=2 \\ k \neq k'}}^{N_u} a_1^{(k)} \sum_{m=0}^{N_c-1} c_m^{(k)} q^{(k')}(t - h^{(k')}T_B - mT_c - a_0^{(k')}\Delta_{bpm} - \tau^{(k')}) \right\} dt.
\end{aligned}
$$

$$(5.32)$$

$\mathcal{Z}^l_{0,mm,A}$ and $\mathcal{Z}^l_{0,mm,B}$ are uncorrelated due to the independency among different users' polarity codes $a_1^{(k)}$ and the scrambling code vector $\mathbf{c}$, hence $\mathsf{E}\{\mathcal{Z}^l_{0,mm,A}\mathcal{Z}^l_{0,mm,B}\} = 0$. The expectation of cross terms self MAI-times-MAI is zero due to the random polarity of the scrambling code. We note that $\mathcal{Z}^l_{0,mm,A}$ and $\mathcal{Z}^l_{0,mm,B}$ are uncorrelated, because of the independency among different user polarity codes and scrambling codes. Meanwhile the expectation of self MAI-times-MAI, using a similar approach as shown for the desired signal in (5.29) with respect to all interfering users' possible TH codes, the code vector $\mathbf{c}$ and distribution of delays transmission τ_k for $k = \{2, 3, \cdots, N_u\}$, can be computed as

$$
\mathsf{E}_{\mathbf{c},h,\tau}\{\mathcal{Z}^l_{0,mm,A}\} = \frac{1}{T_s} \sum_{k=2}^{N_u} \int_{-T_I}^{T_I} \sum_{m=0}^{N_c-1} I_{q^{(k)}}([l-m]T_c - a_0^{(k')}\Delta_{bpm} + x, T_I; 0)dx \quad (5.33)
$$

Meanwhile the cross MAI-times-MAI has zero mean because of the independency among different user's polarity codes and scrambling codes. The second order mo-

ments of $\mathcal{Z}^l_{0,mm}$ can be evaluated as

$$
\begin{aligned}
\mathsf{E}_{\mathbf{c},h,\tau}\{|\mathcal{Z}^l_{0,mm}|^2\} &= \frac{1}{T_s}\sum_{k=2}^{N_u}\int_{-T_I}^{T_I}\sum_{m=0}^{N_c-1} I_{q^{(k)}}([l-m]T_c+x,T_I;0)dx \\
&+ \frac{1}{T_s}\sum_{\substack{k,k'=2 \\ k\neq k'}}^{N_u}\int_{-T_I}^{T_I}\sum_{m=0}^{N_c-1} I_{q^{(k)}}([l-m]T_c-\tau^{(k)},T_I;0)d\tau \\
&+ \frac{1}{T_s}\sum_{k=2}^{N_u}\sum_{h_1=0}^{N_c-1}\sum_{h_2=0}^{N_c-1}\frac{N_h-|h_1|}{N_h}\frac{N_h-|h_2|}{N_h} \\
&\quad \times \int_{-T_I}^{T_I}\Bigg\{\sum_{m=0}^{N_c-1}\sum_{m'=0}^{N_c-1} I_{q^{(k)}}([l-m]T_c,T_I;x) \\
&\quad \times\quad I_{q^{(k)}}([l-m']T_c+[h_1+h_2]N_cT_c,T_I;x) \\
&\quad + \sum_{m=0}^{N_c-1}\sum_{\substack{\mu=-N_c+1 \\ \mu\neq 0}}^{N_c-1} I^2_{q^{(k)}}([l-m-\mu]T_c+[h_1+h_2]N_cT_c,T_I;\mu T_c+x)\Bigg\}dx
\end{aligned}
$$

$$(5.34)$$

5.4.6 Quadratic Noise Term

As we mentioned earlier, the quadratic noise terms $\mathcal{Z}^l_{0,nn}$ can be written as

$$
\mathcal{Z}^l_{0,nn} = \int_{(h^{(1)}N_c+l)T_c}^{(h^{(1)}N_c+l)T_c+T_I} (n(t))^2\ dt
$$

$$(5.35)$$

The mean of the quadratic noise terms $\mathcal{Z}^l_{0,nn}$ is

$$
\mathsf{E}\{\mathcal{Z}^l_{0,nn}\} = N_0 T_I W_{rx} = N_0 T_I.
$$

$$(5.36)$$

The variance of the quadratic noise terms $\mathcal{Z}^l_{0,nn}$ can be evaluated as

$$
\begin{aligned}
\mathsf{E}\{|\mathcal{Z}^l_{0,nn}|^2\} &= \int_0^{T_I}\int_{-t}^{T_I-t} R_{nn}(\varepsilon)R_{nn}(\varepsilon)\ d\varepsilon dt \\
&\cong N_0^2 T_I \int_{-\infty}^{-\infty} \phi_f^2(\varepsilon)\ d\varepsilon \\
&= N_0^2 T_I W'_{rx}
\end{aligned}
$$

$$(5.37)$$

where $W'_{rx} = \| \phi_f(t) \|^2$ is an equivalent receiver bandwidth $W'_{rx} \approx W_{rx}$. It is also to be noted that we have used the assumption that the time-bandwidth product $N_0 T_I$ is large enough to validate the central limit theorem.

5.5 Weighted Energy Detection Receiver

Assuming the desired bit $a_1^{(1)} = 0$ is transmitted, we collect all terms of means and variances for L partitioned integration sub-intervals at the first sample of $\mathcal{Z}_0$ from the previous section.

$$\mu_{0,l} = \mathsf{E}\{|\mathcal{Z}_{0,a}^l|\} + 2\mathsf{E}\{|\mathcal{Z}_{0,an}^l|\} + 2\mathsf{E}\{|\mathcal{Z}_{0,mn}^l|\}$$
$$\sigma_{0,l}^2 = \mathrm{var}\{|\mathcal{Z}_{0,a}^l|\} + 2\mathrm{var}\{|\mathcal{Z}_{0,an}^l|\} + 2\mathrm{var}\{|\mathcal{Z}_{0,mn}^l|\} + 2\mathrm{var}\{|\mathcal{Z}_{0,am}^l|\} \qquad (5.38)$$
$$+ \mathrm{var}\{|\mathcal{Z}_{0,mm}^l|\} + \mathrm{var}\{|\mathcal{Z}_{0,nn}^l|\}.$$

The way to find the weighting coefficients is based on the maximation of the metric function as derived in Appendix A.1. We define the weighting coefficients $\mathbf{w} \triangleq \{w_1, w_2, \cdots, w_L\}$ and the energy desired signal as $\mathbf{h} \triangleq \{E_1, E_2, \cdots, E_L\}$ and assume equal power for all users that is being transmitted. The weighted receiver consists of using the optimal weight vector to estimate the desired user data. The integration interval vector is defined as $\mathbf{t} \triangleq \{T_1, T_2, \cdots, T_L\}$, where $T_l = \frac{2T_I}{N_c T_c}$, and the $\mathbf{T} \triangleq \mathrm{diag}\{\mathbf{t}\}$. The variances of the desired signal are defined as $\mathbf{v} \triangleq \{V_1, V_2, \cdots, V_L\}$ with $\mathbf{V} \triangleq \mathrm{diag}\{\mathbf{v}\}$. The variances of the signal-times-noise are defined as $\mathbf{r} \triangleq \{R_1, R_2, \cdots, R_L\}$, with $\mathbf{R} \triangleq \mathrm{diag}\{\mathbf{r}\}$. The variances of the MAI-times-noise are defined as $\mathbf{s} \triangleq \{S_1, S_2, \cdots, S_L\}$, with $\mathbf{S} \triangleq \mathrm{diag}\{\mathbf{s}\}$. The variances of the desired signal-times-MAI are defined as $\mathbf{y} \triangleq \{Y_1, Y_2, \cdots, Y_L\}$, with $\mathbf{Y} \triangleq \mathrm{diag}\{\mathbf{y}\}$. The variances of MAI-times-MAI are then defined as $\mathbf{x} \triangleq \{X_1, X_2, \cdots, X_L\}$, with $\mathbf{X} \triangleq \mathrm{diag}\{\mathbf{x}\}$.

Then the mean μ_z and variance σ_z^2 in the BER performance (5.7) is evaluated, respectively, as

$$\mu_z = \sum_{l=1}^{L} w_l \mu_l = E_b(\mathbf{w}^T \mathbf{h}), \qquad (5.39)$$

and

$$\sigma_z^2 = \sum_{l=1}^{L} w_l^2 \sigma_l^2 = \mathbf{w}^T \mathbf{V} \mathbf{w} + N_0 \mathbf{w}^T (\mathbf{R} + \mathbf{S}) \mathbf{w} + \mathbf{w}^T Y \mathbf{w} + \mathbf{w}^T \mathbf{X} \mathbf{w} + N_0^2 W'_{rx} N_c T_c \mathbf{w}^T \mathbf{T} \mathbf{w}.$$

$$(5.40)$$

The probability error P_e is rewritten as

$$\begin{aligned}
P_e &= Q(\frac{\mu_z}{\sigma_z}) \\
&= Q(\frac{\mathbf{w}^T\mathbf{h}}{\sqrt{\mathbf{w}^T\Sigma\mathbf{w}}})
\end{aligned} \tag{5.41}$$

where $\Sigma = (\mathbf{V} + \mathbf{Y} + \mathbf{X} + N_0(\mathbf{R} + \mathbf{S}) + N_0^2 W'_{rx} N_c T_c T)/(E_b)^2$. Finally, The weighted coefficients as derived in Appendix A.1 can simply be written as

$$\mathbf{w}_{opt} \cong (\Sigma)^{-1}\mathbf{h}. \tag{5.42}$$

5.5.1 Simulation Results

We conducted BER simulations with and without weighting coefficients (WC). In all experiments, we used the second derivative of Gaussian UWB pulses which are transmitted over non-line-of slight channels with $\tau_{rms} = 10ns$. The channel model assumes a homogeneous Poisson process of ray-arrivals at 5 rays/ns.

Firstly, Fig. 5.2 shows the simulated BER performance of a single-user system over a multipath channel, where the code length $N_c = 4$, the chip width $T_c = 2$ ns, the time of integration $T_I = 20$ ns is set for a conventional energy detection receiver meanwhile $T_I = T_c = 2$ is set for the weighted energy receiver and a symbol duration $T_s = 1024$ ns. The BER performance improves about 3 dB when decreasing the bandwith from (BW) from 1.5 GHz to 0.5 GHz, since the power of the squared noise terms decreases. A close observation of Fig. 5.2 indicates that the weighting affects the TH UWB BPM system performance. It is observed that an energy detection UWB system with weighting coefficients performs more effective which results in lower BER values. Indeed, the noise gets sparsely distributed over the symbol duration to be suppressed.

In Fig. 5.3, the BER performance of energy detection with weighting coefficients is evaluated in a multiuser scenario. It compares the BER performance of a multiuser system ($N_u = 8$) over a multipath channel where we investigate the impact of different combination code lengths for the scrambling code realizations over each symbol, with a fixed data rate=100 Kbps. The IPDP of the channel realization for all users are available in the receiver. We firstly simulate with 500 channel realizations with code length of $N_c = \{16, 64\}$ without weighting. It shows that concentrating the bit energy in a longer code, improves the multiple access performance compared with shorter codes. Furthermore, additional gain can be achieved when the random code of the desired user is known. It can be seen that weighting alleviates the noise and
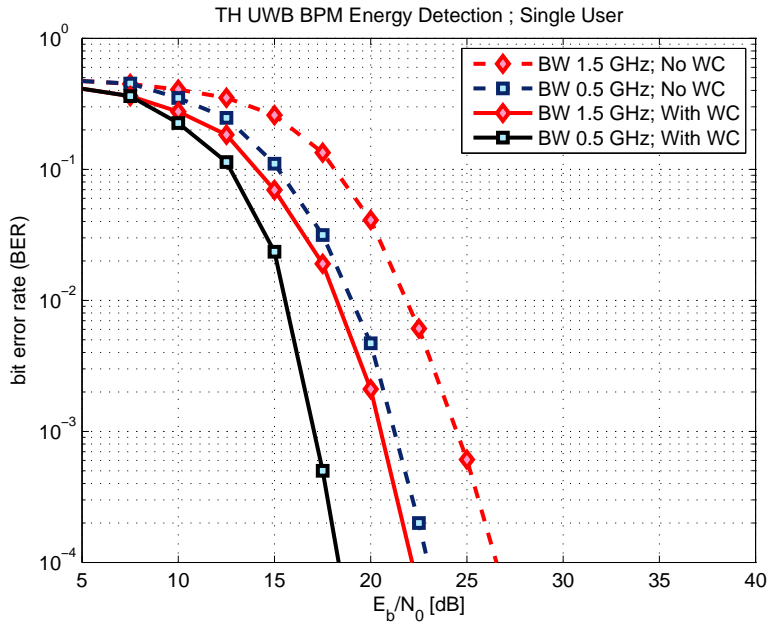
Figure 5.2: Bit error rate versus E_b/N_0 for single user.
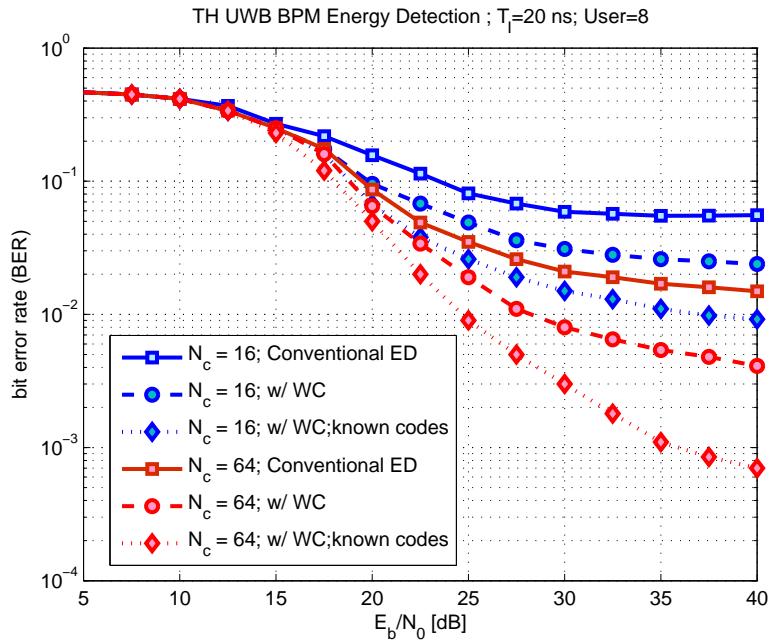
Figure 5.3: Bit error rate versus E_b/N_0 for 8 user case.

interference impact. In Fig. 5.4, we evaluate the performance of a weighted energy detector with impact of different users. We consider a UWB BPM system with TH sequences and the code length $N_c = 64$ and where different numbers of asynchronous UWB users (2-30 users) are active. The bandwidth and signal-to-noise ratio $\frac{E_b}{N_0}$ of the system are 0.5 GHz and 25 dB, respectively. We can see that the presence of MAI interference degrades the BER performance. This reduction is essentially due to the heavy system load and the cross MAI terms which contribute to the overall MAI interference effect. The results show that the proposed weighted noncoherent receiver can reduce the effect of MAI.
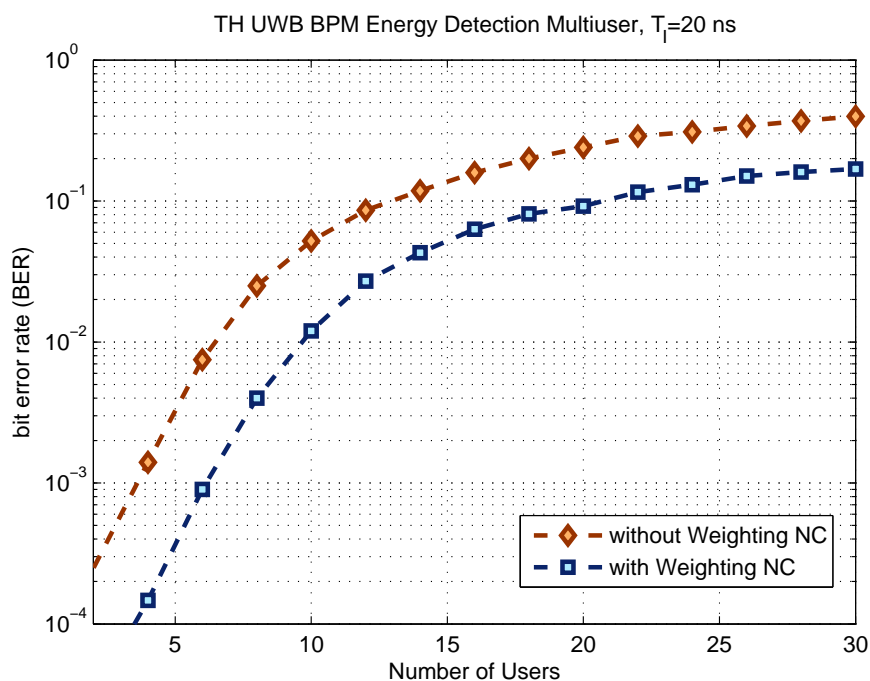
Figure 5.4: Bit error rate versus number of users.

5.6 Summary

We have considered a weighted energy detection receiver that alleviates the noise effect in a single user scenario and the multi-access interference in a multi-access environment. We have shown that concentrating the bit energy in a longer code, improves the multiple access performance compared with shorter codes. The weighted

receiver outperforms the conventional receiver.

6 Conclusions and Recommendations

The objective of this research was to investigate the performance of suboptimal UWB receivers in presence of MAI. Various suboptimal receivers were studied and implemented. This chapter summarizes conclusions that have been drawn and discussed in previous chapters. It comments about this research work and it gives guidelines for future research.

6.1 Conclusions

A comparison of various multiple access schemes has been presented. Simulation results show that a frame-differential scheme achieves better performance than the classical transmitted-reference (TR) technique, by re-using each pulse as a data and as a reference pulse. We also introduce a novel multiple access scheme, which transmits each data symbol as a short burst of differentially modulated pulses. This method, having some penalty in the single-user case due to increased inter-frame-interference, outperforms the others in multiuser scenarios, as collisions between bursts of multiple users are (mostly) avoided in asynchronous transmissions. Moreover, its optimum detector can be a memoryless (joint) ML detector. Blind and semi-blind detection techniques will be simplified due to the memoryless data model [38]. The reduced spacing of pulse-pairs simplifies the implementation of the delay lines in the AcR frontend.

Performance results showed that reference enhancement is an important issue in the hybrid matched filter (HMF) TR UWB receiver. The HMF receiver shows performance gain in absence of ISI when compared to conventional TR UWB systems. Performance evaluation of the HMF TR UWB receiver in the presence of MAI showed that the integration interval is an important design parameter which affects the performance significantly. The results demonstrate that the system performance improves by using the HMF for TR UWB over the conventional multichannel AcR. We have considered the hybrid matched-filter (HMF) transmitted-reference system in single and multiuser scenarios. We have derived a multiuser equivalent system model accounting for MAI to obtain advanced detectors for the HMF receiver. The newly proposed pre-combining MMSE detector has been proven useful by computer simulation although it remains behind the benchmark solutions.

We studied the performance of a dual-pulse TR UWB multiple access system with a memoryless multiuser AcR Volterra equivalent system model. An analytical expression of channel-averaged SIR has been obtained by statistical characterization as a function of system and channel parameters. In the numerical results, the receiver performance has been validated by simulation. The numerical results further show the constraint relationship between the bit rate and the chosen delay hopping code with the impact of MAI in dual-pulse TR UWB. In future work, the results will be applied to evaluate and possibly optimize certain system design choices under various system design constraints.

We have considered a weighting coefficient process that alleviates the noise effect in a single user scenario for BPM energy detection reception and in a multiple-access environment. The weighting coefficient receiver outperforms the conventional receiver without weighting and, in presence of multiuser interference, it is shown to have the better BER performance in dense multiuser scenarios which is achieved by using the considered weighting coefficient.

6.2 Recommendations for Future Work

This research work has opened numerous areas for future work which could be done to better understand the performance of the noncoherent UWB systems in the presence of MAI. Some of the areas are as follows:

1. The multi user case was addressed in this work, but the performance of these receivers in multiuser scenarios with some analytical limitation of the receiver due to MAI should be further studied.

2. Performance of the energy detection receivers should be evaluated for the IEEE channel model IEEE P802.15.4a.

3. Hardware implementation issues related to suboptimal receivers (the HMF TR UWB, energy detection receiver) should be further investigated.

A Derivation of Weighting Coefficients Energy Detection

A.1 Weighting Coefficients Based on Maximized Metric Function

Here we provide the derivation of the optimum weighting coefficients w_{opt}. First, we define the metric function $J(w)$ as

$$J(w) = \frac{\mathbf{w}^T \mathbf{h}}{\sqrt{\mathbf{w}^T \Sigma \mathbf{w}}} \tag{A.1}$$
$$= \frac{u}{v}$$

where the BER is minimized when the metric function is maximzed.

Using the derivation property

$$\frac{dJ(w)}{dw} = \frac{v \frac{du}{d\mathbf{w}} - u \frac{dv}{d\mathbf{w}}}{v^2} \tag{A.2}$$

Then, we are able to calculate

$$v \cdot \frac{du}{d\mathbf{w}} = \sqrt{\mathbf{w}^T \Sigma \mathbf{w}} \, \frac{d(\mathbf{w}^T \mathbf{h})}{d\mathbf{w}} \tag{A.3}$$
$$= \sqrt{\mathbf{w}^T \Sigma \mathbf{w}} \, \mathbf{h}$$

$$u \cdot \frac{dv}{d\mathbf{w}} = (\mathbf{w}^T \mathbf{h}) \frac{d(\sqrt{\mathbf{w}^T \Sigma \mathbf{w}})}{d\mathbf{w}} \tag{A.4}$$
$$= \frac{1}{2 \sqrt{\mathbf{w}^T \Sigma \mathbf{w}}} \mathbf{w}^T \mathbf{h} (\Sigma + \Sigma^T) \mathbf{w}$$

Furthermore, we equate the derivative with respect to $\mathbf{w}$ to zero,

$$\frac{dJ(\mathbf{w})}{d\mathbf{w}} = \frac{(\mathbf{w}^T \Sigma \mathbf{w})^{-\frac{1}{2}} \mathbf{h} - \frac{1}{2} \mathbf{w}^T \mathbf{h} (\mathbf{w}^T \Sigma \mathbf{w})^{\frac{1}{2}} (\Sigma + \Sigma^T) \mathbf{w}}{\mathbf{w}^T \Sigma \mathbf{w}} \tag{A.5}$$
$$= 0$$

resulting in the solution

$$(\mathbf{w}^T\Sigma\mathbf{w})^{\frac{1}{2}}\mathbf{h} - \frac{1}{2}(\mathbf{w}^T\mathbf{h})(\mathbf{w}^T\Sigma\mathbf{w})^{-\frac{1}{2}}(\Sigma + \Sigma^T)\mathbf{w} = 0$$
$$2\mathbf{h} - (\mathbf{w}^T\mathbf{h})(\mathbf{w}^T\Sigma\mathbf{w})^{-1}(\Sigma + \Sigma^T)\mathbf{w} = 0$$
$$2\mathbf{h} - 2(\mathbf{w}^T\mathbf{h})(\mathbf{w}^T\Sigma\mathbf{w})^{-1}\Sigma\mathbf{w} = 0 \tag{A.6}$$
$$(\mathbf{w}^T\Sigma\mathbf{w})\mathbf{h} - (\mathbf{w}^T\mathbf{h})\Sigma\mathbf{w} = 0$$
$$\mathbf{w} = (\mathbf{w}^T\Sigma\mathbf{w})(\mathbf{w}^T\mathbf{h})^{-1}\Sigma^{-1}\mathbf{h}.$$

Finally, we obtain the optimum $\mathbf{w}_{opt}$ as

$$\begin{aligned}
\mathbf{w}_{opt} &= (\mathbf{w}^T\Sigma\mathbf{w})(\mathbf{w}^T\mathbf{h})^{-1}\Sigma^{-1}\mathbf{h} \\
&= \frac{\mathbf{w}^T\Sigma\mathbf{w}}{\mathbf{w}^T\mathbf{h}}\Sigma^{-1}\mathbf{h} \\
&\cong \alpha\Sigma^{-1}\mathbf{h}.
\end{aligned} \tag{A.7}$$

Here $\alpha = \frac{\mathbf{w}^T\Sigma\mathbf{w}}{\mathbf{w}^T\mathbf{h}}$ is a scaling factor dependent on $\mathbf{w}$, while its value does not affect the detection BER, therefore, it can be set $\alpha = 1$, which simplifies the optimal weights to be

$$\mathbf{w}_{opt} = (\Sigma)^{-1}\mathbf{h}. \tag{A.8}$$

Bibliography

[1] C. Steiner and K. Witrisal, "Multiuser interference modeling and suppression for a multichannel differential IR-UWB system," in *IEEE Conference on Ultra Wideband Systems and Technologies*, Zurich, 2005, pp. 667–672.

[2] M. Z. Win and R. A. Scholtz, "Comparisons of analog and digital impulse radio for multiple-access communications," in *IEEE International Conference on Communications, ICC*, Montreal, Canada, June 1997, pp. 91–95.

[3] R. Scholtz, "Multiple access with time-hopping impulse modulation," in *Military Communications Conference, MILCOM*, 1993, pp. 447–450.

[4] M. Z. Win and R. A. Scholtz, "Characterization of ultra-wide bandwidth wireless indoor channels: A communication-theoretic view," *IEEE Journal on Selected Areas in Communications*, vol. 20, no. 9, pp. 1613–1627, 2002.

[5] J. Foerster, "The effects of multipath interference on the performance of UWB systems in an indoor wireless channel," in *IEEE Vehicular Technology Conference, VTC*, Rhodes, Greece, May 2001, pp. 1176–1180.

[6] F. Troesch, F. Althaus, and A. Wittneben, "Modified pulse repetition coding boosting energy detector performance in low data rate systems," in *IEEE Conference on Ultra Wideband Systems and Technologies*, Zurich, Switzerland, 2005, pp. 508–513.

[7] J. Wu, H. Xian, and Z. Tian, "Weighted noncoherent receivers for UWB PPM signals," *IEEE Communications Letters*, vol. 10, no. 9, pp. 655–657, Sept. 2006.

[8] J. Choi and W. Stark, "Performance analysis of RAKE receivers for ultrawideband communications with PPM and OOK in multipath channels," in *IEEE International Conference on Communications, ICC*, 2002, pp. 1969–1973.

[9] D. Cassioli, M. Z. Win, and A. Molisch, "The ultra-wide bandwidth indoor channel: From statistical model to simulations," *IEEE Journal on Selected Areas in Communications*, vol. 20, no. 6, pp. 1247–1257, 2002.

[10] R. Hoctor and H. Tomlinson, "Delay-hopped transmitted-reference RF communications," in *IEEE Conference on Ultra Wideband Systems and Technologies*, 2002, pp. 265–270.

[11] M. Pausini, G. Janssen, and K. Witrisal, "Performance enhancement of differential UWB autocorrelation receiver under IS," *IEEE Journal on Selected Areas in Communications*, vol. 4, no. 24, pp. 815–821, Apr. 2006.

[12] X. Dong, A. Lee, and L. Xiao, "Performance analysis of dual pulse transmission in UWB channels," *IEEE Communications Letters*, vol. 10, no. 8, pp. 626–628, Aug. 2006.

[13] A. Trindade, Q. Dang, and A.-J. van der Veen, "Signal processing model for a transmit-reference UWB wireless communication system," in *IEEE Conference on Ultra Wideband Systems and Technologies*, 2003.

[14] F. Tufvesson, S. Gezici, and A. Molisch, "Ultra-wideband communications using hybrid matched filter correlation receivers," *IEEE Transactions on Wireless Communications*, vol. 11, no. 5, pp. 3119–3129, Nov 2006.

[15] J. Romme and G. Durisi, "Oversampled weighted autocorrelation receivers for transmitted-refence UWB systems," in *IEEE Vehicular Technology Conference, VTC*, Stockholm, Sweden, 2005.

[16] B. J. M.-K. Oh, R. Harjani, and D.Park, "A new noncoherent UWB impulse radio receiver," *IEEE Communications Letters*, vol. 9, no. 2, pp. 151–153, Feb. 2005.

[17] *IEEE P802.15.4a-2007 (Amendement 1), 802.15.4: Wireless Mediaum Access Control (MAC) and Physical Layer (PHY) Specifications for Low-Rate Wireless PANs.* Std., 2007.

[18] A. Forouzan, M. Nasiri-Kenari, and J. Salehi, "Performance analysis of time-hopping spread spectrum multiple-access systems: Uncoded and coded schemes," *IEEE Transactions on Wireless Communications*, no. 4, pp. 671–681, 2002.

[19] S. Gezici, Z. Sahinoglu, H. Kobayashi, and H.V.Poor, "Ultra-wideband impulse radio systems with multiple pulse types," *IEEE Journal on Selected Areas in Communications*, vol. 24, no. 4, pp. 892–898, Apr. 2006.

[20] M. Z. Win and R. A. Scholtz, "Ultra-wide bandwidth time-hopping spread-spectrum impulse radio for wireless multiple-access communications," *IEEE Trans. Commun.*, vol. 48, no. 4, pp. 679–691, Apr. 2000.

[21] G. Durisi and G. Romano, "On the validity of gaussian approximation to characterize the multiuser capacity of UWB TH PPM," in *International Wideband Systems and Technologies*, 2002, pp. 157–161.

[22] K. Witrisal, G. Leus, M. Pausini, and C.Krall, "Equivalent system model and equalization of differential impulse radio UWB systems," *IEEE Journal on Selected Areas in Communications*, vol. 23, no. 9, pp. 1851–1862, Sep. 2005.

[23] C. Steiner, "Multiuser interference modeling and suppression for differential IR-UWB systems," in *Master of Scicence Thesis Graz University of Technology*, Graz, Austria, 2005.

[24] K. Witrisal, M. Pausini, and A. Trindade, "Multiuser interference and inter-frame interference for UWB transmitted reference systems," in *International Workshop on Ultra-Wideband Systems, IWUWBS*, Kyoto, May 2004.

[25] K. Witrisal, "Statistical analysis of the IEEE 802.15.4a UWB PHY over multipath channels," in *IEEE Wireless Communications and Networking Conference, WCNC*, Las Vegas, 2008.

[26] K. Witrisal and M. Pausini, "Statistical analysis of UWB channel correlation function," *IEEE Transactions on Vehicular Technology*, Mar. 2008.

[27] J. Baringbing and K. Witrisal, "Performance evaluation of multiple-access dual-pulse transmitted reference UWB systems," Crete, Greece, Aug. 2008, pp. 214–219.

[28] J. Baringbing, "Multiple access performance of TH UWB BPM energy detection receiver," in *Privatissimum at Signal Processing and Speech Communication Laboratory TUGraz*, Graz, Austria, Oct. 2008.

[29] J. Choi and W. Stark, "Performance of ultra-wideband communications with suboptimal receivers in multipath channels," *IEEE Journal on Selected Areas in Communications*, vol. 20, no. 9, pp. 1754–1766, Dec. 2002.

[30] W. van Etten, "Maximum likelihood receiver for multiple channel transmission systems," *IEEE Trans. Commun.*, vol. 24, no. 2, pp. 276–283, 1976.

[31] J. R. Barry, E. A. Lee, and D. G. Messerschmitt, *Digital Communications*, third ed. ed.   Kluwer Academic Publishers, 2004.

[32] S. Verdú, *Multiuser Detection.*   Cambridge University Press, 2002.

[33] K. Witrisal and Y. D. Alemseged, "Narrowband interference mitigation for differential uwb systems," in *Asilomar Conference on Signals, Systems, and Computers*, Pacific Grove, CA, Oct. 2005.

[34] K. Witrisal, M. Pausini, and A. Trindade, "Multiuser interference and interframe interference for UWB transmitted reference systems," in *International Workshop on Ultra-Wideband Systems, IWUWBS*, Kyoto, May 2004.

[35] A. Vannucci and R. Raheli, "Sequence detection in nonlinear channels: a convenient alternative to analog predistortion," *IEEE Trans. Commun.*, vol. 50, no. 9, pp. 1515–1524, Sept. 2002.

[36] M. V. Eyuboğlu and S. U. H. Qureshi, "Reduced-State Sequence Estimation with Set Partitioning and Decision Feedback," *IEEE Transactions on Communications*, vol. 36, no. 1, pp. 13–20, January 1988.

[37] S. Verdú, "Minimum probability of error for asynchronous gaussian multiple-access channels," *IEEE Trans. Inform. Theory*, vol. 32, no. 1, pp. 85–96, Jan. 1986.

[38] N. Petrochilos and K. Witrisal, "Semi-blind source separation for memoryless volterra channels in UWB and its uniqueness," in *Proc. IEEE Workshop on Sensor Array and Multi-channel Processing, SAM*, Waltham, MA, Jul. 2006.

[39] Y. Chao and R. Scholtz, "Multiple access performance of ultra-wideband transmitted reference systems in multipath envieronments," in *IEEE Wireless Communications and Networking Conference, WCNC*, 2004, pp. 1788– 1793.

[40] M. Win and R. Scholtz, "Ultra-wide bandwith time-hopping spread-spectrum impulse radio for wireless multiple-access communications," *IEEE Transactions on Communications*, vol. 48, pp. 679–691, Apr. 2000.

[41] ——, "Impulse radio: How it works," *IEEE Communications Letters*, vol. 2, pp. 36–38, Feb. 1998.

[42] *Revision of Part 15 of the Commision's Rules Regarding Ultra Wideband Transmission*.   Federal Communications Commision, Washington, DC, ET Docket, 98-153, Apr. 2002.

[43] T.-Q.-S. Quek and M.-Z. Win, "Analysis of UWB transmitted-reference communication systems in dense multipath channels," *IEEE Journal on Selected Areas in Communications*, vol. 9, no. 23, pp. 1863–1874, Sep. 2005.

[44] T. Jia and D. I. Kim, "Analysis of channel-averaged SINR for indoor UWB rake and transmitted reference systems," *IEEE Journal on Selected Areas in Communications*, vol. 55, no. 10, pp. 2022–2032, Oct. 2007.

[45] ——, "Multiple access performance of balanced UWB transmitted-reference systems in multipath," *IEEE Transactions on Wireless Communications*, vol. 7, no. 3, pp. 1084–1094, Mar. 2008.

[46] Y. Alemseged and K. Witrisal, "Modeling and mitigation of narrowband interference for transmitted-reference UWB systems," *IEEE Journal on Selected Areas in Signal Processing*, vol. 1, no. 3, Oct. 2007.

[47] F. Tufvesson and A. Molisch, "Ultra-wideband communication using hybrid matched filter correlation receivers," in *IEEE Vehicular Technology Conference, VTC*, Milan, Italy, May 2004.

[48] J. Baringbing and K. Witrisal, "MMSE optimisation of the hybrid matched-filter receiver for transmitted-reference UWB," in *IEEE UWB Forum on Sensing and Communication*, Linz, Mar. 2007.

[49] ——, "MMSE optimisation of the hybrid matched-filter receiver for transmitted-reference UWB," in *Proc. Int. Symp. on Personal, Indoor, and Mobile Radio Communications, PIMRC*, Athens, Greece, Sep. 2007, pp. 1–5.

[50] M. Win and R. Scholtz, "Ultra-wide bandwith time-hopping spread-spectrum impulse radio for wireless multiple-access communications," *IEEE Transactions on Communications*, vol. 48, pp. 679–691, Apr. 2000.

[51] Y. Chao and R. Scholtz, "Multiple access performance of ultrawideband transmitted reference systems in multipath environments," in *IEEE Wireless Communications and Networking Conference, WCNC*, Mar. 2004.

[52] T. Jia and D. Kim, "Multiuser performance of balanced UWB transmitted-reference system in multipath," in *IEEE Global Telecommunications Conference, GLOBECOM*, Nov. 2006.

[53] K. Witrisal and M. Pausini, "Statistical analysis of transmitted-reference UWB systems on multipath channels," in *IEEE International Conference on Ultra-Wideband, ICUWB*, Waltham, MA, Sep. 2006.

[54] K. Witrisal, "Statistical analysis of the IEEE802.15.4a UWB PHY over multipath channels," in *IEEE Wireless Communications and Networking Conference, WCNC*, Las Vegas, NV, Apr. 2008 (submitted).

[55] M. Pausini and G. Janssen, "Performance analysis of UWB autocorrelation receivers over Nakagami-fading channels," *IEEE Journal on Selected Areas in Signal Processing*, vol. 1, no. 3, pp. 443–455, Oct. 2007.

[56] H. Urkowitz, "Energy detection of unknown deterministic signals," *IEEE Transactions on Communications*, vol. 55, no. 4, pp. 523–531, 1967.

[57] A. Spaulding and D. Middleton, "Optimum reception in an impulsive interference environement-part I: Coherent detection," *IEEE Transactions on Communications*, vol. 25, no. 9, pp. 910–923, 1977.

[58] ——, "Optimum reception in an impulsive interference environement-part II: Incoherent reception," *IEEE Transactions on Communications*, vol. 25, no. 9, pp. 924–934, 1977.

[59] M. Flury, R. Merz, J.-Y. le Boudec, and J. Zory, "Performance evaluation of an ieee 802.15.4a physical layer with energy detection and multi-user interference," in *IEEE Conference on Ultra Wideband Systems and Technologies*, Singapore, Sept. 2007.

[60] M. Weisenhorn and W. Hirt, "ML receiver for pulsed UWB signals and partial channel state information," in *IEEE Conference on Ultra Wideband Systems and Technologies*, Zurich, Sept. 2005.

[61] ——, "Robust noncoherent receiver exploiting UWB channel properties," in *International Workshop on Ultra-Wideband Systems, IWUWBS*, Kyoto, Japan, May 2004, pp. 156–160.

[62] A. A. D'Amico, U. Mengali, and E. Arias-De-Reyna, "Energy-detection UWB receivers with multiple energy measurement," *IEEE Transactions on Wireless Communications*, vol. 6, no. 7, pp. 2652–2659, 2007.

[63] J. Romme and G. Durisi, "Transmitted reference impulse radio systems using weighted correlation," in *International Workshop on Ultra-Wideband Systems, IWUWBS*, Kyoto, May 2004.

[64] *IEEE 802.15.4a Channel Model-Final Report.* IEEE 802.15 TG4a Channel Model Subcommittee, [Online]. Availabe http://www.ieee802.org/15/pub/TG4a.html.

[65] T. Zasowski, F. Troesch, and A. Wittneben, "Partial channel stat information and intersymbol interference in low complexity UWB PPM detection," in *IEEE International Conference on Ultra-Wideband, ICUWB*, Waltham, MA, 2006.

[66] T. Zasowski and A. Wittneben, "UWB transmitted receivers in the presence of co-channel interference," in *Proc. Int. Symp. on Personal, Indoor, and Mobile Radio Communications, PIMRC*, Helsinki, Finland, 2006.